ADVANCED DYNAMICAL DECOUPLING STRATEGIES FOR SIMULATING HAMILTONIAN INTERACTIONS

TECHNISCHE
UNIVERSITÄT
DARMSTADT

Vom Fachbereich Physik
der Technischen Universität Darmstadt

zur Erlangung des Grades
eines Doktors der Naturwissenschaften (Dr. rer. nat.)

genehmigte Dissertation von
M. Sc. Holger Frydrych
aus Lauterbach

Referent: Prof. Dr. Gernot Alber
Korreferent: Prof. Dr. Reinhold Walser

Tag der Einreichung: 12.10.2015
Tag der Prüfung: 14.12.2015

Darmstadt 2016
D17

ABSTRACT

In the field of quantum information, a major challenge is to protect and shield quantum systems from environmental influences, which cause dissipation and decoherence. One approach to address this problem is called dynamical decoupling, where we act on a quantum system with a series of fast and strong local control operations. If done correctly, the system's state gets rotated in discrete steps in its state space in such a way that the effects of the environment cancel up to a certain order. In the first part of this thesis, we will introduce the basics of dynamical decoupling and present a new approach for constructing dynamical decoupling schemes based on sequences of Weyl operators on networks of qudits. This approach goes beyond merely protecting a quantum system, as it is also capable of altering existing Hamiltonian interactions in ways suitable for quantum simulation purposes. We will also investigate how imperfect controls influence the effectiveness of dynamical decoupling and focus particularly on stochastic noise.

In the second part of the thesis, we study concrete scenarios for the application of dynamical decoupling. First, we consider the task of quantum state transfer on a linear chain of qubits and use decoupling to protect the transfer from detrimental influences caused by a bend in the chain. We also look at how to design the specific interaction strengths required on the chain to make the state transfer work and extend this result to chains of qudits. Another chapter deals with decoupling the atomic centre-of-mass motion of a trapped atom or ion in a cavity interacting with a radiation field. Finally, we use decoupling to execute sequences of one- and two-qubit quantum gates on a chain of coupled qubits. Particular care is taken to ensure high fidelity operations in the presence of imperfect decoupling pulses.

ZUSAMMENFASSUNG

Eine der größten Herausforderungen in der Quanteninformationstheorie ist der Schutz von Quantensystemen vor Umgebungseinflüssen, die Dekohärenz und Dissipation verursachen. Eine mögliche Lösung ist Dynamische Entkopplung. Hierbei wird das zu schützende Quantensystem einer Serie von schnellen, lokalen Kontrolloperationen ausgesetzt, die bei korrekter Anwendung den Zustand des Systems im Zustandsraum so rotieren, dass sich die Umgebungseinflüsse im Mittel bis zu einer bestimmten Ordnung aufheben. Im ersten Teil dieser Dissertation werden die Grundlagen dynamischer Entkopplung erklärt und anschließend ein neues Verfahren für die Konstruktion von Entkopplungssequenzen auf Qudit-Netzwerken vorgestellt, deren Kontrolloperationen aus Tensorprodukten von Weyl-Operatoren bestehen. Dieses Verfahren ermöglicht auch Entkopplungssequenzen, die nicht dem reinen Schutz eines Quantensystems dienen, sondern bestehende Wechselwirkungen für den Zweck der Quantensimulation manipulieren können. Abschließend wird auf den Einfluss von imperfekten Kontrollen auf die Effizienz von Entkopplungsverfahren eingegangen und dabei insbesondere der Effekt von stochastischem Rauschen analysiert.

Der zweite Teil der Dissertation beschäftigt sich mit konkreten Anwendungsszenarien für dynamische Entkopplung. Zunächst wird die Zustandsübertragung auf einer linearen Qubit-Kette betrachtet, wobei Entkopplung verwendet wird, um den Transfer vor den Einflüssen eines Knicks in der Kette zu schützen. Anschließend wird gezeigt, wie die für die Zustandsübertragung notwendigen Wechselwirkungsstärken mittels Entkopplung konstruiert werden können. Dieses Resultat wird dann auch auf Ketten von Qudits verallgemeinert. Anschließend wird die Wechselwirkung eines gefangenen Atoms oder Ions in einer optischen Kavität mit einem Strahlungsfeld betrachtet und aufgezeigt, wie die Bewegung des Atoms in der Falle entkoppelt werden kann. Abschließend wird dynamische Entkopplung dazu verwendet, Sequenzen von Quantengattern auf einer stark wechselwirkenden Qubit-Kette zu implementieren. Hierbei wird insbesondere darauf eingegangen, wie trotz imperfekter Entkopplungspulse die Gatter mit hoher Qualität ausgeführt werden können.

ACKNOWLEDGMENTS

I would like to thank Prof. Dr. Gernot Alber for inviting me into and giving me the opportunity to work with his group and for his continued support during the writing of this thesis. I would also like to thank the members of the group for many fruitful discussions and in particular J. Zsolt Bernád, with whom I have had several successful collaborations on dynamical decoupling. Without him, the chapters about the influence of stochastic noise and about decoupling the centre-of-mass motion would not exist. He also graciously agreed to proof-read my thesis.

Furthermore, I would like to extend my gratitude to Prof. Igor Jex and his group in Prague. I was granted numerous opportunities to visit them and benefited greatly from the experience. In particular, I would like to thank Pavel Bažant who helped me understand the basics of dynamical decoupling and who helped me develop my idea for the construction method presented in this thesis. I would also like to thank Antonín Hoskovec, with whom I studied and developed several of the ideas about state transfer in Ch. 6.

Prof. Dr. Reinhold Walser graciously agreed to be the second assessor for this thesis, for which I am very thankful.

Finally, I am grateful to the Crossing project, a collaborative SFB project focussed on cryptography, which I was given the opportunity to join in October 2014 and which paid for half of my salary and several conference visits.

CONTENTS

1 INTRODUCTION

The modern computer is perhaps one of the most significant inventions in recent time. Its ever-increasing capabilities to perform complicated calculations and automate repetitive tasks both in daily life and in industrial production have drastically changed our lives and our society. Computers have enabled advancements in science and engineering that would never have been possible otherwise. Ever since the introduction of smartphones and tablets, many of us carry a small computer around at all times, which allows us instant access to long-range communication and the internet, a vast collection of information on virtually any topic, including maps and navigational aids.

Although the layout and hardware of computers have changed significantly over the years, at its core every digital computer works by manipulating a register of bits. A bit is a discrete unit of information with exactly two possible states, 0 or 1. In hardware, they are typically implemented by the presence or absence of an electric current in a circuit. Several of these bits together can be used to represent any natural number by its binary representation. Other types of information can be encoded as numbers, either by a direct bijective mapping (letters, words, ...) or by approximation (e.g. real numbers). The computer can perform so-called gate operations on individual or groups of bits in a register, which are deterministic and repeatable. A sequence of these gates can form a more complex operation, like the addition of a number.

That such operations can be performed deterministically is not a trivial matter. The bits in a computer are ultimately physical entities and therefore subjected to environmental imperfections. As the size of the electrical circuits on modern computers has been reduced to the point that it reaches atomic scales, they are susceptible to a wide range of disturbances. Indeed, cosmic radiation can cause a bit to inadvertently flip its value. Such random bit flips, if left unchecked, can have wide and potentially catastrophic consequences for the results of any operation performed.

Fortunately, there are ways to deal with these kinds of errors. The solution is to add redundancy - that is, add additional physical bits to a register which do not carry any additional information, but are involved in any operation in such a way that any occuring error can be detected or even corrected. Perhaps the simplest application of this concept is the parity bit. In this case, a register of N logical bits consists of $N + 1$ physical bits, where the additional bit always

represents the parity of the N-bit logical register. This parity bit is 1 if an uneven number of the N bits are in the state 1, and 0 otherwise. If any single bit in the physical register is flipped accidentally, then we can detect this error, since the parity bit will not be in the correct state. We thus know that an error occured and need to repeat the previous operation. However, if more than one error occurs, the parity bit may end up being in the correct state, so we cannot reliably detect errors if the error rate is too high. This is also true of more sophisticated error-correcting codes. They work as long as the overall bit error rate is below a certain threshold.

It is, in fact, this possibility to correct errors which sets the digital computer apart from other potential concepts for computers. At first sight, an analogue computer whose basic entities are not limited to just the discrete values 0 or 1, but can assume any value in-between, would appear more powerful. However, the analogue nature ruins any chance of doing error correction and thus running deterministic operations on such a device. Careful analysis reveals that this problem prevents any known analogue computer from being more powerful than the digital version for a general-purpose computation device. Specialised analogue devices may still be constructed for very specific tasks where exact deterministic results are not required, but they will never replace the classical computer as we know it today.

Recently, a new contender has arisen in the form of the quantum computer. Its origins date back to an idea by Richard Feynman in 1982. He noted that it was not possible to simulate an arbitrary quantum mechanical system on a classical computer due to exponential scaling of the quantum state space. Therefore he suggested that we might need computers which are themselves based on quantum mechanics for the task. In 1985 David Deutsch introduced the notion of a universal quantum computer. However, the quantum computer only gained significant interest when in 1994 Peter Shor presented his now famous algorithm that could efficiently factorise large integers and solve the discrete logarithm problem on a quantum computer. For both of these problems, no efficient algorithm is known on a classical computer. Yet they are at the core of two of our most important public key cryptography algorithms, the RSA public key encryption and the Diffie-Hellman key exchange protocol, so a computer which could efficiently solve these problems would threaten the heart of internet security.

At its core, the quantum computer makes use of qubits as its fundamental building blocks. A qubit describes the quantum-mechanical version of a classical bit. The qubit can assume two fundamental, orthogonal states typically written as $|0\rangle$ and $|1\rangle$. Unlike the classical bit, the qubit can also assume arbitrary superpositions of these two states. At first sight, this might look like the concept of an analogue computer. However, the laws of quantum mechanics dictate

that upon measurement, any superposition will collapse to either one of the two fundamental states with a certain probability, and the only possible measurement results are 0 and 1. This, in fact, makes any readout of the quantum computer digital. This quantum mechanical phenomenon creates a lot of difficulties, including the fact that an arbitrary quantum state cannot be cloned, however, it also enables the possibility to employ error correction on a quantum computer, in contrast to a classical analogue computer.

As with the classical computer, one fundamental idea for error correction is redundancy. Quantum error-correcting codes have been developed which encode a single logical qubit into several physical ones in such a way that potential errors can occur. However, due to the more complex nature of the qubit, there are more types of errors which can appear, and as a consequence the level of redundancy required is significantly higher than for classical bits. Quantum error-correcting codes require 3 or more physical qubits per logical qubit, depending on the class of errors considered to be corrected. Even then, a certain threshold in the error rate must be achieved for these codes to work.

There is another strategy to correct errors in a quantum computer, which works on a lower level and is complementary to quantum error-correcting codes. This method operates on the physical qubits and does not require any redundancy. It can be regarded as an averaging procedure, where the qubits are manipulated in such a way that unwanted environmental influences approximately cancel over time. This method is called *dynamical decoupling*, named so by Lorenza Viola in 1999 when she formalized ideas that had been employed in the nuclear magnetic resonance community since the 1950s. Although dynamical decoupling must in all honesty be called an error suppression technique instead of error correction, it is very effective at protecting the states of qubits. Decoupling has been successfully used in many experiments, and we strongly expect it to be a requirement to achieve the necessary thresholds for operations on the physical qubits so that quantum error-correcting codes can be made to work.

As of the writing of this thesis, the quantum computer is largely still a theoretical idea. Although the main concepts have been successfully demonstrated in small-scale experiments, to this day no quantum computer with a significant amount of controllable qubits exists. It remains to be seen if and when scalability can be achieved. However, it is clear that error correction and dynamical decoupling will be required for this to happen. In this thesis we will investigate advanced dynamical decoupling strategies to protect or even modify quantum systems of the kind we would encounter in quantum computers or quantum information theory.

1.1 OUTLINE

This thesis is divided into two parts. The first part introduces the fundamentals of dynamical decoupling and then presents a new way of constructing decoupling schemes on qubit and qudit networks. We will also look into schemes which are robust against errors in the control as well as analyse the effects of stochastic noise on the performance of dynamical decoupling. This part deals with the topic in a more abstract fashion, although some elementary examples are discussed where appropriate.

The second part presents several scenarios in which dynamical decoupling can be employed to protect quantum systems from imperfections or to engineer interactions for quantum simulation purposes. In each case, we explain the task as well as how the appropriate decoupling schemes are found and how they work in practice, based on numerical simulations.

1.1.1 *Theoretical foundations of dynamical decoupling*

Dynamical decoupling goes back to concepts from the nuclear magnetic resonance community [Hah50, CP54, MG58, Hae76] and was formalized by Viola in 1999 [VKL99].

CHAPTER 2 introduces the fundamental concepts of dynamical decoupling, which adds an external control Hamiltonian to the dynamics of a quantum system such that we may steer the system's time evolution in a beneficial way. The resulting time evolution is then expanded in a Magnus series [Mag54], and the lowest order term of the expansion should match a certain ideal Hamiltonian, provided the external control was applied correctly. As a first approximation, the control is treated as a series of instantaneous unitary pulses to the system (bang-bang scenario [VL98]).

CHAPTER 3 discusses dynamical decoupling in the context of quantum systems comprised of a certain number of qubits. We develop a general method to construct decoupling schemes on such systems which use only local Pauli operators applied to individual qubits. The construction method works by developing the given and the ideal Hamiltonian in the operator basis given by the tensor products of the Pauli operators and constructing a linear system of equations by comparing the two Hamiltonians in the lowest order of the Magnus expansion. Some elementary examples for the application of this method are presented. The ideas and results from this chapter were published in [FAB14].

CHAPTER 4 generalizes the construction method of the previous chapter to apply to networks of qudits. The trick lies in finding the right generalization of the Pauli operators, which for our purposes turns out to be the generalized spin (or Weyl) operators [BBC$^+$93]. With these operators, the approach is very similar to the qubit case, but some of the proofs become a bit more involved. This generalization was also published in [FAB14].

CHAPTER 5 takes a look at the influence of imperfect decoupling controls. We first look at imperfections rising from non-instantaneous pulses or certain systematic errors and look at decoupling sequences which are robust against such imperfections. A first-order correction is accomplished by Eulerian path decoupling schemes [VK03], which we improve upon with higher-order self-stabilizing sequences. We also analyze the influence of stochastic noise on the decoupling process. The higher-order self-stabilizing sequences were published in [BFAJ15]. The stochastic noise analysis was published in [BF14].

APPENDIX A presents several higher-order self-stabilizing decoupling sequences, which were constructed during the investigation of systematic imperfections in the decoupling controls in Sec. 5.1.

1.1.2 *Practical applications of dynamical decoupling*

CHAPTER 6 introduces the problem of perfect state transfer along a linear chain of qubits. Proposals for specially designed Hamiltonians, which implement the state transfer, exist [Bos03, NPL04, CDEL04], but they are susceptible to imperfections along the chain. Specifically, bends in the chain give rise to a loss of transfer fidelity [NHJ12], which we demonstrate can be suppressed by choice of an appropriate dynamical decoupling scheme. We also present an approach to design the special state transfer Hamiltonian from regular nearest-neighbour interactions with the help of decoupling and extend this result to chains of qudits. The approach to decouple the impact of bends in the chain was published in [FMA15].

CHAPTER 7 investigates the influence of the centre-of-mass motion of a trapped atom or ion on its interaction with a radiation field in an optical cavity. An undisturbed atom-field interaction is crucial in the recent proposal of a hybrid quantum repeater [vLS$^+$06, LvLN$^+$06, vLMN08], a device designed to distribute entanglement between distant nodes connected by optical fibres. We will implement a dynamical decoupling scheme acting on the harmonic trap potential to decouple the centre-of-mass motion. The results of this chapter were published in [BFA13].

CHAPTER 8 shows how dynamical decoupling can be used to implement a sequence of one- and two-qubit gates on a linear chain of coupled qubits. Such a scenario is imaginable with e.g. superconducting flux qubits, but not restricted to this particular example. We demonstrate how decoupling can be used to selectively suppress certain couplings in the chain and take the results of Ch. 5 into account to produce decoupling schemes which can implement high-fidelity gate operations. A particular sequence of gates is presented in numerical simulations which will bring the qubits of the chain into an entangled GHZ state [GHZ07]. The results of this chapter were published in [FHJA15].

APPENDIX B derives a specific Baker-Campbell-Hausdorff type formula which is used in Ch. 7.

1.2 FUNDAMENTALS

In this section, we will briefly review the basic components of quantum theory which are needed throughout this thesis. The section is intended to introduce the notation used in the remaining text. It is not meant to be a comprehensive introduction to quantum mechanics, as there is a lot of literature on the subject. For a modern introduction to quantum mechanics, we refer the reader to [Bal14].

1.2.1 *Quantum systems, states and observables*

A quantum system is described on a separable Hilbert space $\mathcal{H}$. In most cases in this thesis, this Hilbert space will be finite-dimensional, but infinite dimensions are possible. The state of a quantum system in its most general form is described by a self-adjoint, non-negative linear operator ρ on $\mathcal{H}$ with unit trace, $\mathrm{Tr}(\rho) = 1$. This operator is called the state or density operator. It can be expressed in terms of its spectral decomposition, which in the case of a discrete spectrum is given as

$$\rho = \sum_n \rho_n |\phi_n\rangle\langle\phi_n|, \tag{1.1}$$

with the real-valued and non-negative eigenvalues ρ_n and corresponding orthonormal eigenvectors $|\phi_n\rangle \in \mathcal{H}$. As a consequence, there is a particular sub-class of states called pure states, for which $\rho = |\Psi\rangle\langle\Psi|$, with $|\Psi\rangle \in \mathcal{H}$ a unit vector. Such a pure state is completely described by the vector $|\Psi\rangle$, however, the description is not unique as any vector $e^{i\varphi}|\Psi\rangle$ results in the same state operator ρ.

Any measurable physical variable (observable) is described by a Hermitian operator on $\mathcal{H}$ whose eigenvalues specify the possible val-

ues this variable can assume. The average value of an observable A for a quantum system in state ρ is given as

$$\langle A \rangle = \mathrm{Tr}(\rho A) = \langle \Psi | A | \Psi \rangle, \text{ for } \rho = |\Psi\rangle\langle\Psi|. \tag{1.2}$$

1.2.2 *Measurement of physical variables*

For an observable represented by an operator A, the possible measurement results are given by the eigenvalues a_n. From the spectral decomposition of A, we can assign to each distinct eigenvalue a_n a projection operator

$$P_n = \sum_{a_j = a_n} |a_j\rangle\langle a_j| \tag{1.3}$$

which projects onto the subspace spanned by the eigenvectors belonging to a_n. The probability to measure a_n, given a state ρ of a quantum system, is then simply

$$\mathrm{Prob}(a_n) = \langle P_n \rangle = \mathrm{Tr}(\rho P_n). \tag{1.4}$$

One of the peculiar properties of quantum mechanics is that a measurement changes the state of a quantum system. If we measure the observable A and get the result a_n, then the state will have changed to

$$\rho' = \frac{P_n \rho P_n}{\mathrm{Tr}(\rho P_n)}. \tag{1.5}$$

This result is called a *selective quantum measurement*, which occurs if we do a post-selection on the measurement result and find that it was a_n. Immediately repeating the measurement on the state ρ' will yield a_n again, since $\mathrm{Tr}(\rho' P_n) = 1$. If a measurement of A is performed without looking at the result (no post-selection), then the resulting state can formally be written as

$$\rho' = \sum_n P_n \rho P_n. \tag{1.6}$$

This is consequently called a *non-selective quantum measurement*.

A more general measurement process is described by *positive-operator valued measures* (POVMs). A POVM is a set of positive-semidefinite operators $\{E_n\}$ which sum to the identity,

$$\sum_n E_n = \mathbb{1}. \tag{1.7}$$

Unlike the projection operators P_n above, the E_n are not necessarily orthogonal. If each operator E_n corresponds again to a possible measurement outcome a_n, then the probability to measure a_n is given by

$$\mathrm{Prob}(a_n) = \mathrm{Tr}(\rho E_n). \tag{1.8}$$

We can formally write $E_n = M_n^\dagger M_n$ with $M_n = \sqrt{E_n}$ a positive-semidefinite operator. The state after measuring a_n is given as

$$\rho' = \frac{M_n^\dagger \rho M_n}{\mathrm{Tr}(M_n^\dagger \rho M_n)}. \tag{1.9}$$

Note that a direct repetition of the measurement may give a different result, since unlike for the projectors P_n, in general we have $M_m M_n \neq \delta_{mn} M_n$. The post-measurement state without post-selection is given by

$$\rho' = \sum_n M_n^\dagger \rho M_n. \tag{1.10}$$

1.2.3 *Evolution of a quantum system*

The evolution of a quantum state over time is governed by a unitary operator $U(t, t_0)$, with t_0 the start of the evolution. This time evolution operator obeys the differential equation

$$\frac{\partial}{\partial t} U(t, t_0) = -\frac{i}{\hbar} H(t) U(t, t_0), \tag{1.11}$$

where $\hbar$ is the reduced Planck constant and $H(t)$ is a Hermitian operator called the Hamiltonian of the system. It corresponds to the energy of the system. The formal solution of Eq. (1.11) is given by the Dyson series, which allows us to express $U(t, t_0)$ as an infinite sum,

$$U(t, t_0) = \mathbb{1} + \sum_{n=1}^{\infty} S_n(t, t_0), \tag{1.12}$$

where each $S_n(t, t_0)$ is a multiple integral with time points ordered in decreasing fashion,

$$S_n(t, t_0) = \left(-\frac{i}{\hbar}\right)^n \int_{t_0}^{t} dt_1 \int_{t_0}^{t_1} dt_2 \cdots \int_{t_0}^{t_n - 1} dt_n H(t_1) H(t_2) \cdots H(t_n). \tag{1.13}$$

It is convenient to introduce a shorthand notation for this series in the form of the Dyson time-ordering operator $\mathcal{T}$,

$$U(t, t_0) = \mathcal{T} \exp\left(-i/\hbar \int_{t_0}^{t} H(t') dt'\right). \tag{1.14}$$

With $U(t, t_0)$ established, the time evolution of a pure state can now be written as

$$|\Psi(t)\rangle = U(t, t_0) |\Psi(t_0)\rangle. \tag{1.15}$$

It obeys the Schrödinger equation

$$i\hbar\frac{d}{dt}|\Psi(t)\rangle = H(t)|\Psi(t)\rangle. \tag{1.16}$$

Consequently, the time evolution of a general state $\rho(t)$ is determined by the equations

$$\rho(t) = U(t,t_0)\rho(t_0)U^\dagger(t,t_0), \tag{1.17}$$

$$i\hbar\frac{d}{dt}\rho(t) = [H(t),\rho(t)], \tag{1.18}$$

with the commutator $[A,B] = AB - BA$.

It is convenient to eliminate the various occurrences of $\hbar$ in the equations above. This can be accomplished by rescaling the Hamiltonian by a factor $1/\hbar$,

$$H(t) \longrightarrow \frac{H(t)}{\hbar}. \tag{1.19}$$

Unless otherwise stated, we adopt this scaling throughout the remainder of this thesis, so that all occurring Hamiltonians have the physical dimension of frequency instead of energy.

1.2.4 *Heisenberg and interaction picture*

There is an alternative formalism for expressing the evolution of a quantum system where the state remains constant over time and merely expresses some initial condition. Instead, the time evolution is carried over to the Hermitian operators representing the observables of the system. If A represents an observable, then in this picture it is replaced by $A_H(t)$ with a time dependence governed by

$$A_H(t) = U^\dagger(t,t_0)AU(t,t_0), \tag{1.20}$$

$$\frac{d}{dt}A_H(t) = i\left[H_H(t),A_H(t)\right], \tag{1.21}$$

$$H_H(t) = U^\dagger(t,t_0)H(t)U(t,t_0). \tag{1.22}$$

This picture is called the Heisenberg picture and yields the same expectation values and measurement probabilities for physical observables as the previous, so-called Schrödinger picture,

$$\begin{aligned}\langle A_H(t)\rangle &= \mathrm{Tr}\left(\rho A_H(t)\right) = \mathrm{Tr}\left(\rho U^\dagger(t,t_0)AU(t,t_0)\right) = \langle A\rangle,\\ \mathrm{Prob}(a_n) &= \mathrm{Tr}\left(\rho U^\dagger(t,t_0)P_nU(t,t_0)\right).\end{aligned} \tag{1.23}$$

As such, both pictures describe the same physics, and either one can be chosen to describe a quantum system based on what is more convenient for a specific task.

It is also possible to split the time evolution on both states and operators, which leads to the interaction (or Dirac) picture. Starting

from a Hamiltonian $H(t) = H_0(t) + H_1(t)$ in the Schrödinger picture, we define the time evolution operator due to $H_0(t)$ alone,

$$U_0(t) = \mathcal{T} \exp\left(-i \int_{t_0}^{t} H(t')dt'\right). \tag{1.24}$$

States and operators in the interaction picture are then given as

$$\begin{aligned} |\Psi_I(t)\rangle &= U_0^\dagger(t)|\Psi(t)\rangle, \\ \rho_I(t) &= U_0^\dagger(t)\rho(t)U_0(t), \\ A_I(t) &= U_0^\dagger(t)AU_0(t). \end{aligned} \tag{1.25}$$

The time evolution in the interaction picture is governed by the equations

$$\begin{aligned} i\frac{d}{dt}|\Psi_I(t)\rangle &= H_{1,I}(t)|\Psi_I(t)\rangle, \\ i\frac{d}{dt}\rho_I(t) &= [H_{1,I}(t), \rho_I(t)], \\ \frac{d}{dt}A_I(t) &= i[H_{0,I}(t), A_I(t)], \end{aligned} \tag{1.26}$$

and we can formally introduce a time evolution operator in the interaction picture due to $H_{1,I}(t)$ as

$$U_I(t) = U_0^\dagger(t)U(t). \tag{1.27}$$

1.2.5 *Composite quantum systems*

Consider two separate quantum systems A and B, with respective Hilbert spaces $\mathcal{H}_A$ and $\mathcal{H}_B$. If these systems are brought into contact, they form a new Hilbert space given by the tensor product

$$\mathcal{H} = \mathcal{H}_A \otimes \mathcal{H}_B, \tag{1.28}$$

which is of dimension $\dim(\mathcal{H}_A)\dim(\mathcal{H}_B)$, leading to an exponential increase in the state space of composite quantum systems. If $\{|\phi_n\rangle\}$ is an orthonormal basis on $\mathcal{H}_A$ and $\{|\psi_m\rangle\}$ is an orthonormal basis on $\mathcal{H}_B$, then a complete orthonormal basis on $\mathcal{H}$ is given by the set of all possible tensor products of these basis vectors, $\{|\phi_n\rangle \otimes |\psi_m\rangle\}$. A composite quantum system truly is larger than the sum of its parts, as the new Hilbert space $\mathcal{H}$ contains states which cannot be written as the tensor product of two vectors on $\mathcal{H}_A$ and $\mathcal{H}_B$. A very simple example for such a state is

$$\frac{1}{\sqrt{2}}\left(|\phi_1\rangle \otimes |\psi_2\rangle + |\phi_2\rangle \otimes |\psi_1\rangle\right). \tag{1.29}$$

These states are called entangled states.

Sometimes the system B is treated as an environment to system A, which influences the evolution of system A in unwanted ways.

In these cases system B is often a very large system whose precise characteristics and evolution are of no interest to us. If ρ is the state of the joint quantum system, we can extract the state of only system A by means of a partial trace over system B,

$$\rho_A = \mathrm{Tr}_B(\rho). \tag{1.30}$$

1.2.6 *Qubits and the Pauli operators*

A qubit is a special two-dimensional quantum system on the Hilbert space $\mathcal{H} = \mathbb{C}^2$. The electron spin is a typical example for a qubit system, but other implementations of such a system exist.

On a qubit system, the so-called Pauli operators σ_1, σ_2 and σ_3 (sometimes also written as X, Y and Z) play a crucial role, as they are both Hermitian and unitary, and together with the identity $\sigma_0 \equiv \mathbb{1}$ they form a complete basis for linear operators on $\mathbb{C}^2$. If we consider the eigenbasis of σ_3, whose two basis states are typically denoted $|0\rangle$ and $|1\rangle$ or $|\uparrow\rangle$ and $|\downarrow\rangle$, then we have the typical matrix representation for these operators:

$$\begin{aligned} I = \sigma_0 &= \begin{pmatrix} 1 & 0 \\ 0 & 1 \end{pmatrix}, & X = \sigma_1 &= \begin{pmatrix} 0 & 1 \\ 1 & 0 \end{pmatrix}, \\ Y = \sigma_2 &= \begin{pmatrix} 0 & -i \\ i & 0 \end{pmatrix}, & Z = \sigma_3 &= \begin{pmatrix} 1 & 0 \\ 0 & -1 \end{pmatrix}. \end{aligned} \tag{1.31}$$

We can also define the Hermitian creation and annihilation operators σ_+ and σ_-, which are convenient to use in some instances. They are defined as

$$\sigma_+ = \frac{1}{2}(\sigma_1 + i\sigma_2) = \begin{pmatrix} 0 & 1 \\ 0 & 0 \end{pmatrix}, \quad \sigma_- = \frac{1}{2}(\sigma_1 - i\sigma_2) = \begin{pmatrix} 0 & 0 \\ 1 & 0 \end{pmatrix}. \tag{1.32}$$

A network of N qubits is comprised of N distinguishable qubits, which together form a composite quantum system on the 2^N-dimensional Hilbert space $\mathcal{H} = (\mathbb{C}^2)^{\otimes N}$. We will regularly deal with such a system in this thesis. Often we want to apply a specific operator, e.g. one of the Pauli operators, to only a specific qubit in the network. We denote this by writing the target qubit as an upper index, e.g. $\sigma_1^{(j)}$. This is a shorthand notation for the following operator on the full system:

$$p^{(j)} = \left(\bigotimes_{i=1}^{j-1} \mathbb{1} \right) \otimes p \otimes \left(\bigotimes_{i=j+1}^{N} \mathbb{1} \right). \tag{1.33}$$

Here, p is an arbitrary operator on the Hilbert space $\mathbb{C}^2$.

1.2.7 *The quantum harmonic oscillator*

Another specific quantum system we will occasionally make use of in this thesis is that of the harmonic oscillator. It originally describes a particle trapped in a harmonic potential, however, the same formalism can be used to, e.g., model a single mode of a radiation field.

The Hamiltonian (in $1/\hbar$ scaling) of the particle in the harmonic potential reads

$$H = \frac{p^2}{2m\hbar} + \frac{m\omega^2 x^2}{2\hbar}, \tag{1.34}$$

where p and x are the momentum and position operators of the particle fulfilling $[x, p] = i\hbar$, m its mass and ω the frequency of oscillation. We introduce two operators

$$a = \sqrt{\frac{m\omega}{2\hbar}}x + i\sqrt{\frac{1}{2m\hbar\omega}}p, \tag{1.35}$$

$$a^\dagger = \sqrt{\frac{m\omega}{2\hbar}}x - i\sqrt{\frac{1}{2m\hbar\omega}}p, \tag{1.36}$$

with $[a, a^\dagger] = 1$. With these operators, the Hamiltonian can be rewritten as

$$H = \omega\left(a^\dagger a + \frac{1}{2}\right). \tag{1.37}$$

The operator $a^\dagger a$ possesses an eigenvector basis $\{|n\rangle\}_{n=0}^{\infty}$ of numbered states with the following relations:

$$a^\dagger a|n\rangle = n\,|n\rangle, \tag{1.38}$$

$$a^\dagger|n\rangle = \sqrt{n+1}\,|n+1\rangle, \tag{1.39}$$

$$a|n\rangle = \sqrt{n}\,|n-1\rangle, \tag{1.40}$$

$$a|0\rangle = 0. \tag{1.41}$$

Because of these relations, the operators a and $a^\dagger$ are typically called the annihilation and creation operators, or the ladder operators. The evolution of an arbitrary pure state can be easily constructed by developing it in the basis of these number states, for which the effects of the Hamiltonian are known completely.

1.2.8 *Fidelity measures*

As the main topic of this thesis is error suppression, we will often need to compare a state ρ of some quantum system to an ideal or expected state σ. For this task we require a distance measure which, given ρ and σ as inputs, produces a number that allows us to quantify the closeness of the two states. Several candidates for such a measure

exist. In this work, we will use a function called the fidelity, which is defined as follows [NCoo]:

$$F(\rho, \sigma) = \mathrm{Tr}\left(\sqrt{\rho^{1/2}\,\sigma\,\rho^{1/2}}\right). \tag{1.42}$$

In the case of pure states, the fidelity simplifies to the following form:

$$F\left(|\psi\rangle, |\phi\rangle\right) = |\langle\psi|\phi\rangle|. \tag{1.43}$$

F can assume any real value between 0 and 1, where 1 signifies the states are identical, and 0 means they are maximally apart, i.e., orthogonal.

Sometimes it is more convenient to compare two time evolution operators $U_1(t)$ and $U_2(t)$ instead of specific states. In this case, we use the following fidelity measure:

$$F(t) = \left|\frac{1}{\dim \mathcal{H}} \mathrm{Tr}\left(U_1^\dagger(t) U_2(t)\right)\right|. \tag{1.44}$$

It relates to the state fidelity (1.43) as follows. If $\{|n\rangle\}$ is a finite orthonormal basis of $\mathcal{H}$, then we can express the trace in Eq. (1.44) as

$$\begin{aligned} F(t) &= \left|\frac{1}{\dim \mathcal{H}} \sum_{n=1}^{\dim \mathcal{H}} \langle n|U_1^\dagger(t) U_2(t)|n\rangle\right| \\ &= \frac{1}{\dim \mathcal{H}} \sum_{n=1}^{\dim \mathcal{H}} F(U_1(t)|n\rangle, U_2(t)|n\rangle) \end{aligned} \tag{1.45}$$

It is thus clear that this fidelity measure also assumes values between 0 and 1. Intuitively, if $U_1(t)$ and $U_2(t)$ are identical, then $U_1^\dagger(t) U_2(t) = \mathbb{1}$, and thus $F(t) = 1$. It is 0, for instance, if $U_1(t) = \sigma_1$ and $U_2(t) = \sigma_2$.

Part I

THEORETICAL FOUNDATIONS OF DYNAMICAL DECOUPLING

2

OVERVIEW OF DYNAMICAL DECOUPLING METHODS

Dynamical decoupling is a method by which the time evolution of a quantum system governed by a Hamiltonian operator is modified by subjecting the system to a series of external control pulses. If done right, this procedure can approximately cancel the influence of certain parts of the Hamiltonian over time. It is typically used to protect a quantum system from the decohering influences of environmental interactions, which helps to significantly improve the life time and fidelity of quantum states in experimental realisations. Dynamical decoupling works best for suppressing weak couplings, as the controls need to be significantly stronger and faster than the Hamiltonian we want to eliminate. Also, the system Hamiltonian must be time-independent, or at least slowly varying so that it is approximately constant on the time scale of the decoupling controls.

The term *dynamical decoupling* was coined by Viola in 1999 [VL98, VKL99] when she introduced a general control-theoretic framework for the method. At the same time, Zanardi [Zan99] developed a procedure for symmetrizing evolutions based on finite groups, which contains Viola's framework in a more abstract manner. However, the principles of decoupling are far older and date back to techniques developed in the nuclear magnetic resonance community [Hah50, CP54, MG58, Hae76]. The best-known example is probably the Hahn spin echo effect [Hah50]. Since then, a lot of advanced decoupling strategies have been developed, and many experiments successfully employ decoupling strategies to increase life times up to several orders. A few more recent experiments are presented in [BUV+09a, BUV+09b, DLDG+09, DRZ+09, BMM+10, dLWR+10, BFN+11, BGY+11, LDGD+11].

Although the majority of decoupling concepts and experimental applications concentrates on fighting decoherence effects, the use of unitary control operations is not limited to these scenarios. Viola *et al.* [VLK99] already showed that dynamical decoupling can also be used to suppress only certain components of a many-particle Hamiltonian selectively. Thus, it is possible to develop control strategies that, within certain limits, are suitable for the purpose of quantum simulation, meaning that the effects of a present Hamiltonian interaction with active controls on a quantum system resemble those of a different Hamiltonian. Wocjan *et al.* [WRJB02b] demonstrated that any quantum system with a non-trivial Hamiltonian can simulate any other Hamiltonian interaction, provided that a suitable finite set of

unitary control operations is available. Dodd *et al.* [DNBT02] showed that any two-body Hamiltonian on a qubit network can be simulated by any two-body entangling Hamiltonian with the help of local unitaries.

In this chapter, we are going to review the basics of dynamical decoupling for a general quantum system with general control and then look in detail at decoupling with instantaneous unitary pulses. The details presented here are the foundation of the techniques we will develop in the later chapters. Additional details to some of the presented techniques are also summarized in [LB13].

The chapter is structured as follows. In Sec. 2.1 we establish the general framework of dynamical decoupling with a general external control and the resulting time evolution, which is then developed into a Magnus series of increasing orders. Basic control strategies are also explained. Then we specialise the general framework to instantaneous unitary pulses in Sec. 2.2, which will be the starting point for many of the techniques in later chapters. Finally, Sec. 2.3 gives a brief outlook on some advanced higher-order decoupling strategies.

2.1 PRINCIPLES OF DYNAMICAL DECOUPLING

We consider a quantum system S whose state space is described by a finite-dimensional Hilbert space $\mathcal{H}_S$. The system S is coupled to an environment E, and the total system is governed by a time-independent Hamiltonian of the form

$$H_0 = H_S \otimes \mathbb{1}_E + \mathbb{1}_S \otimes H_E + H_{SE}, \tag{2.1}$$

where H_S and H_E are the Hamiltonians acting solely on the system S and the environment E, respectively, and H_{SE} describes the coupling between system and environment. Additionally, we are given some control over the system S by means of a time-dependent control Hamiltonian $H_c(t)$ acting only on S, leading to the total time-dependent Hamiltonian

$$H(t) = H_0 + H_c(t) \otimes \mathbb{1}_E. \tag{2.2}$$

Then the time evolution operator of our system is given as

$$U(t) = \mathcal{T} \exp\left(-i \int_0^t H(t')dt'\right). \tag{2.3}$$

The control Hamiltonian $H_c(t)$ gives us influence over $U(t)$, and the goal of dynamical decoupling is to modify the time propagator so that it meets a certain goal. Very often, this goal is to eliminate any time evolution due to H_0 of the system S to protect and conserve the quantum state of S. If this goal were achieved perfectly, S would evolve solely under the influence of the control $H_c(t)$, which is why

dynamical decoupling is typically formulated in a *toggling frame* constructed such that it moves with the control. Formally, this is done by switching to an interaction picture with the transformation operator $U_c(t)$, describing the time evolution induced by the control field $H_c(t)$,

$$U_c(t) = \mathcal{T}\exp\left(-i\int_0^t H_c(t')dt'\right). \tag{2.4}$$

The time evolution in the toggling frame is then described by the operator

$$\tilde{U}(t) = U_c^\dagger(t)U(t) = \mathcal{T}\exp\left(-i\int_0^t \tilde{H}(t')dt'\right), \tag{2.5}$$

with the toggling frame Hamiltonian $\tilde{H}(t) = U_c^\dagger(t)H_0U_c(t)$. This can be seen in the following way. We know that the time derivatives of $U(t)$ and $U_c(t)$ are given as

$$\frac{dU(t)}{dt} = -iH(t)U(t), \quad \frac{dU_c(t)}{dt} = -iH_c(t)U_c(t), \tag{2.6}$$

and by assumption we expect that

$$\frac{d\tilde{U}(t)}{dt} = -i\tilde{H}(t)\tilde{U}(t). \tag{2.7}$$

A simple calculation shows that this assumption is consistent with the time evolution of $U(t)$:

$$\begin{aligned}\frac{dU(t)}{dt} &= \frac{d}{dt}\left(U_c(t)\tilde{U}(t)\right) = \frac{dU_c(t)}{dt}\tilde{U}(t) + U_c(t)\frac{d\tilde{U}(t)}{dt}\\ &= -iH_c(t)U_c(t)\tilde{U}(t) - iU_c(t)U_c^\dagger(t)H_0U_c(t)\tilde{U}(t)\\ &= -i\left(H_c(t) + H_0\right)U(t).\end{aligned} \tag{2.8}$$

2.1.1 *Average Hamiltonian and the Magnus expansion*

Formally, the time evolution of Eq. (2.5) can be expressed with the help of an effective or average Hamiltonian $\overline{H}$ as

$$\tilde{U}(t) = \exp\left(-i\overline{H}t\right), \tag{2.9}$$

where $\overline{H}$ is considered to be a time-independent Hamilton operator, but does depend on the total interaction time t. The goal of dynamical decoupling is to engineer this average Hamiltonian $\overline{H}$ into a desired ideal Hamiltonian $H_{id} \otimes H_E'$, where system and environment are separated from each other and H_{id} is the desired system Hamiltonian. If our goal is the preservation of a quantum state in S, then we would have $H_{id} = 0$. We could also try to engineer a specific system Hamiltonian $H_{id} \neq 0$ which is different from the initial H_S. This case

is sometimes called dynamical recoupling to distinguish it from the former case.

Turning $\overline{H}$ into a desired Hamiltonian H_{id} perfectly is in most cases nearly impossible, so in dynamical decoupling this goal is typically achieved approximately to a certain order. For this purpose, the average Hamiltonian is expressed as an infinite series of self-adjoint operators called the Magnus expansion [Mag54],

$$\overline{H} = \sum_{j=0}^{\infty} \overline{H}^{[j]}, \tag{2.10}$$

such that each partial term $\overline{H}^{[j]}$ is of order $j+1$ in $\tilde{H}(t)$. Unlike the Dyson series, where partial sums are in general not unitary, the Magnus expansion ensures that any partial sum $\sum_{j=0}^{k} \overline{H}^{[j]}$ produces a unitary time evolution in (2.9). However, the terms do not have a simple structure and can therefore not be as easily expressed as the Dyson terms $S_n(t)$. In order to compute the terms of the Magnus expansion, we expand the exponential in (2.9) into an infinite series and compare it with the Dyson expansion (1.12) for $\tilde{U}(t)$,

$$\tilde{U}(t) = \mathbb{1} + \sum_{n=1}^{\infty} \frac{(-it)^n}{n!} \left(\overline{H}^{[0]} + \overline{H}^{[1]} + \dots\right)^n \overset{!}{=} \mathbb{1} + \sum_{n=1}^{\infty} S_n(t). \tag{2.11}$$

We can then arrange each side by orders in $\tilde{H}(t)$, and by comparison we find for the first few orders:

$$\begin{aligned}
S_1(t) &= -it\overline{H}^{[0]} \\
S_2(t) &= -\frac{t^2}{2}\left(\overline{H}^{[0]}\right)^2 - it\overline{H}^{[1]} \\
S_3(t) &= \frac{it^3}{6}\left(\overline{H}^{[0]}\right)^3 - \frac{t^2}{2}\left(\overline{H}^{[0]}\overline{H}^{[1]} + \overline{H}^{[1]}\overline{H}^{[0]}\right) - it\overline{H}^{[2]}.
\end{aligned} \tag{2.12}$$

From these equations, we find the first few terms in the Magnus expansion to be

$$\begin{aligned}
\overline{H}^{[0]} =& \frac{1}{t}\int_0^t dt_1 \tilde{H}(t_1) \\
\overline{H}^{[1]} =& -\frac{i}{2t}\int_0^t dt_1 \int_0^{t_1} dt_2 [\tilde{H}(t_1), \tilde{H}(t_2)] \\
\overline{H}^{[2]} =& -\frac{1}{6t}\int_0^t dt_1 \int_0^{t_1} dt_2 \int_0^{t_2} dt_3 \big([\tilde{H}(t_1), [\tilde{H}(t_2), \tilde{H}(t_3)]] \\
&+ [\tilde{H}(t_3), [\tilde{H}(t_2), \tilde{H}(t_1)]]\big).
\end{aligned} \tag{2.13}$$

In dynamical decoupling, we will typically attempt to match the lowest order of $\overline{H}$ with the desired Hamiltonian H_{id}, so that $\overline{H}^{[0]} = H_{id}$. The higher orders $\overline{H}^{[j]}$ remain as errors, although by careful design of the decoupling controls $H_c(t)$ it is sometimes possible to eliminate certain higher orders.

2.1.2 *Basic control strategies*

In the most common case of dynamical decoupling, the control $H_c(t)$ is specified over a time T and then repeated over and over. This leads to a periodic control action with period T,

$$U_c(t + kT) = U_c(t), \quad k \in \mathbb{N}, \tag{2.14}$$

and this control strategy is therefore called *periodic dynamical decoupling* (PDD). If we only observe the system in sync with the period T, then the time evolution of our system is fully described by the average Hamiltonian $\overline{H}$ at time T,

$$U(kT) = \tilde{U}(kT) = \big(\tilde{U}(T)\big)^k = e^{-ikT\overline{H}}. \tag{2.15}$$

Here we used the fact that $U_c(kT) = \mathbb{1}$.

Since we are considering a finite-dimensional Hilbert space, the Hamilton operator H is bounded, and we can assume $\|H\|_{op} < \kappa$, where κ has units of frequency and $\|\cdot\|_{op}$ is the operator norm

$$\|A\|_{op} = \sup_{\||\psi\rangle\|=1} \|A|\psi\rangle\|, \quad |\psi\rangle \in \mathcal{H}, \tag{2.16}$$

where the vector norm $\||\psi\rangle\| = \sqrt{\langle\psi|\psi\rangle}$ is generated by the inner product. We can then establish upper bounds for the higher orders of the Magnus expansion of $\overline{H}$ from Eqs. (2.13) as

$$\|\overline{H}^{[j]}\|_{op} = \mathcal{O}[\kappa(\kappa T)^j]. \tag{2.17}$$

These bounds tell us that the higher orders of $\overline{H}$ can, in theory, be made arbitrarily small by choosing the control period T as small as possible. The lowest order $\overline{H}^{[0]}$ becomes an exact result for $\overline{H}$ in the limit of infinitely fast control, $T \to 0$.

A common extension of the basic PDD strategy is called *symmetric dynamical decoupling* (SDD). In this case, we place an additional condition on the control of the form

$$U_c(T - t) = U_c(t), \quad t \in [0, T]. \tag{2.18}$$

This means that the control is symmetric in time around the middle point $T/2$. As a consequence of this symmetry, all odd-order terms $\overline{H}^{[2j+1]}$ in the Magnus expansion are eliminated. A proof can be found in [Hae76, Bur81]. The leading remaining error term is therefore given by $\overline{H}^{[2]}$, so that SDD achieves the dynamical decoupling goal to second order.

2.2 DECOUPLING WITH INSTANTANEOUS PULSES

In order to study and design dynamical decoupling controls, it is often advantageous to limit the type of control available through $H_c(t)$

to very short and strong pulses. These pulses can then be approximated as happening instantaneously (*bang-bang control* [VL98]) and can thus be represented by unitary operators. In this scenario, each unitary control pulse p_j is followed by a time τ_j of free evolution under the Hamiltonian H_0, leading to the total time evolution after $M+1$ pulses and time $T = \sum_{j=0}^{M-1} \tau_j$:

$$U(T) = p_M e^{-iH_0\tau_{M-1}} p_{M-1} \cdots e^{-iH_0\tau_1} p_1 e^{-iH_0\tau_0} p_0. \tag{2.19}$$

This time evolution can be rewritten by introducing the toggling operators $g_j = p_j p_{j-1} \cdots p_1 p_0$, which are equivalent to $U_c(t)$ from Eq. (2.4) at times $T_j = \sum_{k=0}^{j-1} \tau_j$. We then have $p_j = g_j g_{j-1}^\dagger$, and so we can write for $T = M\tau$:

$$\begin{aligned} U(T) &= g_M g_{M-1}^\dagger e^{-iH_0\tau_{M-1}} g_{M-1} \cdots g_1^\dagger e^{-iH_0\tau_1} g_1 g_0^\dagger e^{-iH_0\tau_0} g_0 \\ &= g_M e^{-ig_{M-1}^\dagger H_0 g_{M-1}\tau_{M-1}} \cdots e^{-ig_1^\dagger H_0 g_1 \tau_1} e^{-ig_0^\dagger H_0 g_0 \tau_0}. \end{aligned} \tag{2.20}$$

Since the g_j are unitary, we can move them up into the exponent. The operator g_M defines the toggling frame at time T, $\tilde{U}(T) = g_M^\dagger U(T)$.

In order to use any of the basic decoupling control strategies, the operators g_j should be applied in cyclic fashion, and as a consequence we require $g_M = g_0$. Additionally, we will typically choose $p_0 = g_0 = g_M = \mathbb{1}$, so that at the end of each cycle the toggled frame coincides with the untoggled system,

$$\tilde{U}(T) = U(T) = e^{-i\overline{H}T}. \tag{2.21}$$

The lowest two terms of the Magnus expansion for $\overline{H}$ in this bang-bang scenario are given by

$$\overline{H}^{[0]} = \frac{1}{T} \sum_{j=0}^{M-1} \tau_j g_j^\dagger H_0 g_j, \tag{2.22}$$

$$\overline{H}^{[1]} = -\frac{i}{2T} \sum_{i>j=0}^{M-1} \tau_i \tau_j \left[g_i^\dagger H_0 g_i, g_j^\dagger H_0 g_j \right]. \tag{2.23}$$

The set of operators $\{g_j\}_{j=0}^{M-1}$ is called a decoupling scheme if it fulfils the decoupling condition

$$\overline{H}^{[0]} = \frac{1}{T} \sum_{j=0}^{M-1} \tau_j g_j^\dagger H_0 g_j = \frac{1}{D} H_{id}. \tag{2.24}$$

If this condition is met, it means that the average Hamiltonian is, to lowest order, identical to the desired ideal Hamiltonian H_{id}, up to a scaling factor D. If $D \neq 1$, its effect can be compensated by rescaling the overall interaction time by the factor D. Note that the order of the operators g_j does not play a role in the lowest order, so that they can

be reordered at will. This will affect the actual pulses p_j which have to be applied to the system, so a specific ordering may simplify the experimental realization of the required pulses. However, the order of the operators generally does affect the higher orders of $\overline{H}$ and can thus have a significant influence on the quality of the approximation.

Any decoupling scheme $\{g_j\}_{j=0}^{M-1}$ can be turned into a symmetric sequence to perform the SDD strategy and benefit from second-order decoupling. In order to do so, we construct a new decoupling scheme $\{g'_j\}_{j=0}^{2M-1}$ with twice as many operators, which results from appending the reverse of the original scheme to itself, i.e.,

$$g'_j = \begin{cases} g_j & \text{if } j < M, \\ g_{2M-j-1} & \text{if } j \geqslant M. \end{cases} \tag{2.25}$$

The pulse distances τ'_j can be constructed in the same manner from the τ_j. This symmetrized scheme preserves the lowest order $\overline{H}^{[0]}$ from the original scheme, but eliminates all odd orders in the Magnus expansion.

2.3 HIGHER-ORDER DECOUPLING STRATEGIES

The SDD strategy offers a generic way to achieve dynamical decoupling to second order. Unfortunately, no general strategy is known to achieve decoupling to arbitrary orders. There are, however, promising concepts which can be applied in a multitude of situations. We shall give a brief overview of these methods here; further detail can be found in the cited primary references below and in [LB13].

Khodjasteh and Lidar introduced the idea of *concatenated decoupling* [KL05, KL07]. Here, an inner decoupling sequence is embedded into an outer sequence. Consider a decoupling scheme $\{g_j\}_{j=0}^{M-1}$ which produces the time evolution operator $e^{-i\overline{H}T}$. We now take a second decoupling scheme $\{G_k\}_{k=0}^{N-1}$ which is applied on a larger time scale to produce the time evolution

$$U(NT) = G_{N-1}^{\dagger} e^{-i\overline{H}T} G_{N-1} \cdots G_0^{\dagger} e^{-i\overline{H}T} G_0. \tag{2.26}$$

Actual decoupling pulses are now determined by both the inner and outer decoupling sequence. This strategy can be repeated indefinitely for an arbitrary level of embedding. This strategy works extremely well if our goal is to eliminate a given Hamiltonian H completely and if we have a so-called annihilator scheme $\{g_j\}_{j=0}^{M-1}$ which can decouple any Hamiltonian. In this case, the outer scheme can be identical to the inner scheme and will eliminate additional orders of $\overline{H}$.

Another high-order decoupling method is *Uhrig decoupling* [Uhr07]. Uhrig's method can decouple a system up to N-th order by applying

an appropriate instantaneous pulse p for N times. The trick is in the choice of time points at which each pulse application occurs, namely

$$T_j = T \sin^2\left(\frac{j\pi}{2(N+1)}\right). \tag{2.27}$$

It has been shown to use the minimum number of pulses for a given decoupling order. Non-equidistant pulse strategies were further developed in [WS07, LWDS08, GKL08, SÁS11].

Finally, we briefly mention *randomized decoupling* strategies, which were first suggested in [KAS05, VK05]. The idea is fairly simple. Given a set of decoupling operators $\{g_j\}$, we randomly choose from these operators to form a randomized decoupling scheme. Since this is not a deterministic strategy, its effects on higher orders of $\overline{H}$, or in fact even the lowest order, are not immediately clear. It has been shown that, averaged over many implementations, randomized strategies have beneficial properties on the fidelity decay rate in long-term applications of decoupling. Of particular interest, however, are strategies which combine deterministic decoupling schemes with randomized decoupling [KA05, SV06] to potentially combine the strengths of both approaches.

3

DESIGNING PAULI PULSE DECOUPLING SEQUENCES

For purposes of quantum information processing, we are typically dealing with networks of distinguishable qubits (or qudits) as the building blocks of both quantum registers and memories. It is therefore of particular interest to develop error-suppressing dynamical decoupling schemes and quantum simulation schemes for such networks. For these systems, a special case of decoupling controls is frequently discussed where all control operations consist of instantaneously applied Pauli operations acting locally on each qubit separately. Numerous efficient schemes of this kind have been developed which are capable of suppressing environmental errors or unwanted inter-qubit couplings in many-qubit systems. Stollsteimer and Mahler [SM01], for example, proposed a construction based on orthogonal arrays, while Leung [Leu02] presented a decoupling method based on Hadamard matrices. Both approaches were eventually unified by Rötteler and Wocjan [RW06]. Wocjan *et al.* also discussed applications of similar constructions to quantum simulation scenarios [WRJB02a].

Despite these interesting developments, it remains a challenge to find and implement suitable Pauli pulse schemes for the purpose of quantum simulation. While specific constructions for specific scenarios have been developed, so far there has been no systematic method for constructing dynamical decoupling schemes from simple Pauli pulses for a general scenario that applies to both error suppression and quantum simulation for arbitrary many-body Hamiltonians.

In this chapter, we will develop a systematic method for constructing decoupling schemes from local Pauli pulses on networks of qubits which are capable of changing the action of a given arbitrary Hamiltonian H_0 to that of a wanted "ideal" Hamiltonian H_{id}. This method is not only useful for protecting specific inter-particle couplings against unwanted couplings or environmental influences, but also for simulating ideal Hamiltonian dynamics within certain limits.

The restriction to local Pauli operations leads to a particularly simple, but still powerful procedure which exploits two basic properties of the Pauli operators, namely that they are both Hermitian and unitary and that they fulfil characteristic Clifford-type algebraic relations. We will later see in Ch. 4 that certain aspects of these properties carry over to generalized spin operators, allowing our method to be generalized to qudit networks of arbitrary dimension. Although the method does not work for all possible pairs of H_0 and H_{id}, its

limitations are easily understood and still allow for a multitude of interesting applications.

This chapter begins with a short introduction to qubit networks and Pauli pulses in Sec. 3.1. We then develop our systematic method for constructing Pauli pulse decoupling schemes in Sec. 3.2, before we have a look at a few interesting applications in Sec. 3.3.

3.1 NETWORKS OF QUBITS AND DECOUPLING WITH PAULI PULSES

We consider a quantum system comprised of N distinguishable qubits in an arbitrary layout and with arbitrary inter-qubit couplings. The Hilbert space for our system is

$$\mathcal{H}_S = \left(\mathbb{C}^2\right)^{\otimes N}. \tag{3.1}$$

Our system is governed by a Hamiltonian operator H_0 of the form (2.1), which we would like to turn into the ideal Hamiltonian H_{id} by means of dynamical decoupling.

The three Pauli operators $\sigma_1, \sigma_2, \sigma_3$ combined with the identity $\mathbb{1} \equiv \sigma_0$ form a basis for all linear operators on the Hilbert space $\mathbb{C}^2$. By constructing all 4^N possible N-tensor products of these operators, we get an operator basis for $\mathcal{H}_S$, the set of operators $\{S_j\}_{j=0}^{4^N-1}$ with

$$S_j = \sigma_{j_1} \otimes \sigma_{j_2} \otimes \cdots \otimes \sigma_{j_N}, \quad j_i \in [0, 1, 2, 3], \tag{3.2}$$

with the base-4 representation $j = j_1 j_2 \ldots j_N$. We can then expand both N-qubit system Hamiltonians H_0 and H_{id} in this basis with coefficients μ_k and ν_k, i.e.,

$$\begin{aligned} H_0 &= \sum_{k=1}^{4^N-1} \mu_k S_k \otimes E_k + H_E, \\ H_{id} &= \sum_{k=1}^{4^N-1} \nu_k S_k \otimes \mathbb{1}_{env} + H_E. \end{aligned} \tag{3.3}$$

Here the arbitrary linear operators E_k act on the Hilbert space $\mathcal{H}_E$ of the environment. Furthermore, it is assumed that we are looking for a dynamical decoupling scheme which removes all possible couplings between the N-qubit system and the environment. The part of the Hamiltonians H_0 and H_{id} which acts on the environment only is denoted H_E and its precise form is not important for our subsequent discussion. For the sake of convenience, let us also assume that both H_0 and H_{id} are traceless so that the operator $S_0 \equiv \mathbb{1}$ can be omitted from the expansion (3.3).

For the decoupling, we assume that we can apply approximately instantaneous pulses to individual qubits in the form of the Pauli operators, where pulses can be applied in parallel to any number of the N qubits. This means that the decoupling pulses p_k can be any of

the basis operators S_j. Due to the specific multiplication rules of the Pauli operators, we find that the toggling frame operators g_k are then also just one of the basis operators S_j, up to a phase factor. However, since the operators always appear in pairs $g_k, g_k^\dagger$, this phase vanishes in the time evolution of the system, and even if it did not, it would be a global phase and therefore not measurable. In the remainder of the chapter, we will therefore omit this phase. We assume further that the pulses are applied equidistantly, so that the intervals between consecutive pulses are all equal to τ.

3.2 CONSTRUCTING PAULI DECOUPLING SCHEMES

Restricting ourselves to equidistant Pauli pulses on the qubit network significantly reduces the complexity of the decoupling task, both theoretically and experimentally. However, we still need to determine which pulses need to be applied in what order to turn a given Hamiltonian H_0 into the desired Hamiltonian H_{id}, at least in the lowest order of the average Hamiltonian $\overline{H}$.

In this section, we will develop a general method to find such suitable decoupling schemes by solving a linear set of equations. The method depends only on the form of H_0 and H_{id} and works for any scenario, be it the protection of a quantum memory ($H_{id} = 0$) or simulating a different Hamiltonian. The restriction to Pauli pulse decoupling will pose certain limitations on which Hamiltonians can actually be simulated with a given Hamiltonian H_0, and these limitations are directly linked to the question of whether our set of equations has any solution.

3.2.1 *Constructing a linear set of equations from the decoupling condition*

Our goal is to find a set of decoupling operators $\{g_j\}$ which fulfil the decoupling condition (2.24). As a first step, we insert the basis expansion (3.3) of H_0 and H_{id} into Eq. (2.24), and with $\tau_j = \tau = T/M$ we obtain the relations

$$\frac{D}{M}\sum_{k=1}^{4^N-1}\sum_{j=0}^{M-1}\mu_k\left(g_j^\dagger S_k g_j\right)\otimes E_k = \sum_{k=1}^{4^N-1}\nu_k S_k\otimes\mathbb{1}, \tag{3.4}$$

$$\Rightarrow \frac{D}{M}\sum_{k=1}^{4^N-1}\sum_{j=0}^{4^N-1}\mu_k c_j\left(S_j^\dagger S_k S_j\right)\otimes E_k = \sum_{k=1}^{4^N-1}\nu_k S_k\otimes\mathbb{1}, \tag{3.5}$$

$$\Rightarrow \frac{D}{M}\sum_{k=1}^{4^N-1}\sum_{j=0}^{4^N-1}\mu_k c_j a_{kj} S_k\otimes E_k = \sum_{k=1}^{4^N-1}\nu_k S_k\otimes\mathbb{1}. \tag{3.6}$$

Since all of operators g_j can be represented by one of the basis operators S_j, we can replace the sum over the operators g_j in (3.4) by a sum

over the basis operators S_j, where we introduce natural number variables c_j which count how often each basis operator S_j occurs in our decoupling scheme $\{g_j\}$. With this replacement, we arrive at relation (3.5). Since for all Pauli operators (including the identity operation) the Clifford-type relation

$$\sigma_k^\dagger \sigma_j^\dagger \sigma_k \sigma_j = \pm \mathbb{1} \tag{3.7}$$

holds, it is also true that $S_k^\dagger S_j^\dagger S_k S_j = \pm \mathbb{1}$. If we incorporate these signs into the variables a_{kj} of unit modulus, we finally arrive at relation (3.6).

Due to the linear independence of the operators S_k in (3.2), their coefficients can be compared individually in Eq. (3.6). This comparison yields a system of, at most, $4^N - 1$ linear equations for the 4^N unknown natural numbers c_j. However, we immediately notice a restriction concerning the solvability of this linear system of equations: If for any $k \in [1, 4^N - 1]$ either $\mu_k = 0$ or $E_k \neq \mathbb{1}$, then the corresponding expansion coefficient of H_{id} has to vanish, i.e., $\nu_k = 0$. This reflects the fact that any term not present in the originally given Hamiltonian H_0 cannot be created by our decoupling scheme in the ideal Hamiltonian H_{id}. Furthermore, any operator S_k of the original Hamiltonian H_0 which is coupled to the environment, i.e., $E_k \neq \mathbb{1}$, can only be suppressed completely and thus cannot appear in the ideal Hamiltonian H_{id}.

We obtain the following set of linear equations:

$$\frac{D}{M} \sum_{j=0}^{4^N-1} a_{kj} c_j = \frac{\nu_k}{\mu_k}, \quad k \in \mathcal{K}, \tag{3.8}$$

$$\mathcal{K} = \{k \in [1, 4^N - 1] : \mu_k \neq 0\},$$

with $\mathcal{K}$ denoting the set of indices of operators S_k which are present in the basis expansion of the original Hamiltonian H_0. We need to solve for the non-negative natural numbers c_j as well as for D and M which are not all independent. This is due to the fact that, since M is the total number of operators in our decoupling scheme, the relation $\sum c_j = M$ must be fulfilled. Introducing variables $e_j = Dc_j/M$, we can formulate another system of equations as

$$\sum_{j=0}^{4^N-1} a_{kj} e_j = \frac{\nu_k}{\mu_k}, \quad k \in \mathcal{K}. \tag{3.9}$$

By construction, the e_j fulfil the relation $\sum e_j = D$, and M can be found by determining M as the lowest common denominator for the rational numbers e_j/D. One could also choose a larger denominator for M. However, this would result in a structurally identical scheme that consists of repetitions of the shorter scheme.

3.2.2 *Existence of solutions*

Let us now address the question under which conditions the system of linear equations (3.9) has suitable solutions.

Let us first analyze the set of all possible real-valued solutions for the quantities e_j. The system of equations depends on the previously introduced variables $a_{kj} = \pm 1$, which can be computed from the algebraic properties of the operators S_k and S_j. Doing so for all pairs of our operator basis yields a $4^N \times 4^N$ square matrix $A^{(N)}$ with entries $A^{(N)}_{kj} \equiv a_{kj} = \pm 1$. For $N = 1$, we can calculate $A^{(1)}$ directly from the Pauli operators and obtain the matrix

$$A^{(1)} = \begin{pmatrix} 1 & 1 & 1 & 1 \\ 1 & 1 & -1 & -1 \\ 1 & -1 & 1 & -1 \\ 1 & -1 & -1 & 1 \end{pmatrix}. \tag{3.10}$$

This matrix has a number of interesting properties. Notice that for each row (and column) except the first, the sum over the entries is zero,

$$\sum_{j=0}^{3} A^{(1)}_{kj} = \begin{cases} 0 & \text{if } k \neq 0, \\ 4 & \text{if } k = 0. \end{cases} \tag{3.11}$$

Furthermore, the rows and columns are mutually orthogonal, since the dot product between any two row (or column) vectors $\vec{A}^{(1)}_j \cdot \vec{A}^{(1)}_k = 0$, as can be easily checked. This also means that the row vectors are linearly independent.

Due to the way the operators S_k are constructed as tensor products of Pauli operators, it follows that higher-order matrices $A^{(N)}$ can be constructed from lower-order ones by the recursive relation

$$A^{(N)} = A^{(1)} \otimes A^{(N-1)}. \tag{3.12}$$

This relation preserves the mentioned properties of $A^{(1)}$ for any order, as can be seen with the help of induction. First, let us consider the sum of the entries in any row $\vec{A}^{(N)}_l$ of $A^{(N)}$. The row is given by the recursion relation as

$$\vec{A}^{(N)}_l = \vec{A}^{(1)}_j \otimes \vec{A}^{(N-1)}_k, \quad l = j \cdot 4^{N-1} + k. \tag{3.13}$$

We can write the sum over the entries of this vector as

$$\sum_{s=0}^{4^N-1} A^{(N)}_{ls} = \sum_{q=0}^{3} A^{(1)}_{jq} \sum_{r=0}^{4^{N-1}-1} A^{(N-1)}_{kr}. \tag{3.14}$$

By assumption, if $k \neq 0$, then the sum over r vanishes, and the term is 0, as expected. For the case of $k = 0$, the sum over r yields 4^{N-1}, so that we have

$$\sum_{s=0}^{4^N-1} A_{ls}^{(N)} = 4^{N-1} \sum_{q=0}^{3} A_{jq}^{(1)}. \tag{3.15}$$

From Eq. (3.11) we know this is 0 if $j \neq 0$. Only if $k = j = 0$, we get the non-zero answer 4^N, which concludes the proof by induction.

The orthogonality of the rows can be similarly proven by induction. Consider two row vectors $\vec{A}_l^{(N)}$ and $\vec{A}_m^{(N)}$. From the recursion relations, these vectors can be expressed as

$$\vec{A}_l^{(N)} = \vec{A}_q^{(1)} \otimes \vec{A}_j^{(N-1)}, \quad l = q \cdot 4^{N-1} + j, \tag{3.16}$$

$$\vec{A}_m^{(N)} = \vec{A}_r^{(1)} \otimes \vec{A}_k^{(N-1)}, \quad m = r \cdot 4^{N-1} + k. \tag{3.17}$$

We then immediately find that the dot product between the two vectors is given as

$$\vec{A}_l^{(N)} \cdot \vec{A}_m^{(N)} = \left(\vec{A}_q^{(1)} \cdot \vec{A}_r^{(1)}\right) \left(\vec{A}_j^{(N-1)} \cdot \vec{A}_k^{(N-1)}\right). \tag{3.18}$$

This product is 0 by assumption if either $q \neq r$ or $j \neq k$. Only in the case $l = m$ is the dot product non-zero, concluding the proof by induction.

Matrices of the form $A^{(N)}$ which have entries ± 1 and whose rows are mutually orthogonal are called Hadamard matrices. Indeed, the recursive construction in Eq. (3.12) is very similar to the well-known Sylvester construction for Hadamard matrices [Syl67]. Since Hadamard matrices have full rank due to their linearly independent rows and since we use only $\dim \mathcal{K} < 4^N$ rows from the matrix in our system of equations (3.9), our system is under-determined and free of contradictions, and we can conclude that the system has infinitely many real-valued solutions for the variables e_j. Now, let $A_{\mathcal{K}}^{(N)}$ be the $\dim \mathcal{K} \times 4^N$ matrix resulting from the matrix $A^{(N)}$ by including only the rows $\vec{A}_k^{(N)}$ with $k \in \mathcal{K}$. Then we can express our system of equations (3.9) in compact vector form:

$$A_{\mathcal{K}}^{(N)} \cdot \vec{e} = \vec{r}, \qquad \vec{r} = \left(\frac{\nu_k}{\mu_k}\right)_{k \in \mathcal{K}}. \tag{3.19}$$

Here, $\vec{e}$ is the 4^N-dimensional vector of our variables e_j, and $\vec{r}$ is the $\dim \mathcal{K}$-dimensional vector of the right-hand side of (3.9). In order to find the general solution of this linear system of equations, we first solve for the homogeneous part, $A_{\mathcal{K}}^{(N)} \cdot \vec{e} = 0$. The linear space of these solutions has dimension $4^N - \dim \mathcal{K}$. As the rows of the Hadamard matrix $A^{(N)}$ are orthogonal and the scalar product of any two row vectors $\vec{A}_j^{(N)}$ and $\vec{A}_k^{(N)}$ fulfils the relation

$$\vec{A}_j^{(N)} \cdot \vec{A}_k^{(N)} = 4^N \delta_{jk}, \tag{3.20}$$

we conclude that any multiple of a row of $A^{(N)}$ not contained in $A^{(N)}_{\mathcal{K}}$ is a solution of the homogeneous equation. Therefore, the most general homogeneous solution $\vec{e}_0$ is of the form

$$\vec{e}_0 = \sum_{k \notin \mathcal{K}} \gamma_k (\vec{A}^{(N)}_k)^T, \quad \gamma_k \in \mathbb{R}. \tag{3.21}$$

A particular solution of the inhomogeneous equation can be constructed by noticing that from relation (3.20), one can conclude that

$$A^{(N)}_{\mathcal{K}} \cdot \left(A^{(N)}_{\mathcal{K}}\right)^T = 4^N \mathbb{1}_{\dim \mathcal{K}}. \tag{3.22}$$

This yields the particular solution

$$\vec{e}_r = \frac{1}{4^N} \left(A^{(N)}_{\mathcal{K}}\right)^T \cdot \vec{r}. \tag{3.23}$$

Therefore, the most general solution of the system of equations is given by

$$\vec{e} = \vec{e}_0 + \vec{e}_r. \tag{3.24}$$

Starting from this result, we now need to construct a set of c_j with non-negative integer values. Let us address the issue of non-negativity first. In order for c_j to be non-negative the quantities e_j must be non-negative, too. This latter requirement can be met by starting from an arbitrary solution of the system of equations $\vec{e}$. Because the first row of the Hadamard matrix $\vec{A}^{(N)}_0 = (1111\ldots)$ is never a part of $A^{(N)}_{\mathcal{K}}$ (due to the Hamiltonians being traceless), it is a solution to the homogeneous equation, and so an arbitrary multiple γ_0 of this first row can always be added to $\vec{e}$. In particular, one can choose the multiple as $\gamma_0 = -\min\{e_j\}$ over all entries in a given $\vec{e}$. Adding $\gamma_0 \vec{A}^{(N)}_0$ to $\vec{e}$ ensures that all entries in the resulting solution are non-negative.

Starting from such a non-negative solution, the quantities c_j will be integral if the numbers e_j/D are rational. Whether such solutions exist depends entirely on the particular solution $\vec{e}_r$ and therefore on the structure of the vector $\vec{r}$. For this purpose, it is required that all entries of $\vec{r}$ are rational or that they share at most a common real multiplier so that $\vec{r} = d\vec{r}_0$, with $\vec{r}_0$ denoting a rational vector. However, for practical purposes, we can relax this rather stringent condition. Even if the entries of $\vec{r}$ are not rational, it is quite acceptable from a practical point of view to round these quantities to suitable rational numbers. This is possible because dynamical decoupling is already approximate in nature and the lowest order $\overline{H}^{[0]}$ is linear in the quantities c_j. Therefore, any error originating from rounding will affect $\overline{H}^{[0]}$ linearly only, and we conclude that we can always find solutions c_j suitable for decoupling from the linear system (3.9), at least approximately.

3.2.3 *Practical considerations*

The presented system of linear equations allows us to calculate solutions for the variables c_j which determine how often each of the basis operators S_k appears in the constructed decoupling scheme. Thus, these variables describe our decoupling scheme completely. This means that we can always find a decoupling scheme for any given original Hamiltonian H_0 provided the ideal Hamiltonian H_{id} does not contain operators S_k which are either missing in H_0 or which are coupled with the environment.

However, the linear system has infinitely many solutions, and consequently infinitely many decoupling schemes exist. Although they all simulate the Hamiltonian H_{id} to lowest order, the remaining higher orders $\overline{H}^{[k]}$ can differ drastically, thus affecting the practical performance of the scheme. The higher orders are beyond approach with the linear system, but there are two other parameters of a scheme which have practical relevance. These are the number of pulses in a scheme, M, and the scaling constant D. For practical applications, it is preferable to find a scheme which is as short as possible. This simplifies implementation and makes it more feasible to employ techniques like symmetric or concatenated decoupling to deal with the higher orders of $\overline{H}$. For applications where the ideal Hamiltonian H_{id} is non-zero, the scaling constant D should ideally be 1, as otherwise the overall interaction time would have to be extended.

The most straightforward construction of a decoupling scheme is based on the particular solution $\vec{e}_r$, which can be readily calculated and then modified, as described, to yield a positive solution for the c_j. Unfortunately, it turns out that the particular solution often produces very large decoupling schemes with large scaling factors D. To improve the generated decoupling scheme, we need to exploit the freedom presented by the general homogeneous solution. However, it is not apparent how to modify the particular solution in such a way that the resulting scheme has minimal M and D.

There is a way to find solutions to the linear system which are guaranteed to have minimal scaling D. This is done by employing linear programming. Linear programming is a technique to optimize a linear objective function of a set of variables under certain linear equality and inequality constraints. In our case, we can use linear programming for the set of variables e_j and minimize $D = \sum e_j$ subject to the linear equality constraints (3.9), which will return a solution that is guaranteed to have minimal scaling. However, this approach does not guarantee a minimal scheme size M. For small qubit systems with $N \leqslant 5$ the particular solutions generated by typical linear programming solvers often produce sufficiently short decoupling schemes which are practically usable, but in some instances it is still

possible to manually construct shorter schemes with the same minimal scaling D.

Given that the number of variables and the set of equations grow exponentially with the number N of qubits, constructing solutions by any method will become increasingly difficult with growing N. To find schemes for larger numbers of qubits, it is often better to calculate a solution for a smaller problem instance and then induce a scheme for the full system from the smaller solution. Working with a smaller problem instance may also allow us to optimize the scheme in certain ways. For example, in some experimental settings, the Pauli σ_1 and σ_2 pulses are readily available, but the σ_3 pulse may be more difficult to implement. This is the case, for instance, with the superconducting flux qubits we will study in Ch. 8. By reordering the scheme operators appropriately or replacing them adequately, the need for σ_3 pulses may be avoided in many schemes. We will see examples of such manual optimizations and extensions to higher N throughout the remainder of this thesis.

3.3 EXAMPLE APPLICATIONS

Now that we have a method to design decoupling schemes, it is time to apply it to a number of scenarios. In the following, we will look at how to protect two-qubit interactions from an environment as well as how to modify certain couplings in a qubit network. We will also run a few numerical simulations to see how well some of these schemes perform.

3.3.1 *Protecting a two-qubit interaction from environmentally induced decoherence*

Let us consider two physically separated, distinguishable qubits 1 and 2, which interact according to a time-independent interaction Hamiltonian H_{id}. Furthermore, both qubits are coupled to independent environments $\mathcal{A}$ and $\mathcal{B}$, which may introduce decoherence and

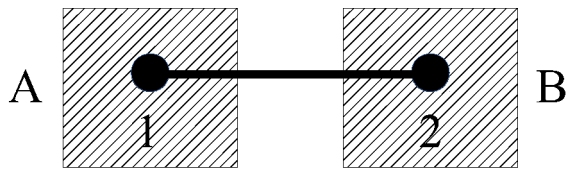

Figure 3.1: Two interacting qubits a and b coupled to separate environments $\mathcal{A}$ and $\mathcal{B}$.

damping. See Fig. 3.1 for a visual depiction. The full dynamics of the system is then described by the most general Hamiltonian,

$$\begin{aligned} H_0 &= H_{id} + H_{err}, \\ H_{id} &= \sum_{i,j=1}^{3} h_{ij} \sigma_i^{(1)} \sigma_j^{(2)}, \\ H_{err} &= \sum_{i=1}^{3} \sigma_i^{(1)} \otimes A_i + \sum_{i=1}^{3} \sigma_i^{(2)} \otimes B_i, \end{aligned} \tag{3.25}$$

where A_i and B_i are arbitrary Hermitian operators on their corresponding environments. We ignore potential interactions within and between the environments as they are not relevant to our discussion.

Our goal is to find a decoupling scheme to turn the acting Hamiltonian H_0 into the ideal Hamiltonian H_{id} by eliminating H_{err}. For this purpose, we have to solve the system of linear equations (3.6). The system matrix $A^{(2)} = A^{(1)} \otimes A^{(1)}$ is known and independent of the two Hamiltonians involved. For the coefficients of the vector $\vec{r}$, which determine the inhomogeneous part of the set of equations, we find

$$\frac{\nu_k}{\mu_k} = \begin{cases} 1 & \text{if } S_k \text{ acts on both qubits,} \\ 0 & \text{if } S_k \text{ acts only on one of the qubits.} \end{cases} \tag{3.26}$$

From the particular solution $\vec{e}_r$ to the set of equations we can construct the following decoupling scheme by following the steps outlined in Sec. 3.2.2:

$$\begin{array}{cccccccccccc} 0 & 0 & 0 & 1 & 1 & 1 & 2 & 2 & 2 & 3 & 3 & 3 \\ 0 & 0 & 0 & 1 & 2 & 3 & 1 & 2 & 3 & 1 & 2 & 3. \end{array} \tag{3.27}$$

Here, the two numbers i and j of each column represent an operator $g_k = \sigma_i \otimes \sigma_j$ of our decoupling scheme. We see that the scheme consists of a total sequence of $M = 12$ operators. They involve free evolution (identity pulses applied three times) and a sequence in which all combinations of Pauli operators appear exactly once. The scaling constant for this decoupling scheme is $D = 3$. This is the minimal possible value of D, as can be verified by linear programming.

3.3.2 *Protecting a $\sqrt{SWAP}$ gate implementation*

Let us now consider a specific interaction Hamiltonian in the form of a two-qubit Heisenberg Hamiltonian,

$$H_{id} = \sum_{i=1}^{3} \sigma_i^{(1)} \sigma_i^{(2)}. \tag{3.28}$$

This Hamiltonian can be used to implement the entangling $\sqrt{\text{SWAP}}$ gate if applied over a time interval of duration $T = \frac{\pi}{8}$ (see, e.g., [SS03]).

Entangling gates are particularly interesting in quantum information because they can create an entangled state from a separable two-qubit state.

For the interaction with the environment, let us now assume that each qubit is coupled to a harmonic oscillator as described by the Hamiltonian

$$H_{\text{err}} = \lambda(\sigma_+^{(1)} a + \sigma_-^{(1)} a^\dagger + \sigma_+^{(2)} b + \sigma_-^{(2)} b^\dagger). \tag{3.29}$$

Here, a, $a^\dagger$ and b, $b^\dagger$ are the annihilation and creation operators of the two oscillators, and $\sigma_\pm = \frac{1}{2}(\sigma_1 \pm i\sigma_2)$. λ characterizes the common strength of the coupling.

The general two-qubit protection scheme (3.27) can be used to protect this $\sqrt{\text{SWAP}}$ gate implementation. However, the Hamiltonian in (3.28) contains only three out of nine possible two-qubit basis operators and the error terms in (3.29) involve only four out of six possible operators. Taking these special circumstances into account, we can simplify the system of equations (3.6) by omitting eight equations. As a result, we find the significantly simpler dynamical decoupling scheme:

$$\begin{array}{cccc} 0 & 1 & 3 & 2 \\ 0 & 1 & 3 & 2. \end{array} \tag{3.30}$$

This particular protection scheme involves only four decoupling operators and has an improved scaling factor of $D = 1$. This means that no rescaling of the interaction time is necessary, therefore allowing the gate to be implemented faster. Furthermore, the control operators g_k required for the special scheme can be implemented with the help of only σ_1 and σ_2 pulses, whereas the general scheme also requires σ_3 pulses, so it might be easier to implement experimentally.

3.3.3 *Protecting arbitrary two-qubit interactions on an N-qubit network from environmental influences*

We can also study a generalization of the example in Sec. 3.3.1. Consider a network of N qubits, where any two qubits can interact with each other, and any qubit may also be in contact with an environment. In the time-independent case, the most general Hamiltonian is then given by

$$\begin{aligned} H_0 &= H_{\text{id}} + H_{\text{err}}, \\ H_{\text{id}} &= \sum_{n,m=1}^{N} \sum_{i,j=1}^{3} h_{nm,ij} \sigma_i^{(n)} \sigma_j^{(m)}, \\ H_{\text{err}} &= \sum_{n=1}^{N} \sum_{i=1}^{3} \sigma_i^{(n)} \otimes E_i^{(n)}, \end{aligned} \tag{3.31}$$

where the $E_i^{(n)}$ are arbitrary operators acting on the n-th qubit's environment. Our goal is to protect all of the two-qubit interactions in H_{id} against the influence of H_{err}.

Constructing and solving the equation system (3.6) for arbitrary N is not feasible, since the size of the system grows exponentially with N. However, we already know the solution for $N = 2$, which is just the case that we studied in Sec. 3.3.1. The solution (3.27) consists of two parts, the first being three identity operators, and the second part a sequence where all the combinations $\sigma_a \otimes \sigma_b$, with $a, b \in [1, 2, 3]$ appear exactly once as scheme operators. Since we can repeat a decoupling scheme any number of times and also change the order of operators in that scheme without affecting the lowest order $\overline{H}^{[0]}$, it follows that any scheme is a solution to the two-qubit case if it fulfils the following two conditions: it must contain all of the combinations $\sigma_a \otimes \sigma_b$ the same number of times, and exactly one fourth of the operators in the scheme must be identity operators.

Due to the fact that the Hamiltonian H_0 contains at most two-qubit operations, we can conclude that a decoupling scheme for arbitrary N protects all of the two-qubit interactions to lowest order if any two rows of the scheme are a solution to the two-qubit case. For example, for $N = 3$ it is easy to add a third row to the original solution such that this condition is fulfilled:

$$\begin{array}{cccccccccccc} 0 & 0 & 0 & 1 & 1 & 1 & 2 & 2 & 2 & 3 & 3 & 3 \\ 0 & 0 & 0 & 1 & 2 & 3 & 1 & 2 & 3 & 1 & 2 & 3 \\ 0 & 0 & 0 & 1 & 2 & 3 & 3 & 1 & 2 & 2 & 3 & 1. \end{array} \tag{3.32}$$

However, constructing solutions for arbitrary N is still no trivial task. Thankfully, we can make use of extensive mathematical research if we recognize that what we are looking for is in fact an *orthogonal array*.

Orthogonal arrays are defined as follows. If $\mathcal{A}$ is an alphabet containing a symbols, then an orthogonal array with a levels, strength t and index λ is an $N \times M$ matrix A with entries from $\mathcal{A}$ such that any $s \times M$ sub-matrix constructed from any s rows from A ($s \leqslant t$) contains any s-tuple of elements from $\mathcal{A}$ exactly λ times as a column.

In our case, we are looking for an orthogonal array with $a = 3$ levels and strength $t = 2$, which describes the second part of our decoupling scheme. If we can find an array of suitable dimensions, we can construct our decoupling scheme for N qubits from it by adding the necessary identity operators. A construction method for strength-2 orthogonal arrays based on Hamming codes can be found in [HSS99], so that in principle we can construct a decoupling scheme for any number of qubits N. Note, however, that the size M of our decoupling scheme grows approximately linearly with N.

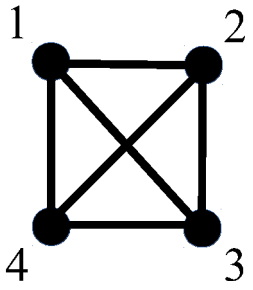

Figure 3.2: A quadratic closed chain of four qubits with diagonal couplings.

A solution for $N = 6$ obtained from a suitable orthogonal array looks like this:

000000	1	1	1	1	1	1	2	2	2	2	2	2	3	3	3	3	3	3
000000	1	2	1	3	2	3	1	3	2	3	1	2	2	3	1	2	1	3
000000	1	2	3	3	1	2	2	3	1	1	2	3	3	1	2	2	3	1
000000	1	2	3	1	3	2	3	1	2	3	2	1	3	2	2	1	1	3
000000	1	3	3	2	2	1	2	3	2	1	3	1	1	2	1	3	2	3
000000	1	3	2	3	1	2	3	2	2	1	1	3	2	1	3	1	2	3.

3.3.4 *Removing diagonal couplings in a closed 4-qubit chain*

As another example, let us consider a closed chain of four qubits with Ising couplings between each qubit pair, as depicted in Fig. 3.2. We can describe the couplings by the Hamiltonian

$$H_0 = \sum_{\substack{i,j=1 \\ i<j}}^{4} h_{i,j}\sigma_3^{(i)}\sigma_3^{(j)}. \tag{3.33}$$

Our goal is to eliminate the diagonal couplings between qubits 2 and 4 and between qubits 1 and 3. The ideal Hamiltonian without these diagonal couplings can be written as

$$H_{id} = \sum_{i=1}^{4} h_{i,i+1}\sigma_3^{(i)}\sigma_3^{(i+1)}, \tag{3.34}$$

if we assume that the indexes wrap around, i.e., qubit 5 is just qubit 1. This scenario is an example of selective decoupling where we want to remove only certain parts of the given Hamiltonian.

Setting up the linear system is straight-forward. The system matrix is $A^{(4)} = A^{(1)} \otimes A^{(1)} \otimes A^{(1)} \otimes A^{(1)}$. Our set $\mathcal{K}$ of basis operator indices occurring in H_0 consists of $\{3300, 0330, 0033, 3003, 3030, 0303\}$, with the numbers in base-4 notation so that a number corresponds to

Figure 3.3: A linear chain of four qubits with nearest-neighbour interactions, where the inner coupling is twice as strong as the two outer couplings.

an operator $abcd \Rightarrow \sigma_a \otimes \sigma_b \otimes \sigma_c \otimes \sigma_d$. Finally, we set the vector $\vec{r} = (1,1,1,1,0,0)$, meaning that we want to keep the first four operators in $\mathcal{K}$ and eliminate the other two.

We employ linear programming to construct a decoupling scheme for this scenario. The solution given by our linear programming solver leads to the following decoupling scheme:

$$\begin{array}{cccc} 0 & 0 & 1 & 0 \\ 0 & 0 & 1 & 1 \\ 0 & 0 & 0 & 1 \\ 0 & 0 & 0 & 0. \end{array} \tag{3.35}$$

The scaling factor of this scheme is $D = 2$, meaning that the interaction time has to be doubled to compensate for the reduced interaction strength.

3.3.5 *Modifying individual interaction strengths*

As a final example, let us look at how to construct schemes which can modify individual coupling strengths between qubits. Consider a linear chain of four qubits with nearest-neighbor XX interactions which are all equally strong. The Hamiltonian describing these interactions is

$$H_0 = \sum_{i=1}^{3} J(\sigma_1^{(i)}\sigma_1^{(i+1)} + \sigma_2^{(i)}\sigma_2^{(i+1)}), \tag{3.36}$$

with J an arbitrary coupling strength. Imagine that we would like to reduce the coupling strengths between qubits 1 and 2 and between qubits 3 and 4 by half, as depicted in Fig. 3.3. The resulting Hamiltonian would be

$$\begin{aligned} H_{id} =& J(\sigma_1^{(2)}\sigma_1^{(3)} + \sigma_2^{(2)}\sigma_2^{(3)}) \\ &+ \frac{1}{2}J(\sigma_1^{(1)}\sigma_1^{(2)} + \sigma_2^{(1)}\sigma_2^{(2)} + \sigma_1^{(3)}\sigma_1^{(4)} + \sigma_2^{(3)}\sigma_2^{(4)}). \end{aligned} \tag{3.37}$$

Our system matrix is $A^{(4)}$ as before; the relevant operator indices in our set $\mathcal{K}$ are $\{1100, 2200, 0110, 0220, 0011, 0022\}$ with corresponding entries in the vector $\vec{r} = (0.5, 0.5, 1.0, 1.0, 0.5, 0.5)$. This way we ensure

that the couplings in the middle are kept intact, while the couplings at the outer edges are reduced.

By employing linear programming again, we find the following decoupling scheme with a scaling $D = 1$:

$$\begin{matrix} 0 & 0 & 0 & 0 \\ 0 & 0 & 0 & 3 \\ 0 & 0 & 0 & 3 \\ 0 & 0 & 0 & 0. \end{matrix} \tag{3.38}$$

3.4 NUMERICAL SIMULATIONS

As a conclusion to this chapter, let us look at a few numerical simulations to get a feel for the effectiveness of the presented schemes. We are going to simulate the scenario outlined in Sec. 3.3.2 for both the general scheme (3.27) and the specialized scheme (3.30).

We assume that two qubits are initially prepared in a separable state $|\Psi_0\rangle$ and evolve under the influence of the Hamiltonian $H_0 = H_{id} + H_{err}$ as given by Eqs. (3.28) and (3.29). Without the environmental interaction of H_{err}, this state would, after a time $T = \frac{\pi}{8}$, evolve to the quantum state $|\Psi(T)\rangle = U_{id}(T)|\Psi\rangle$ under the action of the ideal Heisenberg Hamiltonian H_{id}. The final state of the two qubits resulting from time evolution under the total Hamiltonian H_0 with active decoupling controls can be obtained by a partial trace over the environment as

$$\rho_{Tr}(T) = \mathrm{Tr}_E \left(U(DT) \left(|\Psi\rangle \otimes |0\rangle_E \right) \left(\langle\Psi| \otimes \langle 0|_E \right) U^\dagger(DT) \right). \tag{3.39}$$

($|0\rangle_E$ denotes the initially prepared ground state of the environmental harmonic oscillators.) We have taken into account that the interaction time may need to be rescaled by the factor D of the decoupling scheme which is used. This result can be compared with the ideal case by means of the state fidelity

$$F(T) = \sqrt{\langle\Psi(T)|\rho_{Tr}(T)|\Psi(T)\rangle} \tag{3.40}$$

in a convenient way.

In Fig. 3.4, the results of numerical simulations of the general two-qubit protection scheme (3.27) are presented for different choices of the coupling strengths λ. The left graph shows the final fidelity $F(T)$ after the gate implementation time T and its dependence on the number n of times the decoupling scheme has been applied. The pulse sequences of the dynamical decoupling scheme are distributed equally over the whole interaction time DT. Therefore, in order to apply the decoupling scheme n times it is necessary to implement a control pulse frequency of magnitude

$$\frac{1}{\tau} = \frac{Mn}{DT}, \tag{3.41}$$

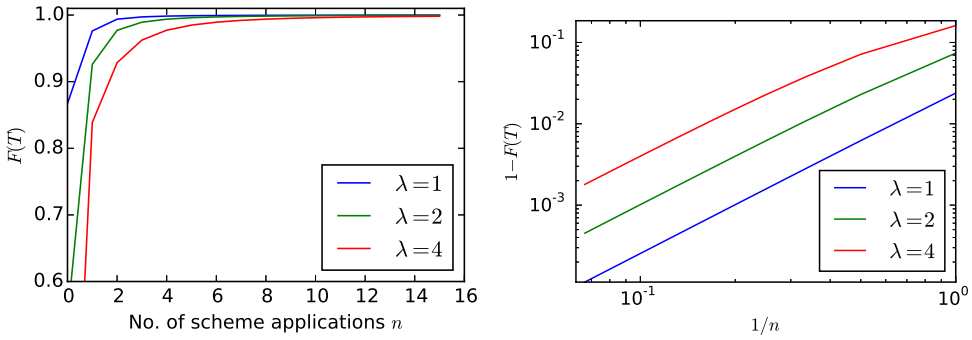

Figure 3.4: Performance of the general two-qubit interaction scheme for protecting the two-qubit gate against different strengths λ of environmental couplings, with dependence of the fidelity $F(T)$ on the number of applications n of the dynamical decoupling scheme. On the left $F(T)$ is plotted over n, on the right side the same results are shown in log-log scale with $1-F(T)$ plotted over $1/n$. The scaling $D=3$ of the dynamical decoupling scheme has been compensated by extending the actual interaction time from its ideal value T to $3T$.

with $M=12$ and $D=3$ for the general two-qubit protection scheme (3.27). It is apparent that with increasing values of n and consequently smaller times τ between subsequent control pulses, the performance of the decoupling procedure increases. This is expected as the higher-order terms $\overline{H}^{[k]}$ in the average Hamiltonian are of the order of τ^k. But even if the scheme is applied only once or twice, the increase of the fidelity is noticeable, particularly in the presence of stronger couplings to the environment.

In the right graph, we plotted the error $1-F(T)$ over $1/n$ for the same data points $(n, F(T))$ and on logarithmic scales. From the fact that we get what appear to be straight lines, we can conjecture that the relationship between the fidelity $F(T)$ and the number of repetitions n should be given by

$$1-F(T) \sim \frac{1}{n^\alpha} \sim \tau^\alpha. \tag{3.42}$$

By analysing the slope of the lines, we find $\alpha \approx 2$ for all three values of λ, meaning that the loss of fidelity scales with τ^2. If we assume that the error is dominated by $e^{-i\overline{H}^{[1]}DT}$, then with $\|\overline{H}^{[1]}\|_{op} \sim \tau$ and $DT = Mn\tau$ we expect the error to scale with τ^2, just as we found.

Figure 3.5 presents results from the same numerical simulations, but this time employing the specialized decoupling scheme (3.30). Compared to the performance of the general two-qubit scheme, the fidelity is slightly improved. This is an additional practical advantage of the specialized scheme over the general one, besides those mentioned in Sec. 3.3.2. The slopes of the straight lines in the log-log plot on the right again yield $\alpha \approx 2$, so that the error still scales with τ^2.

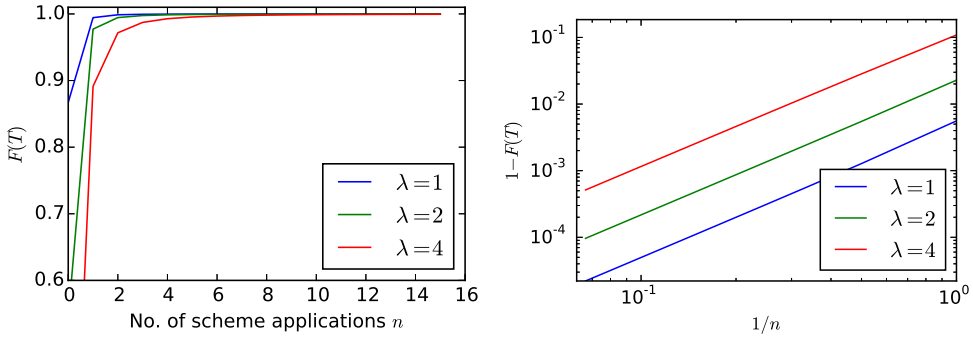

Figure 3.5: Performance of the special Heisenberg protection scheme (3.30): The fidelity of the system after the gate interaction time T and its dependence on the number n of applications of the dynamical decoupling scheme are plotted. Left is plotted $F(T)$ over n, on the right $1 - F(T)$ is plotted in log-log scale over $1/n$.

4

EXTENSION TO HIGHER-DIMENSIONAL SYSTEMS

Qubits are a convenient system to explore concepts of quantum information, since they are relatively easy quantum systems to describe in theory, and several experimental implementations exist which are well understood. Furthermore, they are the natural quantum analogue of a classical bit. However, there is no fundamental reason that would dictate that quantum computation must be done with qubits as the building blocks. We can, in principle, use higher-dimensional systems, so called *qudits*, which are defined on the Hilbert space $\mathcal{H}_d = \mathbb{C}^d$, with dimension $d > 2$. Indeed, many practical systems used to implement qubits (like atoms and ions, for instance) actually have more than two distinct energy levels, and extra care must be taken that only two levels are significantly populated to achieve an approximate two-level system.

Given that the computational power of a quantum register is tied to the dimension of its Hilbert space, we would need fewer qudits to achieve a comparable computational power to a register of qubits. This means that we would have to control fewer qudits, which also means that environmental disturbances may be less severe. On the other hand, as a single qudit is now a more complex system, the task of implementing all necessary operations to achieve universal quantum computation might be even more challenging than it already is for qubits. So far, the majority of ongoing research efforts both in theory and experiment seems to be focussed on qubits, and so the question of whether qudits could be advantageous for quantum computation is still open.

Nevertheless, dynamical decoupling methods will be hugely beneficial for any practical qudit implementation, so in this chapter we will study how decoupling schemes can be constructed for networks of qudits.

4.1 GENERALIZING THE PAULI OPERATORS

In Sec. 3.2 we used tensor products of the Pauli operators as a complete basis to express both the Hamiltonians and the available pulses on a network of N qubits. This allowed us to derive a convenient linear set of equations from the basic decoupling condition (2.24). If we want to generalize this method to qudits, we first need to generalize the Pauli operators to higher dimensions.

In dimension $d = 2$, the Pauli operators are both unitary and Hermitian. Unfortunately, we cannot keep both of these properties in

higher dimensions, which leads to two different ways of extending the Pauli operators.

4.1.1 *The generalized Gell-Mann operators*

Let $\{|k\rangle\}_{k=0}^{d-1}$ be an arbitrary orthonormal vector basis for $\mathcal{H}_d$. Then we can construct a set of d^2-1 generators of the special unitary group $SU(d)$ as follows [HE81]. The set consists of $d(d-1)/2$ symmetric operators

$$u_{jk} = |j\rangle\langle k| + |k\rangle\langle j|, \quad 0 \leqslant j < k < d, \tag{4.1}$$

$d(d-1)/2$ antisymmetric operators

$$v_{jk} = -i(|j\rangle\langle k| - |k\rangle\langle j|), \quad 0 \leqslant j < k < d, \tag{4.2}$$

and finally $d-1$ diagonal operators

$$w_l = \sqrt{\frac{2}{l(l+1)}} \left(\sum_{k=0}^{l-1} |k\rangle\langle k| - l|l\rangle\langle l| \right), \quad 1 \leqslant l < d. \tag{4.3}$$

Each of these operators is by definition traceless and Hermitian, but in general not unitary. By adding the identity operator $w_0 \equiv \mathbb{1}$ to this set of operators, we get a complete orthonormal operator basis with respects to the Hilbert-Schmidt inner product. A proof can be found in [BK08].

In the case of $d = 2$, these operators reproduce the Pauli operators. In the case of $d = 3$, we get the so-called Gell-Mann operators, which is why these operators are often called the generalized Gell-Mann operators. The Gell-Mann operators in $d = 3$ dimensions are given by their matrix representation as:

$$u_{01} = \begin{pmatrix} 0 & 1 & 0 \\ 1 & 0 & 0 \\ 0 & 0 & 0 \end{pmatrix}, \quad u_{02} = \begin{pmatrix} 0 & 0 & 1 \\ 0 & 0 & 0 \\ 1 & 0 & 0 \end{pmatrix}, \quad u_{12} = \begin{pmatrix} 0 & 0 & 0 \\ 0 & 0 & 1 \\ 0 & 1 & 0 \end{pmatrix},$$

$$v_{01} = \begin{pmatrix} 0 & -i & 0 \\ i & 0 & 0 \\ 0 & 0 & 0 \end{pmatrix}, \quad v_{02} = \begin{pmatrix} 0 & 0 & -i \\ 0 & 0 & 0 \\ i & 0 & 0 \end{pmatrix}, \quad v_{12} = \begin{pmatrix} 0 & 0 & 0 \\ 0 & 0 & -i \\ 0 & i & 0 \end{pmatrix},$$

$$w_1 = \begin{pmatrix} 1 & 0 & 0 \\ 0 & -1 & 0 \\ 0 & 0 & 0 \end{pmatrix}, \qquad w_2 = \frac{1}{\sqrt{3}} \begin{pmatrix} 1 & 0 & 0 \\ 0 & 1 & 0 \\ 0 & 0 & -2 \end{pmatrix}. \tag{4.4}$$

4.1.2 *The generalized spin operators*

Where the generalized Gell-Mann operators are a Hermitian generalization of the Pauli operators, we will now define a set of d^2 unitary operators,

$$\sigma_{j,k} = \sum_{l=0}^{d-1} \omega^{jl} |l\rangle\langle l+k|, \quad j,k \in [0, d-1], \tag{4.5}$$

with $\omega = e^{2\pi i/d}$ and $|l\rangle \equiv |l \bmod d\rangle$. These operators were first introduced in [BBC+93] in the context of teleporting qudit states. They are typically known as Weyl operators or generalized spin operators [PR04], and in the case of $d = 2$ they reproduce the Pauli operators up to phase factors. The operators form an orthonormal operator basis with regards to the Hilbert-Schmidt inner product, a proof of which can be found in [BK08].

In the case of $d = 3$, the operators have the following matrix representation:

$$\sigma_{00} = \begin{pmatrix} 1 & 0 & 0 \\ 0 & 1 & 0 \\ 0 & 0 & 1 \end{pmatrix}, \quad \sigma_{01} = \begin{pmatrix} 0 & 1 & 0 \\ 0 & 0 & 1 \\ 1 & 0 & 0 \end{pmatrix}, \quad \sigma_{02} = \begin{pmatrix} 0 & 0 & 1 \\ 1 & 0 & 0 \\ 0 & 1 & 0 \end{pmatrix},$$

$$\sigma_{10} = \begin{pmatrix} 1 & 0 & 0 \\ 0 & \omega & 0 \\ 0 & 0 & \omega^2 \end{pmatrix}, \quad \sigma_{11} = \begin{pmatrix} 0 & 1 & 0 \\ 0 & 0 & \omega \\ \omega^2 & 0 & 0 \end{pmatrix}, \quad \sigma_{12} = \begin{pmatrix} 0 & 0 & 1 \\ \omega & 0 & 0 \\ 0 & \omega^2 & 0 \end{pmatrix},$$

$$\sigma_{20} = \begin{pmatrix} 1 & 0 & 0 \\ 0 & \omega^2 & 0 \\ 0 & 0 & \omega \end{pmatrix}, \quad \sigma_{21} = \begin{pmatrix} 0 & 1 & 0 \\ 0 & 0 & \omega^2 \\ \omega & 0 & 0 \end{pmatrix}, \quad \sigma_{22} = \begin{pmatrix} 0 & 0 & 1 \\ \omega^2 & 0 & 0 \\ 0 & \omega & 0 \end{pmatrix}. \tag{4.6}$$

4.2 DERIVING THE LINEAR SET OF EQUATIONS FOR QUDITS

We will now discuss how the construction of Pauli pulse decoupling schemes on qubit networks that we derived in Sec. 3.2 can be extended to networks of qudits. As before, we will assume that the available decoupling operations are comprised of local instantaneous pulses to the individual qudits, this time selected from the set of generalized spin operators defined in (4.5). Since the pulses need to be unitary, we cannot use the Gell-Mann operators for this purpose.

For an N-qudit system, the d^{2N} tensor products of these generalized spin operators, i.e.

$$S_{j,k} = \sigma_{j_1,k_1} \otimes \sigma_{j_2,k_2} \otimes \cdots \otimes \sigma_{j_N,k_N}, \tag{4.7}$$

with $j = j_1 j_2 \ldots j_N$ and $k = k_1 k_2 \ldots k_N$ in base-d representation, form a complete operator basis on the N-qudit network's Hilbert space

$\mathcal{H}_d^{\otimes N}$. This means that we can again express the Hamiltonian operators H_0 and H_{id} in this operator basis. Given that the Hamiltonians must be Hermitian operators, the generalized Gell-Mann operators from Sec. 4.1.1 would, in principle, be a more convenient basis. However, our qubit method exploited the particular property (3.7) of the Pauli operators, and we will see in Sec. 4.2.1 that this property is generalized by the spin operators. For this reason, we choose the generalized spin operators as our operator basis.

4.2.1 *Basic spin operator properties*

Let us start with obtaining a few vital algebraic properties of the generalized spin operators $\sigma_{j,k}$, which we need in the following calculations. First, the adjoint of an operator $\sigma_{j,k}$ is given by

$$\begin{aligned}\sigma_{j,k}^\dagger &= \sum_{l=0}^{d-1} (\omega^*)^{jl} |l+k\rangle\langle l| = \sum_{l=0}^{d-1} \omega^{(d-j)l} |l+k\rangle\langle l| \\ &= \omega^{jk} \sum_{m=k}^{d+k-1} \omega^{(d-j)m} |m\rangle\langle m+(d-k)| \\ &= \omega^{jk} \sigma_{d-j,d-k}. \end{aligned} \tag{4.8}$$

The adjoint of a tensor product operator follows as

$$S_{j,k}^\dagger = \bigotimes_{i=N-1}^{0} \omega^{j_i k_i} \sigma_{d-j_i,d-k_i} \tag{4.9}$$

$$= \omega^{\vec{j}\cdot\vec{k}} S_{d^N-j,d^N-k}, \tag{4.10}$$

with $\vec{j}\cdot\vec{k} := \sum_{i=0}^{N-1} j_i k_i$ a scalar product of the base-d representations of j and k.

The product of two spin operators yields

$$\begin{aligned}\sigma_{j,k}\sigma_{s,t} &= \sum_{l=0}^{d-1} \omega^{jl+s(l+k)} |l\rangle\langle l+k+t| \\ &= \omega^{sk} \sigma_{j+s,k+t}. \end{aligned} \tag{4.11}$$

We can then quickly show that the generalized spin operators are indeed unitary, because

$$\sigma_{j,k}\sigma_{j,k}^\dagger = \omega^{jk} \sigma_{j,k}\sigma_{d-j,d-k} = \omega^{jk}\omega^{(d-j)k}\sigma_{0,0} = \mathbb{1}. \tag{4.12}$$

Finally, we obtain the characteristic relation

$$\begin{aligned}\sigma_{j,k}^\dagger \sigma_{s,t} \sigma_{j,k} &= \omega^{jk}\omega^{tj}\omega^{(s+j)(d-k)} \sigma_{d+s,d+t} \\ &= \omega^{jt-ks} \sigma_{s,t}, \end{aligned} \tag{4.13}$$

which generalizes the Pauli operator relation (3.7) and enables us to extend our method to the qudit case. We can follow for the tensor product operators that

$$\begin{aligned} S_{j,k}^{\dagger} S_{s,t} S_{j,k} &= \bigotimes_{i=N-1}^{0} \omega^{j_i t_i - k_i s_i} \sigma_{s_i,t_i} \\ &= \omega^{\vec{j}\cdot\vec{t}-\vec{k}\cdot\vec{s}} S_{s,t}. \end{aligned} \tag{4.14}$$

4.2.2 *Deriving the linear set of equations*

In the tensor basis of the generalized spin operators, our Hamiltonians are given as

$$H_0 = \sum_{(j,k)\in\mathcal{K}} \mu_{j,k} S_{j,k} \otimes E_{j,k} + H_E, \tag{4.15}$$

$$H_{id} = \sum_{(j,k)\in\mathcal{K}} \nu_{j,k} S_{j,k} \otimes \mathbb{1}_{env} + H_E, \tag{4.16}$$

where $\mathcal{K}$ is a subset of $[0,\dots,d^N-1]\times[0,\dots,d^N-1]$ and does not contain the pair $(0,0)$. Therefore, these Hamiltonians are traceless. However, due to the Hermitian nature of the Hamiltonians, we have additional constraints, namely that if an operator $S_{j,k}$ is part of the expansion, then so must be its adjoint. In other words, if we have $(j,k)\in\mathcal{K}$, then we must also have $(d^N-j,d^N-k)\in\mathcal{K}$, and the coefficients must be related as $\mu_{j,k} = \omega^{\vec{j}\cdot\vec{k}}\mu^*_{d^N-j,d^N-k}$, $\nu_{j,k} = \omega^{\vec{j}\cdot\vec{k}}\nu^*_{d^N-j,d^N-k}$. This yields the relation

$$\frac{\nu_{j,k}}{\mu_{j,k}} = \left(\frac{\nu_{d^N-j,d^N-k}}{\mu_{d^N-j,d^N-k}}\right)^*. \tag{4.17}$$

Inserting these expansions into the decoupling condition (2.24) and following the same steps as in Sec. 3.2.1, we arrive at the complex system of linear equations

$$A^{(N)}_{\mathcal{K}}\cdot\vec{e} = \vec{r}, \qquad \vec{r} = \left(\frac{\nu_{j,k}}{\mu_{j,k}}\right)_{(j,k)\in\mathcal{K}}, \tag{4.18}$$

with $A^{(N)}_{\mathcal{K}}$ being the sub-matrix of $A^{(N)}$ consisting of all the rows $\vec{A}^{(N)}_{(j,k)}$ for $(j,k)\in\mathcal{K}$. The entries of the full matrix $A^{(N)}$ are determined by the characteristic property of the operators $S_{j,k}$ given in (4.14):

$$A^{(N)}_{(s,t),(j,k)} = \omega^{\vec{j}\cdot\vec{t}-\vec{k}\cdot\vec{s}}. \tag{4.19}$$

As in the qubit case, this system of equations is only solvable if, for any $\mu_{j,k}=0$, the corresponding $\nu_{j,k}$ also vanishes. (Compare with the discussion in Sec. 3.2.1.) In the following, it is therefore assumed that $\mu_{j,k}\neq 0$ for any $(j,k)\in\mathcal{K}$. The linear system in (4.18) is complex, however, we still need rational or at least real-valued solutions for $\vec{e}$. Whether such solutions exist will be discussed in the following.

4.2.3 *The properties of the system matrix* $A^{(N)}$

In the qubit case, the system matrix turned out to be a Hadamard matrix. We will now see that all of the relevant properties carry over naturally to the qudit case, and in this sense the matrix $A^{(N)}$ could now be called a complex Hadamard matrix. Its entries consist exclusively of the d-th unit roots ω^k, with $k \in [0, \ldots, d-1]$. The matrix $A^{(N)}$ is Hermitian because

$$\left(A^{(N)}_{(s,t),(j,k)}\right)^* = \left(\omega^{\vec{j}\cdot\vec{t}-\vec{k}\cdot\vec{s}}\right)^* = \omega^{-\vec{j}\cdot\vec{t}+\vec{k}\cdot\vec{s}} = A^{(N)}_{(j,k),(s,t)}. \tag{4.20}$$

The entries of any row vector $\vec{A}^{(N)}_{(s,t)}$ of $A^{(N)}$ sum up to zero with the only exception being the first row $\vec{A}_{(0,0)}$. This follows from the fact that for any integral power $k \neq 0$ of the unit root, ω^k, it holds that $\sum_{j=0}^{d-1} \omega^{kj} = 0$. We assume that s_n is a non-zero component of the base-d representation of s. Thus, we find for the sum over the row $\vec{A}^{(N)}_{(s,t)}$ the expression

$$\begin{aligned}
&\sum_{j=0}^{d^N-1} \sum_{k=0}^{d^N-1} A^{(N)}_{(s,t),(j,k)} = \sum_{\substack{j_0,\ldots,j_{N-1}=0 \\ k_0,\ldots,k_{N-1}=0}}^{d-1} \prod_{i=0}^{N-1} \omega^{j_i t_i} \omega^{-k_i s_i} \\
&= \sum_{\substack{j_0,\ldots,j_{N-1}=0 \\ k_0,\ldots,k_{n-1},k_{n+1}, \\ \ldots,k_{N-1}=0}}^{d-1} \prod_{\substack{i=0 \\ i\neq n}}^{N-1} \omega^{j_i t_i} \omega^{-k_i s_i} \omega^{j_n t_n} \sum_{k_n=0}^{d-1} \omega^{-k_n s_n} \\
&= 0.
\end{aligned} \tag{4.21}$$

The same result is obtained if any component t_n of the base-d representation of t is non-zero. Only if $s = t = 0$ does the sum not vanish. In this case, all terms in the sum are equal to 1 and performing the sums yields the result d^{2N}. As a direct consequence, we find for the scalar product between any two row vectors $\vec{A}^{(N)}_{(s,t)}$ and $\vec{A}^{(N)}_{(u,v)}$,

$$\begin{aligned}
\vec{A}^{(N)}_{(s,t)} \cdot \vec{A}^{(N)}_{(u,v)} &= \sum_{j,k=0}^{d^N-1} \omega^{\vec{j}\cdot\vec{t}-\vec{k}\cdot\vec{s}} \omega^{-\vec{j}\cdot\vec{v}+\vec{k}\cdot\vec{u}} \\
&= \sum_{j,k=0}^{d^N-1} \omega^{\vec{j}\cdot(\vec{t}-\vec{v})-\vec{k}\cdot(\vec{s}-\vec{u})} \\
&= d^{2N} \delta_{s,u} \delta_{t,v},
\end{aligned} \tag{4.22}$$

which corresponds to the sum over the row $\vec{A}^{(N)}_{(s-u,t-v)}$.

From Eq. (4.19), it follows that for any row vector $\vec{A}^{(N)}_{(s,t)}$, there is another row vector $\vec{A}^{(N)}_{(d^N-s,d^N-t)}$ whose entries are the complex conjugate of the former, i.e.,

$$\begin{aligned} A^{(N)}_{(s,t),(j,k)} &= \omega^{\vec{j}\cdot\vec{t}-\vec{k}\cdot\vec{s}} = \left(\omega^{-\vec{j}\cdot\vec{t}+\vec{k}\cdot\vec{s}}\right)^* \\ &= \left(A^{(N)}_{(-s,-t),(j,k)}\right)^* = \left(A^{(N)}_{(d^N-s,d^N-t),(j,k)}\right)^*. \end{aligned} \tag{4.23}$$

4.2.4 *The particular solution and construction of a decoupling scheme*

With our knowledge of the scalar products of $A^{(N)}$'s row vectors, we can conclude that a particular solution to the linear system (4.18) is given by

$$\vec{e}_r = \frac{1}{d^{2N}} \left(A^{(N)}_{\mathcal{K}}\right)^\dagger \cdot \vec{r}, \tag{4.24}$$

since $\frac{1}{d^{2N}} A^{(N)}_{\mathcal{K}} \left(A^{(N)}_{\mathcal{K}}\right)^\dagger = \mathbb{1}_{\mathcal{K}}$. This particular solution is real-valued because for any entry of the vector $\vec{e}_r$, we find with the help of the Hermitian condition (4.17)

$$\begin{aligned} (\vec{e}_r)_{(s,t)} &= \frac{1}{d^{2N}} \sum_{(j,k)\in\mathcal{K}} \left(A^{(N)}_{(s,t),(j,k)}\right)^* \frac{\nu_{j,k}}{\mu_{j,k}} \\ &= \frac{1}{d^{2N}} \sum_{(j,k)\in\mathcal{K}} \frac{1}{2}\Bigg[\left(A^{(N)}_{(s,t),(j,k)}\right)^* \frac{\nu_{j,k}}{\mu_{j,k}} \\ &+ \left(A^{(N)}_{(d^N-s,d^N-t),(d^N-j,d^N-k)}\right)^* \frac{\nu_{d^N-j,d^N-k}}{\mu_{d^N-j,d^N-k}}\Bigg] \\ &= \frac{1}{2d^{2N}} \sum_{(j,k)\in\mathcal{K}} \Bigg[\left(A^{(N)}_{(s,t),(j,k)}\right)^* \frac{\nu_{(j,k)}}{\mu_{(j,k)}} \\ &+ A^{(N)}_{(s,t),(j,k)} \left(\frac{\nu_{j,k}}{\mu_{j,k}}\right)^* \Bigg]. \end{aligned} \tag{4.25}$$

The expression in brackets in (4.25) is of the form $c + c^*$ and is therefore real-valued. Adding a solution of the homogeneous equation $A_{\mathcal{K}} \cdot \vec{e}_0 = 0$ to $\vec{e}_r$ yields again a solution of the linear system of Eq. (4.18). From the scalar products in Eq. (4.22), we can conclude that any row vector $\vec{A}_{(j,k)}$, $(j,k) \notin \mathcal{K}$ is a solution of the homogeneous system of equations. Therefore, the most general solution of the linear system of equations is given by

$$\vec{e} = \frac{1}{d^{2N}} A^\dagger_{\mathcal{K}} \cdot \vec{r} + \sum_{(j,k)\notin\mathcal{K}} \alpha_{(j,k)} \vec{A}_{(j,k)}. \tag{4.26}$$

As $(0,0) \notin \mathcal{K}$, this construction allows us to find at least one real-valued and non-negative solution of the form $\vec{e} = \vec{e}_r + \alpha\vec{A}_{(0,0)}$ with α chosen so that all entries in $\vec{e}$ are non-negative. Approximating the real values by rational numbers allows us to construct a decoupling scheme from $\vec{e}$, as explained in Sec. 3.2.2.

5 IMPERFECTIONS IN DECOUPLING CONTROLS

So far, we have only considered the ideal approximation of instantaneous unitary control pulses. This assumption is a good starting point for constructing decoupling schemes, as it makes the analysis of the expected system behaviour relatively easy. However, it is clear that these kinds of controls cannot exist in practice.

In actual experiments, any kind of decoupling control is described by an additional time-dependent Hamiltonian, as indicated in Eq. (2.2). In practice, this Hamiltonian is switched on for a short duration, following a certain pulse shape, and then switched off again. This is done in such a way that the time evolution due to this control Hamiltonian alone would ideally be identical to the unitary pulse we were trying to achieve. However, this means that the pulse has a finite implementation time, during which the pulse will be disturbed. For one, it is acting together with the system Hamiltonian H_0, and since these two Hamiltonians do not commute in general, the pulse is disturbed. Likewise, experimental imperfections may occur which could mean a deviation of the intended pulse shape or additional environmental interactions not taken into account.

These issues affect and limit the achievable fidelity of our decoupling procedures. Furthermore, our simple assumption that higher orders of the average Hamiltonian $\overline{H}$ could be dealt with by choosing the pulse distance τ small enough no longer holds. Since the now imperfect controls introduce additional errors to the system, there is a certain threshold at which point further reducing τ introduces more errors than we correct.

Fortunately, there are ways to deal with these imperfections. The errors introduced by these bounded controls (as opposed to bang-bang control) can be analysed in the resulting average Hamiltonian. Viola and Knill [VK03] showed that they can be suppressed in first order under certain conditions by choosing an appropriate decoupling sequence. Such carefully crafted decoupling schemes can be called self-decoupling since they are robust against errors in the controls. We will have a look at their results and will also show an extension to higher-order self-decoupling sequences.

Bounded controls are a form of systematic error in the controls. However, in experiments we are typically also confronted with statistical errors. In [KL05], a jitter pulse with uniformly distributed random parameters was introduced, and its effects on a concatenated dynamical decoupling sequence examined. We will investigate a different stochastic noise model where the decoupling pulses are subject

to a time-dependent uncertainty. We will derive and analyse the time evolution under this stochastic noise and look at the effects it has on decoupling procedures on a number of exemplary scenarios.

The outline of this chapter is as follows. In Sec. 5.1 we review the Eulerian path decoupling method introduced in [VK03] to deal with bounded controls. These results are then extended to higher-order sequences. In Sec. 5.2 we introduce our stochastic noise model. We derive the resulting time evolution with the help of Ito calculus. In section 5.3 we explore the effects of our noise model on a few exemplary systems both in finite and infinite-dimensional Hilbert spaces. Several higher-order self-decoupling sequences are collected in App. A.

5.1 SELF-DECOUPLING CONTROL SEQUENCES

In this section we look at systematic errors in decoupling controls, which regularly arise when the controls are bounded and not instantaneous. Unsurprisingly, these errors degrade the performance of dynamical decoupling. However, decoupling sequences exist which are robust against such orders to a certain extent. We call these sequences self-decoupling or self-stabilizing as they decouple their own errors up to a certain order. The first sequences of this kind were presented in [VK03]. Here, we develop additional higher-order self-stabilizing sequences.

5.1.1 *The error of bounded controls*

In the limit of instantaneous controls, we treat each decoupling pulse as a unitary operator P_j, and a decoupling sequence consists of several such pulses applied to the system at certain times. This aproach is very convenient for the construction and analysis of decoupling schemes. In practice, however, the implementation of the pulses takes a certain amount of time and is implemented with an additional control Hamiltonian, as in Eq. (2.2). Our control pulses P_j can then be written as

$$P_j = U_{P_j}(t_{P_j}), \quad U_{P_j}(t) = \mathcal{T}\exp\left(-i\int_0^t H_{P_j}(t')dt'\right), \tag{5.1}$$

where the pulse is implemented by a pulse-specific Hamiltonian $H_{P_j}(t)$ and lasts a pulse-specific time t_{P_j}.

The error comes from the fact that this control Hamiltonian $H_{P_j}(t)$ does not act alone, since we generally still have the system Hamilto-

nian H_0 to consider. We therefore get a disturbed pulse $\tilde{p}_j$, which is given as

$$\begin{aligned}\tilde{p}_j &= \mathcal{T}\exp\left(-i\int_0^{t_{p_j}}(H_{p_j}(t)+H_0)dt\right)\\ &= p_j p_j^\dagger \mathcal{T}\exp\left(-i\int_0^{t_{p_j}}(H_{p_j}(t)+H_0)dt\right)\\ &= p_j \mathcal{T}\exp\left(-i\int_0^{t_{p_j}} U_{p_j}^\dagger(t) H_0 U_{p_j}(t)dt\right)\\ &\equiv p_j e^{-i\Phi_j}. \end{aligned} \tag{5.2}$$

We made use of Eq. (2.5) to separate the imperfect pulse into the ideal pulse p_j and an error operator, which we formally denote as $e^{-i\Phi_j}$. We can do a Magnus expansion on the pulse error $\Phi_j = \Phi_j^{[0]} + \Phi_j^{[1]} + \ldots$, where the lowest order is given by

$$\Phi_j^{[0]} = \int_0^{t_{p_j}} U_{p_j}^\dagger(t) H_0 U_{p_j}(t)dt. \tag{5.3}$$

If we now replace the pulses p_j in Eq. (2.19) with the imperfect pulses $\tilde{p}_j$, then we arrive at the following time evolution after M pulses

$$\begin{aligned}U(T=M\tau) =& p_M e^{-i\Phi_M} e^{-iH_0\tau} p_{M-1} e^{-i\Phi_{M-1}} e^{-iH_0\tau}\\ &\cdots e^{-iH_0\tau} p_1 e^{-i\Phi_1} e^{-iH_0\tau}\\ =& e^{-ig_{M-1}^\dagger \Phi_M g_{M-1}} e^{-ig_{M-1}^\dagger H_0 g_{M-1}\tau}\\ &\cdots e^{-ig_1^\dagger \Phi_2 g_1} e^{-ig_1^\dagger H_0 g_1 \tau} e^{-ig_0^\dagger \Phi_1 g_0} e^{-ig_0^\dagger H_0 g_0 \tau}\\ &\equiv e^{-i\overline{H}T}, \end{aligned} \tag{5.4}$$

where the toggling operators are still $g_j = p_j \cdots p_1 p_0$ and we assume for convenience that $g_M = g_0 = \mathbb{1}$ and thus $p_0 = \tilde{p}_0 = \mathbb{1}$. We further assume that all pulses are equidistant, i.e. $\tau_j = \tau$. If we now look at the average Hamiltonian $\overline{H}$ for this time evolution with the pulse errors, we find for the lowest order

$$\overline{H}^{[0]} = \frac{1}{M}\sum_{j=0}^{M-1} g_j^\dagger H_0 g_j + \frac{1}{T}\sum_{j=0}^{M-1} g_j^\dagger \Phi_{j+1}^{[0]} g_j. \tag{5.5}$$

We see that even in the lowest order we get an additional term from the pulse errors. This means that even though a particular decoupling scheme $\{g_j\}$ may fulfil the original decoupling condition (2.24), these pulse errors remain and thus affect decoupling performance.

5.1.2 *A single-qubit self-stabilizing decoupling sequence*

From the structure of Eq. (5.5) we see that the pulse error terms are very similar to the terms involving the Hamiltonian H_0. This immediately leads to the question if we can design a decoupling scheme in

a way that it removes these terms in the lowest order. We call such a scheme self-decoupling or self-stabilizing. However, sandwiched in-between the g_j the pulse errors $\Phi_{j+1}^{[0]}$ are not all the same, which makes them more difficult to decouple than H_0. Indeed, the pulse errors stem from the actual pulses p_j, which depend on the order of the operators g_j in the scheme, so for these pulse errors the order in which the operators g_j are placed matters. As a consequence, constructing a self-decoupling scheme in general may be very hard or even impossible. Let us therefore focus on a specific scenario, namely that of a single qubit which we want to decouple completely ($H_{id} = 0$). This is currently the most relevant scenario in experiments.

For a single qubit, there is a simple decoupling scheme which can eliminate any Hamiltonian in the lowest order. It is formed by the operators

$$\{g_j\}_{j=0}^{3} = \{\sigma_j\}_{j=0}^{3} = \{\mathbb{1}, \sigma_1, \sigma_2, \sigma_3\}. \tag{5.6}$$

Since any (traceless) Hermitian operator on $\mathcal{H} = \mathbb{C}^2$ can be written as a linear combination of the Pauli operators σ_j, it is easy to verify that this decoupling scheme can indeed eliminate any Hamiltonian in the lowest order (2.24). For the pulses p_j needed to implement this scheme, we can use any two of the Pauli operators. For example, the pulse sequence

$$g_0 = \mathbb{1} \overset{p_1=\sigma_1}{\longrightarrow} \sigma_1 \overset{\sigma_2}{\longrightarrow} \sigma_3 \overset{\sigma_1}{\longrightarrow} \sigma_2 \overset{\sigma_2}{\longrightarrow} \mathbb{1} \tag{5.7}$$

is a suitable implementation. Since the pulses are repeating and we can assume that identical pulses produce (at least approximately) the same error, this means that we only need to deal with the error operators Φ_1 and Φ_2 in Eq. (5.5). Now consider the following extended sequence:

$$\mathbb{1} \overset{\sigma_1}{\longrightarrow} \sigma_1 \overset{\sigma_2}{\longrightarrow} \sigma_3 \overset{\sigma_1}{\longrightarrow} \sigma_2 \overset{\sigma_2}{\longrightarrow} \mathbb{1} \overset{\sigma_2}{\longrightarrow} \sigma_2 \overset{\sigma_1}{\longrightarrow} \sigma_3 \overset{\sigma_2}{\longrightarrow} \sigma_1 \overset{\sigma_1}{\longrightarrow} \mathbb{1} \tag{5.8}$$

It consists of $M = 8$ pulses, and it is clearly just the original decoupling scheme applied twice in a slightly different order. So it still fulfils the decoupling condition (2.24). However, look closely at the decoupling operator g_j preceding each pulse p_j. If we insert this particular pulse order into Eq. (5.5), we get

$$\overline{H}^{[0]} = \frac{2}{8}\sum_{j=0}^{3} \sigma_j H_0 \sigma_j + \frac{1}{T}\sum_{j=0}^{3} \sigma_j \Phi_1^{[0]} \sigma_j + \frac{1}{T}\sum_{j=0}^{3} \sigma_j \Phi_2^{[0]} \sigma_j = 0. \tag{5.9}$$

Now all three Hermitian operators H_0, $\Phi_1^{[0]}$ and $\Phi_2^{[0]}$ are inside the full original decoupling scheme (5.6) and thus all three are eliminated in this lowest order. Notice, however, that unlike before, the order of the scheme operators g_j in (5.8) matters now even in the lowest order. It is therefore appropriate to speak of a decoupling sequence to emphasize this fact.

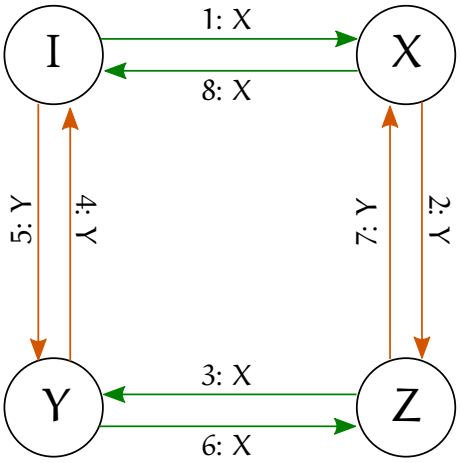

Figure 5.1: Self-stabilizing sequences can be constructed as a Eulerian path. The toggling operators g_j form the nodes of the graph, while the pulses p_j are directed edges which implement transitions between the toggling operators. In a Eulerian path, all edges must be visited exactly once. This figure shows one particular Eulerian path for the single-qubit annihilator scheme.

5.1.3 *Eulerian path decoupling*

As it turns out, the decoupling sequence (5.8) has an intuitive visual representation. If we consider the decoupling operators g_j as the nodes of a graph and connect these with directed edges formed by the pulses σ_1 and σ_2, then our self-decoupling sequence is simply a Eulerian path along this graph. In a Eulerian path, all edges of the graph are visited exactly once. Figure 5.1 shows the resulting graph along with the Eulerian path. The depicted path is not the only possible Eulerian path. Picking an alternative path results in an alternative self-decoupling sequence.

This connection between self-decoupling sequences and Eulerian paths was first published by Viola in 2003 [VK03]. It results in a construction method for self-decoupling schemes which is more general than the single-qubit case. Consider a finite set of operators $\Gamma = \{p_j\}_{j=0}^{K-1}$ which generate a finite group $\mathcal{G} = \{g_j\}_{j=0}^{M-1}$, where each element in $\mathcal{G}$ can be written as an ordered product of operators in Γ. (We ignore possible phase factors, so g_j and $e^{i\varphi}g_j$ are considered the same group element.) As an example, $\Gamma = \{\sigma_1, \sigma_2\}$ generates the group $\mathcal{G} = \{\mathbb{1}, \sigma_1, \sigma_2, \sigma_3\}$. The Cayley graph $G(\mathcal{G}, \Gamma)$ of $\mathcal{G}$ with respect to the generators Γ visualizes the generation of all group elements of $\mathcal{G}$ by the generators p_j. The group elements form the vertices of the graph, and there is a directed edge connecting g_j and g_k if and only if $g_k = p_i g_j$. Each vertex has thus K outgoing edges, and the total number of edges is KM. Each of the generators p_j generates exactly one of the outgoing edges of each vertex g_j.

Every Cayley graph $G(\mathcal{G}, \Gamma)$ possesses at least one Eulerian cycle which visits every edge in the graph exactly once. If we take such a Eulerian cycle and use it as a decoupling sequence, then by construction the lowest order of the resulting average Hamiltonian is given by

$$\overline{H}^{[0]} = \frac{1}{M} \sum_{j=0}^{M-1} g_j^\dagger H_0 g_j + \frac{1}{T} \sum_{k=0}^{K-1} \sum_{j=0}^{M-1} g_j^\dagger \Phi_k^{[0]} g_j. \tag{5.10}$$

For the group $\mathcal{G}$ we can define a subspace $\Omega \subseteq B(\mathcal{H})$ of traceless operators on the Hilbert space $\mathcal{H}$ for which

$$\sum_{j=0}^{M-1} g_j^\dagger E g_j = 0 \quad \forall E \in \Omega. \tag{5.11}$$

If H_0 and all the pulse errors $\Phi_j^{[0]}$ are elements of this subspace Ω, then by Eq. (5.10) any Eulerian path on $G(\mathcal{G}, \Gamma)$ is a self-decoupling sequence.

5.1.4 *Higher-order self-decoupling sequences and numerical results*

When talking about the order of decoupling, so far we considered the lowest order of the Magnus expansion of $\overline{H}$ which remains as an error. However, in the case of imperfect controls, it makes sense to distinguish between the errors from the original Hamiltonian interaction and the pulse errors. Generally, we can write

$$\overline{H} \in \mathcal{O}(\|H_0\tau\|_{op}^{\omega_H+1}) + \mathcal{O}(\|\Phi_{max}\|_{op}^{\omega_\Phi+1}) + \mathcal{O}(\|H_0\tau\|_{op} \cdot \|\Phi_{max}\|_{op}), \tag{5.12}$$

where Φ_{max} is the pulse error with the largest norm. In this formulation, a decoupling scheme decouples the Hamiltonian H_0 to ω_H-th order and the pulse error to ω_Φ-th order. There are also mixed terms which are usually not so easy to decouple.

The decoupling sequences produced by the Eulerian path method generally only decouple the pulse errors to the first order ($\omega_\Phi = 1$). There is no known general construction method for sequences which decouple higher orders of the pulse errors. However, for the single qubit case, such sequences can be found with the help of a computer search program. A method that searches for an $\omega_\Phi + 1$-th order self-decoupling sequence by creating candidate sequences from lower-order self-decoupling sequences was developed in [BFAJ15]. Candidates are generated by concatenating two different ω_Φ-th order sequences. Different sequences of the same order ω_Φ can be constructed by cyclic permutations, sequence reversal and swapping of the involved pulse operators σ_1 and σ_2. We then need to check the self-decoupling order of each candidate. On the Hilbert space of the

single qubit, we can express the Hamiltonian H_0 and the pulse errors Φ_j in the most general form [1] as

$$H_0 = \sum_{i=1}^{3} h_i \sigma_i, \quad \Phi_j = \sum_{i=1}^{3} \alpha_{ji} \sigma_i. \tag{5.13}$$

If we insert these expresions into the full time evolution (5.4), a symbolic calculation on a computer can tell us the occurring powers of the coefficients h_i and α_{ji}. The lowest power of any of the h_i indicates $\omega_H + 1$, and the lowest power of any of the α_{ji} gives $\omega_\Phi + 1$.

It is not clear whether this approach produces decoupling sequences of arbitrary order, but we were able to produce sequences for smaller orders ω_Φ [BFAJ15]. For example, a second order self-decoupling sequence is given by

$$\begin{aligned} &\mathbb{1} \xrightarrow{\sigma_2} \sigma_2 \xrightarrow{\sigma_2} \mathbb{1} \xrightarrow{\sigma_1} \sigma_1 \xrightarrow{\sigma_2} \sigma_3 \xrightarrow{\sigma_1} \sigma_2 \xrightarrow{\sigma_1} \sigma_3 \xrightarrow{\sigma_2} \sigma_1 \xrightarrow{\sigma_1} \\ &\mathbb{1} \xrightarrow{\sigma_2} \sigma_2 \xrightarrow{\sigma_1} \sigma_3 \xrightarrow{\sigma_2} \sigma_1 \xrightarrow{\sigma_2} \sigma_3 \xrightarrow{\sigma_1} \sigma_2 \xrightarrow{\sigma_2} \mathbb{1} \xrightarrow{\sigma_1} \sigma_1 \xrightarrow{\sigma_1} \mathbb{1} \end{aligned} \tag{5.14}$$

Additional self-decoupling sequences of up to order $\omega_\Phi = 9$ in the pulse errors are listed in App. A. Due to the sequence length doubling from order to order in this construction method, higher-order schemes will quickly become impractical, even if they could be constructed by this approach.

Note that the mixed terms in Eq. (5.12) are in general not decoupled by these higher-order schemes. At first sight one might question then if they even offer any benefit over the first-order self-decoupling sequences. However, the mixed terms, like the errors from H_0, scale with the pulse distance τ and can thus potentially be made quite small. By reducing τ far enough, the pulse errors become dominant, and then higher-order self-decoupling sequences will perform better.

In order to demonstrate the effectiveness of the self-decoupling sequences compared to a regular decoupling scheme, we ran some numerical simulations. In the simulation scenario, we consider a single qubit coupled to a bath of 7 additional qubits. The system Hamiltonian is of the form

$$H_0 = \omega \sigma_3^{(1)} + \lambda \sum_{j=2}^{8} \left(\sigma_1^{(1)} \sigma_1^{(j)} + \sigma_2^{(1)} \sigma_2^{(j)} \right). \tag{5.15}$$

The qubit is prepared in the superposition $(|0\rangle + |1\rangle)/\sqrt{2}$, which we would like to protect for as long as possible. For the pulse errors of the decoupling pulses σ_1 and σ_2, we use a rather simple model

$$\Phi_1 = e^{-i\theta\sigma_1}, \quad \Phi_2 = e^{-i\theta\sigma_2}, \tag{5.16}$$

1 Technically, either of those operators could also be coupled to an environment, however, for the decoupling orders, only their structure on the qubit space is relevant.

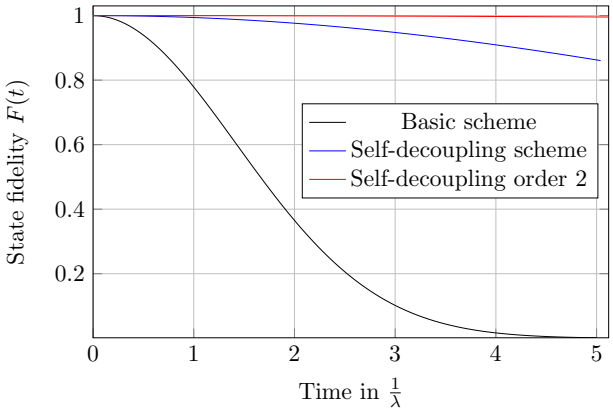

Figure 5.2: Numerical results for the fidelity of a single-qubit state coupled to a bath of additional qubits, as specified by the Hamiltonian (5.15). The results show the performances of the original decoupling scheme as well as the first- and second-order self-decoupling sequences with faulty decoupling pulses. We used $\omega = 10\lambda$, a pulse error of $\theta = 0.02\pi$ and a pulse distance of $\tau = 0.01/\lambda$.

which can be interpreted as a systematic rotation error in these pulses. For the simulation, we set $\omega = 10\lambda$ and $\theta = 0.02\pi$. Figure 5.2 shows the numerical results of the state fidelity obtained for the original annihilator scheme (5.6) as well as the first-order (5.8) and second-order (5.14) self-decoupling sequences. We can see that the fidelity with the original scheme very quickly drops to 0, whereas the self-decoupling sequences can maintain higher fidelities for a longer time. As expected, the second-order self-decoupling sequence performs better than the first-order one. A pulse distance of $\tau = 0.01/\lambda$ was used for all three decoupling sequences.

5.2 INFLUENCE OF STOCHASTIC NOISE ON DYNAMICAL DECOUPLING

In this section we investigate a different source of imperfection in the dynamical decoupling controls, where the pulses are described by a linear quantum stochastic differential equation with a standard Wiener process. For this model, we derive the generator of the time evolution and study its form in the limit of continuous control, which allows us to predict the robustness of different decoupling sequences against decoherence in our error model. Numerical simulations for finite numbers of pulses are also provided. While the model is phenomenological in nature, it is our hope that the results can help gain a deeper understanding of certain real-world decoupling procedures. For instance, a recent experimental publication [PSK+13] demonstrated, for different pulse sequences, that individual pulse

imperfections can accumulate, but also compensate each other. Our model offers one possible explanation of these findings.

5.2.1 *Decoupling pulses with stochastic noise*

For the following treatment, let us return to the basic principles of dynamical decoupling with instantaneous pulses, as outlined in Sec. 2.2. In the following we assume that the apparatus implementing the decoupling pulses p_j causes a stochastic error over time to the controlled system. Mathematically we introduce this error by means of an Ito stochastic differential equation for the applied unitary pulses:

$$dp_j(t) = \left(-\frac{\gamma}{2}B^2 dt - i\sqrt{\gamma}B dW_t\right) p_j(t), \quad p_j(0) = p_j, \tag{5.17}$$

where $p_j(0)$ is the original ideal pulse, the parameter γ stands for the strength of the disturbance and W_t is a classical Wiener process. The operator B stands for a physical quantity, i.e. a self-adjoint operator, which describes the nature of the disturbance. B^2 is always a positive operator [Rud91]. W_t is defined as a Gaussian random variable with expectation value 0 and variance t:

$$\begin{aligned} \langle W_t \rangle &= 0, \\ \langle W_t^2 \rangle - \langle W_t \rangle^2 &= t. \end{aligned} \tag{5.18}$$

In order to work with this equation we employ the quantum Ito rules [2] in the sense that the differential equation deals with operators, however the used Wiener process is still a classical and not an operator-valued process.

We need to ensure that the differential equation (5.17) always results in a unitary operator for $t > 0$. Using the properties of the Wiener process

$$dW_t^2 = dt, \; dW_t^n = 0, \, n > 2, \tag{5.19}$$

a straight-forward calculation yields

$$\begin{aligned} d\left(p_j^\dagger(t)\, p_j(t)\right) &= dp_j^\dagger(t)\, p_j(t) + p_j^\dagger(t)\, dp_j(t) + dp_j^\dagger(t)\, dp_j(t) \\ &= 0 = d\left(p_j(t)\, p_j^\dagger(t)\right), \end{aligned} \tag{5.20}$$

which means that the solution $p_j(t)$ is unitary for all $t \geqslant 0$. The term $dp_j^\dagger(t)\, dp_j(t)$ is a consequence of stochastic differentiation rules, see also Eq. (5.25).

Note that the time parameter t is not meant to imply the implementation time of a finite-width pulse, but rather an increasing uncertainty in the instantaneous pulse p_j as time moves forward. Our

2 In mathematics, quantum Ito's formula is related to stochastic integrals for operator-valued processes, see [Par92].

model ensures that the distance between the ideal pulse p_j and the average of $p_j(t)$ (over a large sample size) increases with t. From the property $\langle dW_t \rangle = 0$ it follows for the averaged pulse

$$\frac{d\langle p_j(t)\rangle}{dt} = -\frac{\gamma}{2} B^2 \langle p_j(t)\rangle. \tag{5.21}$$

The equation describes a decaying effect, due to the fact that B^2 is positive. As an example, consider B^2 to be the identity operator and the distance between two operators to be quantified by the operator norm (2.16). In this case we have

$$\|p_j - \langle p_j(t)\rangle\|_{op} = \| \left(1 - e^{-\frac{\gamma t}{2}}\right) p_j\|_{op} = 1 - e^{-\frac{\gamma t}{2}}. \tag{5.22}$$

5.2.2 *Time evolution with stochastic noise*

We now derive the time evolution of the full system generated by a Hamiltonian H_0 and N decoupling pulses, applied evenly over the whole interaction time t with a distance between pulses of $\tau = t/N$ and the stochastic noise as described by Eq. (5.17). After time t the time evolution is given by the unitary operator

$$U_N(t) = \prod_{k=0}^{N-1} p_{N-k}(\tau/N) e^{-iH_0\tau}. \tag{5.23}$$

The time parameter of $\frac{\tau}{N}$ for the pulses is a mathematical consequence of our intended noise: we want to study a global noise induced by the pulse-generating device which is governed by W_t. Mathematically we express the error by partitioning it over the N pulses applied to the system, and due to the particular rescaling properties of the Wiener process, $W_t = 1/\sqrt{a} W_{at}$ for $a > 0$, we therefore have

$$e^{-iW_t} = e^{-iNW_{t/N^2}} = \left(e^{-iW_{\tau/N}}\right)^N. \tag{5.24}$$

Our model is phenomenological in nature. Since all pulses share the same random variable W_t, they will introduce the same error to the system during a single run of the experiment. However, the error will be different for subsequent repetitions of the experiment. As such, this model captures imperfections due to changing conditions between experimental runs, which cannot typically be avoided perfectly or might even happen deliberately, e.g. through necessary recalibrations of the experimental apparatus.

Our aim is to calculate the derivative $dU_N(t)$ in order to determine the time evolution of the system with N stochastic pulses applied. We use the Ito formula for an N-term product which states

$$\begin{aligned} d(A_1 A_2 .... A_N) &= d(A_1) A_2 .... A_N + ... + A_1 A_2 .... d(A_N) \\ &+ \sum_{\substack{\text{all possible} \\ \text{pairings}}} A_1 ... d(A_i) ... d(A_j) ... A_N. \end{aligned} \tag{5.25}$$

We introduce the operators

$$u_j(\tau) = \prod_{k=0}^{j-1} p_{N-k}(\tau/N) e^{-iH_0\tau}, \tag{5.26}$$

and with these, we find for the time derivative of the evolution operator

$$dU_N(t) = \Big(-iH_N(t)dt - i\sqrt{\gamma}B_N(t)dW_t - \frac{\gamma}{2}C_N(t)dt \Big) U_N(t), \tag{5.27}$$

where

$$H_N(t) = \frac{1}{N}\sum_{k=0}^{N-1} u_k(\tau) p_{N-k}(\tau/N) H_0 p^\dagger_{N-k}(\tau/N) u^\dagger_k(\tau), \tag{5.28}$$

$$B_N(t) = \frac{1}{N}\sum_{k=0}^{N-1} u_k(\tau) B u^\dagger_k(\tau), \tag{5.29}$$

$$\begin{aligned} C_N(t) =& \frac{1}{N^2}\sum_{k=0}^{N-1} u_k(\tau) B^2 u^\dagger_k(\tau) \\ &+ \frac{2}{N^2}\sum_{j=0}^{N-2}\sum_{k=j+1}^{N-1} u_j(\tau) B u^\dagger_j(\tau) u_k(\tau) B u^\dagger_k(\tau), \end{aligned} \tag{5.30}$$

$H_N(t)$ is the Hamiltonian operator generating the error-free time evolution. The operators $B_N(t)$ and $C_N(t)$ express the error due to the stochastic noise and are related as

$$\frac{C_N(t) + C^\dagger_N(t)}{2} = B^2_N(t). \tag{5.31}$$

5.2.3 *The limit of continuous control*

We are particularly interested in the limit of $N \to \infty$, the limit of continuous control. The time evolution in this limit,

$$d\mathcal{U}(t) = -i\mathcal{H}\mathcal{U}(t)dt - i\sqrt{\gamma}\mathcal{B}\mathcal{U}(t)dW_t - \frac{\gamma}{2}\mathcal{B}^2\mathcal{U}(t)dt, \tag{5.32}$$

with

$$\mathcal{U}(t=0) = \lim_{N\to\infty}\prod_{k=0}^{N-1} p_{N-k}, \tag{5.33}$$

defines the time evolution of any observable $O(t) = \mathcal{U}^\dagger(t) O \mathcal{U}(t)$ and of any density operator $\rho(t) = \mathcal{U}(t)\rho\mathcal{U}^\dagger(t)$. The initial condition $\mathcal{U}(t = 0)$ is a unitary operator due to the fact that unitary operators are

closed under multiplication. Most of the experiments are designed such that $\mathcal{U}(t=0)=\mathbb{1}$. We introduced the following notations

$$\mathcal{U}(t) = \lim_{N\to\infty} U_N(t),\ \mathcal{H} = \lim_{N\to\infty} H_N(t), \tag{5.34}$$

$$\mathcal{B} = \lim_{N\to\infty} B_N(t),\ \mathcal{B}^2 = \lim_{N\to\infty} C_N(t). \tag{5.35}$$

Using the Ito rules, a straight-forward calculation for the dynamical evolution of the density operator yields

$$d\rho(t) = \mathcal{L}\rho(t)dt - i\sqrt{\gamma}\,[\mathcal{B},\rho(t)]\,dW_t, \tag{5.36}$$

where the Kossakowski-Lindblad generator [GKS76, Lin75] is given by

$$\mathcal{L}\rho = -i\,[\mathcal{H},\rho] + \gamma\mathcal{B}\rho\mathcal{B} - \frac{\gamma}{2}\left(\mathcal{B}^2\rho + \rho\mathcal{B}^2\right). \tag{5.37}$$

Let us now turn to our usual case where we have a finite number of repeating pulses in the PDD strategy (compare Sec. 2.1.2). We take a scheme of size M with the cyclic condition $g_M = \mathbb{1}$, which is repeated L times for a total of $N = LM$ pulses. Now, in the continuous control limit $L\to\infty$, we have $\tau\to 0$, and Eqs. (5.28),(5.29) and (5.30) simplify. Specifically, we find for $\mathcal{H}$ and $\mathcal{B}$

$$\mathcal{H} = \frac{1}{M}\sum_{j=0}^{M-1} g_j^\dagger H g_j, \tag{5.38}$$

$$\mathcal{B} = \frac{1}{M}\sum_{j=0}^{M-1} g_j^\dagger B g_j, \tag{5.39}$$

where the g_j are the toggling operators defined in Sec. 2.2. We have thus reproduced our typical decoupling condition known from Eq. (2.24). The structure of $\mathcal{H}$ and $\mathcal{B}$ is formally equivalent and suggests the possibility that a carefully designed decoupling scheme may eliminate both operators.

5.3 EXAMPLES WITH STOCHASTIC NOISE

In this section we study the effects of the stochastic noise from Sec. 5.2 on various quantum systems. First we look at two qubits coupled by a Hamiltonian interaction. Despite this system's simplicity we are able to derive a number of properties of our noise model which carry over to more complex systems. This is demonstrated in our study of an electron spin coupling to a nuclear spin bath. Finally, we briefly look at two coupled harmonic oscillators as an example of a quantum system in an infinite-dimensional Hilbert space.

5.3.1 *Two coupled qubits*

We consider two coupled qubits with energy eigenstates $|0\rangle_i$ and $|1\rangle_i$ ($i \in \{1,2\}$) under the influence of the Hamiltonian

$$H_0 = \frac{\omega}{2}\sigma_3^{(1)} + \frac{\omega}{2}\sigma_3^{(2)} + g\sigma_1^{(1)}\sigma_1^{(2)}, \tag{5.40}$$

with ω the frequency difference between the levels of the qubits and g being the coupling constant between the two qubits. By means of dynamical decoupling we want to protect the evolution of qubit 1 against the effects of the interaction with qubit 2, which induces transitions between the energy eigenstates of the two qubits. Although this model is very primitive from a physical viewpoint, it is very useful to showcase quite a few properties of our noisy decoupling. These properties can then directly be applied to more sophisticated systems.

In order to decouple the two qubits, a single pulse is sufficient. We choose

$$p = \sigma_3^{(1)}, \tag{5.41}$$

which, if repeated in pairs of two pulses, results in two scheme operators $g_1 = p$ and $g_2 = \mathbb{1}$. In the limit of $N \to \infty$ it follows from Eq. (5.38) that

$$\mathcal{H} = \frac{\omega}{2}\sigma_3^{(1)} + \frac{\omega}{2}\sigma_3^{(2)}, \tag{5.42}$$

which is the original model Hamiltonian minus the interaction between the two qubits, just as we intended.

For the self-adjoint error operator B we consider the most general form:

$$\begin{aligned} B &= B_1^{(1)} B_2^{(2)}, \\ B_1 &= (\alpha_0 \mathbb{1} + \alpha_1\sigma_1 + \alpha_2\sigma_2 + \alpha_3\sigma_3), \\ B_2 &= (\beta_0 \mathbb{1} + \beta_1\sigma_1 + \beta_2\sigma_2 + \beta_3\sigma_3), \\ &\quad \alpha_0, \alpha_1, \alpha_2, \alpha_3, \beta_0, \beta_1, \beta_2, \beta_3 \in \mathbb{R}. \end{aligned} \tag{5.43}$$

Let us first study the effects of the error operator B in the limit of continuous control $N \to \infty$. Substituting B into Eq. (5.39) we obtain

$$\mathcal{B} = \left(\alpha_0 \mathbb{1}^{(1)} + \alpha_3\sigma_3^{(1)}\right) B_2^{(2)}. \tag{5.44}$$

This implies the time evolution

$$d\rho = -i\,[\mathcal{H}, \rho]\,dt - \frac{\gamma}{2}\,[\mathcal{B}, [\mathcal{B}, \rho]]\,dt - i\sqrt{\gamma}\,[\mathcal{B}, \rho]\,dW_t. \tag{5.45}$$

We assume an initially separable state $\rho(0) = \rho_1 \otimes \rho_2$, where we try to protect the free evolution of $\rho_1(t)$ governed by the first term of the Hamiltonian (5.40). In the case of ideal unitary pulses ($B = 0$) the

whole system dynamics is governed by the Hamiltonian of Eq. (5.42) (in the limit of $N \to \infty$), so this is indeed achievable. With active errors, the dynamics for $\rho_1(t) = \mathrm{Tr}_2\{\rho(t)\}$, with $\rho(t)$ a solution of Eq. (5.45), will depend on the nature of $\mathcal{B}$, and may display a complicated time evolution.

First, we note that in the case of a specific subset of initial conditions, namely

$$\rho(0) = \rho_1 \otimes \rho_2, \ \forall \rho_1 \in \left\{\rho \,\middle|\, [\rho, \sigma_3] = 0\right\}, \tag{5.46}$$

there is no effect induced by the imperfections. This is a direct consequence of Eq. (5.45) and the form of $\mathcal{B}$ in Eq. (5.44). ρ_2 is taken as an arbitrary density matrix of qubit 2. In the following we consider a simple example for the initial condition

$$\begin{aligned} \rho(0) &= |\Psi\rangle\langle\Psi| \otimes \rho_2, \, |\Psi\rangle = (|0\rangle + |1\rangle)/\sqrt{2}, \\ \rho_2 &= \frac{1}{2}\mathbb{1}, \end{aligned} \tag{5.47}$$

which does not fall into the definition of Eq. (5.46). We determine the fidelity between the ideal evolution of the pure state

$$|\Psi(t)\rangle = e^{-i\omega\sigma_3 t/2}\Big(|0\rangle + |1\rangle\Big)/\sqrt{2} \tag{5.48}$$

and the mixed state $\mathrm{Tr}_2\{\rho(t)\}$ given by

$$F(t) = \sqrt{\langle\Psi(t)|\mathrm{Tr}_2\{\rho(t)\}|\Psi(t)\rangle}. \tag{5.49}$$

In Fig. 5.3, numerical results are presented for characterizing the fidelity as a distance measure of the ideal state evolution and the state emerging from the imperfect decoupling scheme. The average fidelity describes the average over many runs, which must be prepared similarly. From an ensemble of realizations the average fidelity is determined by

$$\bar{F} = \frac{1}{M}\sum_{i=i}^{M} \sqrt{\langle\Psi(t)|\mathrm{Tr}_2\{\rho_i(t)\}|\Psi(t)\rangle}, \tag{5.50}$$

where $\rho_i(t)$ is one realization of Eq. (5.45) and M is the size of the ensemble. The corresponding standard deviation σ_t is given by

$$\sigma_t^2 = \frac{1}{M}\sum_{i=i}^{M} \left(\sqrt{\langle\Psi(t)|\mathrm{Tr}_2\{\rho_i(t)\}|\Psi(t)\rangle} - \bar{F}\right)^2. \tag{5.51}$$

Instead of using algorithms for stochastic evolution, we simply generated several realizations of the Wiener process W_t and substituted into the integrated form of Eq. (5.45). We found that for 1000 different realizations the average fidelity coincides with the analytical solution of

$$\frac{d\rho}{dt} = -i\,[\mathcal{H}, \rho] - \frac{\gamma}{2}\,[\mathcal{B}, [\mathcal{B}, \rho]]\,. \tag{5.52}$$

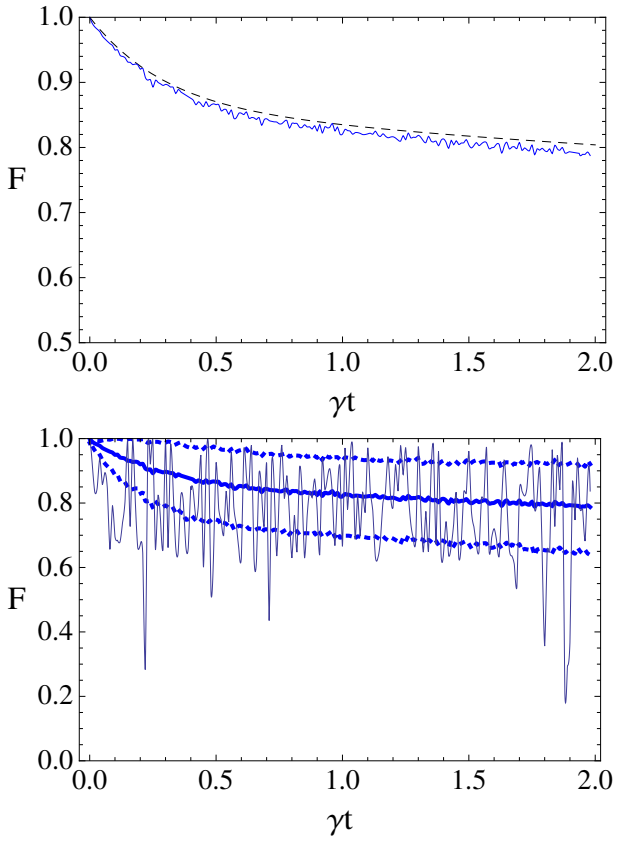

Figure 5.3: Dependence of fidelity on γt. The first figure shows the average over 1000 realizations of Eq. (5.45), where the dashed line gives the analytical result. The second figure shows a single realization of Eq. (5.45), plotted as a solid line. The thick solid line corresponds to the average over 1000 realizations and the thick dotted lines define the standard deviation of the averaged fidelity. The parameters of Eq. (5.44), describing the nature of the error, are set to be $\alpha_0 = \beta_0 = \beta_1 = \beta_2 = \beta_3 = 1$ and $\alpha_3 = 1/2$.

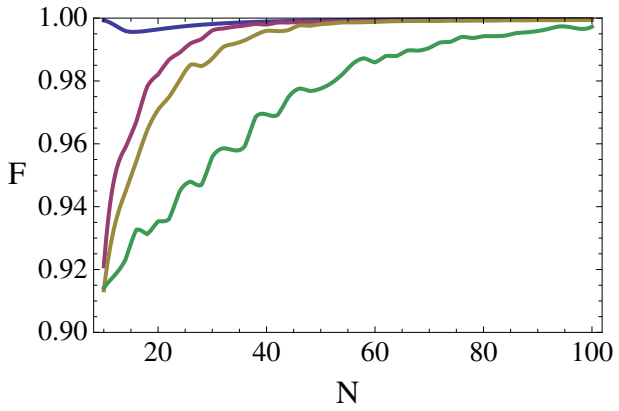

Figure 5.4: Dependence of fidelity on number of pulses. Plotted is the fidelity $F(t)$ over the number of decoupling pulses N. The initial state of qubit 1 is $\rho_1 = |0\rangle\langle 0|$, and the error is chosen to be $B = \sigma_2^{(1)}\sigma_2^{(2)}$. The remaining parameters are chosen as $\omega t = 10$ and $\gamma t \in \{0, 50, 100, 500\}$, where the values of γt are in the order of the highest to lowest graph in the plot.

The figures tell us that even in the limit $N \to \infty$ there is a decay of fidelity over time due to the error $\mathcal{B}$ which is not present in the ideal decoupling scenario. However, as we see in Eq. (5.44), only those parts of the error operator B survive which commute with p. If we choose a different decoupling operator $p = \sigma_y^{(1)}$, then we would find $\mathcal{H} = 0$ and $\mathcal{B} = \left(\alpha_0 \mathbb{1}^{(1)} + \alpha_2 \sigma_2^{(1)}\right) B_2^{(2)}$. Depending on the actual parameter values α_i of B this offers one explanation for fidelity differences between different decoupling operators as observed in experiments.

So far we have only studied the limit $N \to \infty$ which is obviously not achievable in experimental implementations of a dynamical decoupling scheme. In the following, we look at finite numbers of pulses where the noncommuting terms of the error operator B do play a role and reinduce transitions between the two qubits, with a decreasing contribution as N increases. We conducted a series of numerical simulations to capture the effects of the stochastic error for finite numbers of pulses. For the initial state of the first qubit we look at an eigenstate of the Hamiltonian, $|\Psi\rangle = |0\rangle$, and at the superposition $|\Psi\rangle = \frac{1}{\sqrt{2}}(|0\rangle + |1\rangle)$. The state of qubit 2 is the totally mixed state. We investigate cases of commuting and noncommuting error operators, $B = \sigma_3^{(1)}\sigma_3^{(2)}$ and $B = \sigma_2^{(1)}\sigma_2^{(2)}$, respectively. Fig. 5.4 shows results for the case of the eigenstate and a noncommuting error. Plotted is the achieved fidelity (averaged over 1000 runs) after a fixed time t depending on the number of pulses N applied during that time. We can see that for large N the fidelity approaches 1, which is in agreement with our analysis of the limit $N \to \infty$. For smaller N, however,

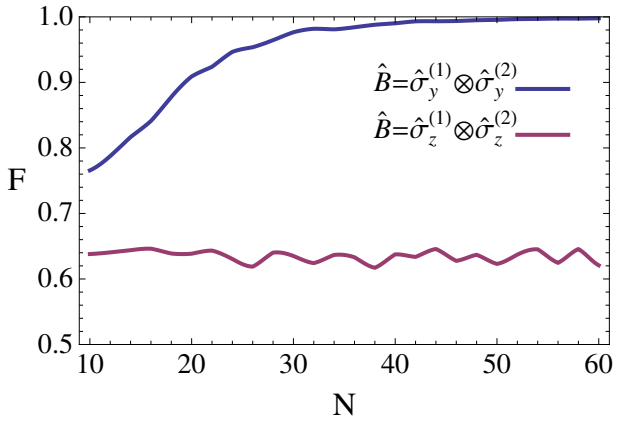

Figure 5.5: Dependence of fidelity on number of pulses. Plotted is the fidelity $F(t)$ over the number of decoupling pulses N. The initial state of qubit 1 is $\rho_1 = \frac{1}{2}(|0\rangle + |1\rangle)(\langle 0| + \langle 1|)$, and the error is chosen to be $B = \sigma_2^{(1)}\sigma_2^{(2)}$ (upper curve) or $B = \sigma_3^{(1)}\sigma_3^{(2)}$ (lower curve). The remaining parameters are chosen as $\omega/g = 10$, $\omega t = 10$ and $\gamma t = 50$.

there is a drop in the fidelity which depends on the strength of the error.

Fig. 5.5 shows results for the simulations which were conducted with the superposition as the initial state. The two depicted plots show the achieved fidelity after a fixed time t depending on the number of pulses N for a noncommuting and commuting B, respectively. In the noncommuting case we approach fidelity 1 with increasing N as expected, however, the drop in fidelity for lower numbers of pulses is stronger than in the case of the eigenstate. In the case of the commuting error we see a constant drop of the fidelity independent of N which is expected, since the decoupling scheme has no effect on the commuting error. The case of a commuting error B acting on an initial eigenstate was not depicted because in this case the error has no effect on the qubit state. The simulation results show that, with increasing N, we approach the dynamics of the continuous control limit which we studied earlier.

5.3.2 *A spin interacting with a bath of nuclear spins*

We now regard a system-environment model where a single electron spin qubit is coupled to K nuclear spins. We consider an interaction Hamiltonian which is given by the Fermi contact hyperfine interaction [SK03, CL04]. Formally we can describe both the electron spin and the nuclear spins as simple qubits, where we label the electron

spin with the index (1) and the nuclear spins with indices from (2) to $(K+1)$. The Hamiltonian of our model is of the form

$$\begin{aligned} H_0 &= \sum_{k=2}^{K+1} A_k \left(\sigma_1^{(1)} \sigma_1^{(k)} + \sigma_2^{(1)} \sigma_2^{(k)} + \sigma_3^{(1)} \sigma_3^{(k)} \right) + \\ &+ \sum_{k=1}^{K+1} \frac{\omega_k}{2} \sigma_3^{(k)} \end{aligned} \tag{5.53}$$

where the hyperfine coupling constant with index k is given by $A_k \sim |\psi(\vec{r}_k)|^2$. $\psi(\vec{r}_k)$ is the electron envelope wave function, evaluated at $\vec{r}_k$, the position of the k^{th} nuclear spin. ω_k is the split frequency for each individual spin qubit. From our perspective we consider the electron spin qubit as the system we want to protect, whereas the nuclear spins should be regarded as an environment whose influence on the electron spin we want to eliminate. Interactions between the nuclear spins are not considered as they have no direct effect on the electron spin.

This model is a natural extension of the two-qubit case we studied in the previous section. The difference is that our system qubit is now coupled to more than one other qubit, and the interaction involves all three Pauli operators. Despite these differences, the results we obtained for the two-qubit case generalize in a natural way. Analogous to Eqs. (5.41) and (5.43), we choose for the decoupling operator p and the error operator B

$$p = \sigma_3^{(1)}, \tag{5.54}$$

$$B = B_1^{(1)} B_2^{(2)} \cdots B_{K+1}^{(K+1)}. \tag{5.55}$$

As we know from the two-qubit model, only those terms in H and B which commute with p survive in the limit $N \to \infty$. Therefore, we find for the effective Hamiltonian

$$\mathcal{H} = \sum_{k=1}^{K+1} \frac{\omega_k}{2} \sigma_3^{(k)} + \sum_{k=2}^{K+1} A_k \sigma_3^{(1)} \sigma_3^{(k)}, \tag{5.56}$$

which, compared to Eq. (5.42), includes the surviving interaction term $\sigma_3 \otimes \sigma_3$. The effective error $\mathcal{B}$ is still equivalent to Eq. (5.44) and is given by

$$\mathcal{B} = \left(\alpha_0 \mathbb{1}^{(1)} + \alpha_3 \sigma_3^{(1)} \right) B_2^{(2)} \cdots B_{K+1}^{(K+1)}. \tag{5.57}$$

As before, initial states of the form of Eq. (5.46) remain unaffected over time in the limit. However, if the electron spin is in a superposition, it will be affected by the surviving $\sigma_3 \otimes \sigma_3$ coupling to the nuclear spins, which means that the achievable state fidelity is limited by this interaction. We ran numerical simulations for an electron spin coupled to 5 nuclear spins for both cases with finite numbers of

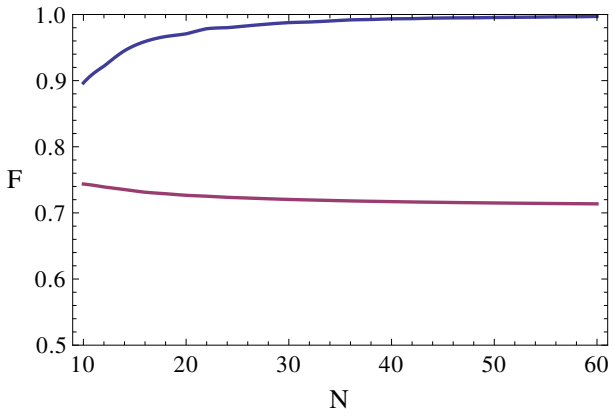

Figure 5.6: Dependence of fidelity on number of pulses for an electron spin coupled to 5 nuclear spins. Plotted is the fidelity F over the number of decoupling pulses N. The upper curve depicts behaviour of the fidelity for the electron spin in the initial state $\rho_1 = |0\rangle\langle 0|$, whereas the lower curve starts with the electron spin in the state $\rho_1 = \frac{1}{2}(|0\rangle + |1\rangle)(\langle 0| + \langle 1|)$. The error is chosen to be $B = \sigma_1^{(1)}\sigma_1^{(2)}\cdots\sigma_1^{(K+1)}$ with $\gamma t = 5$. The remaining parameters are chosen as $\omega t = 2$ and (compare [CL04]) $A_k/\omega = \exp\left[-\left(\frac{k}{5}\right)^{1/3}\right]$.

pulses. As we can see from the results depicted in Fig. 5.6, the eigenstate approaches fidelity 1 for larger numbers of pulses, as predicted for the limit $N \to \infty$. The fidelity of the superposition state, however, is severely limited by the remaining coupling.

In order to get rid of the remaining nuclear spin interaction in $\mathcal{H}$, we need a two-pulse decoupling sequence. We can use the scheme from Eq. (5.6) and implement it with the pulse sequence

$$\sigma_1^{(1)} \to \sigma_3^{(1)} \to \sigma_1^{(1)} \to \sigma_3^{(1)} \to \ldots, \tag{5.58}$$

which means that the cycle length is 4. Looking at the limits and using Eqs. (5.38) and (5.39) with $M = 4$, we now find

$$\mathcal{H} = \mathcal{B} = 0, \tag{5.59}$$

which is independent of the choice of error operator B.

This means that, in the limit $N \to \infty$, this decoupling scheme not only eliminates the influence of the nuclear spins on the electron spin completely, it is also robust against our stochastic noise model. Fig. 5.7 shows the performance of this scheme for both an eigenstate and a superposition state, depending on the number of pulses N. As we see, this scheme is a vast improvement in the superposition case and is able to achieve a fidelity close to 1. For the eigenstate it also approaches a fidelity of 1, however, compared with the single pulse decoupling, it is not an improvement. The lesson here is that it is

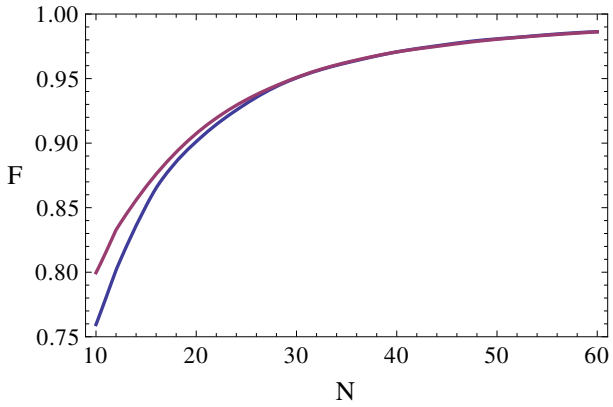

Figure 5.7: Dependence of fidelity on number of pulses for an electron spin coupled to 5 nuclear spins. Plotted is the fidelity F over the number of decoupling pulses N for the case of the two-pulse decoupling scheme. The lower (blue) curve shows results for an eigenstate, whereas the upper (purple) curve corresponds to a superposition state. All parameters are chosen identically to Fig. 5.6.

beneficial to keep decoupling schemes as simple as possible for a specific application.

5.3.3 *Two coupled harmonic oscillators*

So far we discussed in detail the effects of our noise model on systems in finite dimensional Hilbert spaces. In the following, we consider an infinite-dimensional Hilbert space. Due to the added complexity of dealing with infinite Hilbert spaces, we restrict ourselves to investigating the limit of large N only.

Let us consider a model of two coupled quantum harmonic oscillators. We model the system by the Hamiltonian

$$H_0 = \omega_A a^\dagger a + \omega_B b^\dagger b + g\left(a^\dagger + a\right)\left(b^\dagger + b\right), \tag{5.60}$$

where ω_A (ω_B) is the frequency of oscillator A (B) and g is the strength of the interaction. a ($a^\dagger$) and b ($b^\dagger$) are the creation (annihilation) operators of oscillators A and B.

To decouple system A from system B, we can use a decoupling pulse of the form

$$p = e^{i\varphi a^\dagger a} \otimes \mathbb{1}_B, \ \varphi \in (0, \pi], \tag{5.61}$$

a result which will be derived in Sec. 7.2.1. Here we restrict ourselves to the special case $\varphi = \pi$, so that the decoupling pulse is equal to $\mathcal{P}_A \otimes \mathbb{1}_B$, with $\mathcal{P}_A$ the parity operator [VT99] acting on system A. At

the limit $N \to \infty$, the joint system is governed by the Hamiltonian (see Eq. (5.38))

$$\mathcal{H} = \omega_A a^\dagger a + \omega_B b^\dagger b. \tag{5.62}$$

Next, we define the nature of the error by the self-adjoint operator

$$B = \left(a^\dagger a + a^\dagger + a\right) \otimes \mathbb{1}_B. \tag{5.63}$$

Substituting B into Eq. (5.39), we find

$$\mathcal{B} = a^\dagger a \otimes \mathbb{1}_B. \tag{5.64}$$

One observes that in the limit $N \to \infty$ system B evolves freely and system A is governed by

$$\begin{aligned} d\rho_A =& -i\omega_A[a^\dagger a, \rho_A]dt - \frac{\gamma}{2}[a^\dagger a, [a^\dagger a, \rho_A]]dt \\ & - i\sqrt{\gamma}[a^\dagger a, \rho_A]dW_t. \end{aligned} \tag{5.65}$$

Considering the expansion of the density operator into number states $|n\rangle_A$,

$$\rho_A = \sum_{n,m=0}^{\infty} \rho_{n,m}(t)|n\rangle_A\langle m|_A, \tag{5.66}$$

and averaging over all realisations, the time evolution yields the model of a phase-damped oscillator,

$$\frac{d\rho}{dt} = -i\omega_A[a^\dagger a, \rho_A] - \frac{\gamma}{2}[a^\dagger a, [a^\dagger a, \rho_A]], \tag{5.67}$$

which has the solution

$$\rho_{n,m}(t) = e^{-i\omega_A(n-m)t}e^{-(n-m)^2\frac{\gamma t}{2}}\rho_{n,m}(0). \tag{5.68}$$

The coherence between number states is damped, whereas diagonal terms are not affected by the error of the pulse. This shows that prepared number states can be protected in the context of this model. Despite the fact that two harmonic oscillators are decoupled for large numbers of pulses, initially prepared coherent states of system A are dephased by the imperfectness of the pulses.

The model of two coupled harmonic oscillators can be extended to a model where a harmonic oscillator (subsystem) interacts with a collection of independent harmonic oscillators (environment) [CL83]. For the case of $N \to \infty$ the environment and the subsystem can be decoupled completely by repeated application of the unitary pulse defined in Eq. (5.61). As already seen, the pulse error only affects states which are superpositions of number states.

Part II

PRACTICAL APPLICATIONS OF DYNAMICAL DECOUPLING

6

STATE TRANSFER ON QUBIT AND QUDIT NETWORKS

The no-cloning theorem [WZ82] is a central result in quantum information theory. While the impossibility to copy arbitrary quantum states is the very reason that enables quantum cryptography, it is a significant obstacle for quantum computation. Thankfully, we can at least transport quantum information, and thus it is important to develop quantum state transfer protocols which are capable of transferring an arbitrary quantum state within a quantum network from one position to any other. Such quantum state transfer protocols have been developed independently by Bose [Bos03], Nikolopoulos *et al.* [NPL04] and Christandl *et al.* [CDEL04] for linear qubit chains. These *passive* protocols propose specific Hamiltonians governing the dynamics of these chains which implement a state transfer from one end of the chain to the other in a particular interaction time without any additional external control or ancillary quantum systems. A comprehensive introduction to the topic of quantum state transfer and current developments can be found in [NJ13, Kay10].

Although the simplicity of these protocols is very appealing, engineering the necessary non-uniform interaction strengths can be a challenge. Furthermore, they are susceptible to imperfections in the structure of the qubit chain. The effects of diagonal and off-diagonal disorder in the governing system Hamiltonian have been studied for spin chains in [PNL10, YBB10, PSB14]. And while linear qubit chains with nearest neighbour interactions are convenient for exploring basic theoretical aspects of quantum state transfer, experimental implementations typically involve more complicated and higher-dimensional scenarios. A particular arrangement, which can arise naturally in two- or three-dimensional qubit networks, is a qubit chain with a bend around a specific qubit. In such a case additional strong couplings between qubits may arise close to the position of the bend so that simple one-dimensional models with nearest-neighbour couplings no longer describe these situations adequately. Such configurations have been studied recently in detail [NHJ12]. In particular, it has been demonstrated that the additional interactions arising from qubits close to the position of the bend significantly affect quantum state transfer in a detrimental way.

All of these practical problems can, in principle, be attacked with the help of dynamical decoupling. Suppression of disorder effects and unwanted additional couplings as well as engineering the required coupling strengths on the qubit chain are all tasks which are

well within the capabilities we developed in Ch. 3, and in this chapter we will put them to practice. However, the introduction of decoupling will require active control on the network, which may be a problem for longer distance transfers, for which the passive protocols are usually particularly appealing. Therefore, we expect a decoupling approach to be suitable primarily for small to medium-sized qubit networks and particularly for state transfer within a quantum register where single-qubit gates are already available.

The outline of the chapter is as follows. In Sec. 6.1 we will introduce and explain a perfect state transfer protocol on qubit chains. Then, Sec. 6.2 adds an imperfection to this protocol in the form of a bend in the underlying qubit chain. We devise several potential dynamical decoupling schemes to correct this imperfection and present numerical simulations of the performance of these schemes. In Sec. 6.3 we analyze how to engineer the state transfer Hamiltonian from a nearest-neighbour Hamiltonian by means of dynamical decoupling. This example also gives us new insight into how to apply our method of finding decoupling schemes when the search space becomes too large. Finally, in Sec. 6.4, we extend this state transfer protocol to qudit chains and explain how the decoupling schemes of Sec. 6.3 can be applied on qudit systems.

6.1 PERFECT STATE TRANSFER ON QUBIT CHAINS

Let us consider a system of N qubits in a linear chain configuration with nearest-neighbour interactions, such that qubit i interacts only with its direct neighbours $i-1$ and $i+1$. Qubits 1 and N mark the ends of the chain. In the following, we restrict ourselves to the study of an XX type nearest-neighbour interaction on the qubit chain, which in the ideal case is given by a Hamiltonian

$$H_{PST} = \sum_{i=1}^{N} \frac{\omega_i}{2}\sigma_3^{(i)} + \sum_{i=1}^{N-1} J_i \left(\sigma_1^{(i)}\sigma_1^{(i+1)} + \sigma_2^{(i)}\sigma_2^{(i+1)}\right). \tag{6.1}$$

Here, the eigenenergies ω_i and coupling strengths J_i are determined by the specific implementation of the qubit chain. It has been shown that for specific choices of the coupling strengths J_i this Hamiltonian can transfer a single excitation from one end of the chain to the other one and thus can be used for purposes of perfect state transfer along the qubit chain. A particular choice for the coupling strengths J_i has been discovered independently in [NPL04] and [CDEL04], namely

$$J_i = \frac{\lambda}{4}\sqrt{i(N-i)}. \tag{6.2}$$

If the qubit chain is prepared in the initial state

$$|\Psi(0)\rangle = (a|0\rangle + b|1\rangle) \otimes |0\rangle \otimes \cdots \otimes |0\rangle, \quad |a|^2 + |b|^2 = 1, \tag{6.3}$$

this particular choice of coupling strengths leads to the final state

$$|\Psi(T)\rangle = |0\rangle \otimes \cdots \otimes |0\rangle \otimes (a|0\rangle + e^{i\varphi} b|1\rangle), \tag{6.4}$$

after a time $T = \pi/\lambda$. The phase φ depends on the length of the chain N and on the eigenenergies ω_i and should ideally be zero in order to accomplish perfect state transfer. Alternatively, the phase needs to be corrected by applying an appropriate phase gate at the end of the quantum state transfer. In the case where all eigenenergies are identical, $\omega_i = \omega$, the phase is given by

$$e^{i\varphi} = (-i)^{N-1} e^{i\omega T}. \tag{6.5}$$

In particular, if the eigenenergies can be engineered to equal $\omega = (N-1)\lambda/2$, then there is no phase shift. If the ω_i differ from each other, the state transfer is disturbed. The effects of this diagonal disorder were studied in [PNL10] and [YBB10].

Let us quickly outline the proof for this state transfer protocol, where we closely follow the presentation given in [CDEL04]. We first notice that the state $|000\ldots0\rangle$, where all qubits are prepared in the ground state, is an eigenstate of H_{PST} and does not change. Furthermore, the operator $Z = \sum_i \sigma_3^{(i)}$ commutes with the Hamiltonian, $[H_{PST}, Z] = 0$, which means that the number of excitations is preserved by the time evolution under H_{PST}. Let us declare the N vectors $\{|k\rangle_e\}_{k=1}^N$, where $|k\rangle_e$ means that qubit k is in the excited state $|1\rangle$ and all other qubits are in the ground state $|0\rangle$. Then the initial state $|1\rangle_e$ evolves within the subspace spanned by the vectors $|k\rangle_e$. In this N-dimensional subspace, the interaction part of the Hamiltonian H_{PST},

$$H_{int} = \sum_{i=1}^{N-1} J_i \left(\sigma_1^{(i)} \sigma_1^{(i+1)} + \sigma_2^{(i)} \sigma_2^{(i+1)} \right), \tag{6.6}$$

can be represented by an $N \times N$ matrix, which looks like this:

$$H_{int} = \begin{pmatrix} 0 & J_1 & 0 & \cdots & 0 \\ J_1 & 0 & J_2 & \cdots & 0 \\ 0 & J_2 & 0 & \cdots & 0 \\ \vdots & \vdots & \vdots & \ddots & J_{N-1} \\ 0 & 0 & 0 & J_{N-1} & 0 \end{pmatrix}. \tag{6.7}$$

With the particular coupling strengths (6.2), this matrix is identical to the representation of a spin $\frac{1}{2}(N-1)$ particle Hamiltonian $H = \lambda S_x$, with S_x being the x component angular momentum operator. Then the time evolution $e^{-i\lambda t S_x}$ represents a rotation of this spin particle. The matrix elements of these rotations are well known and were first

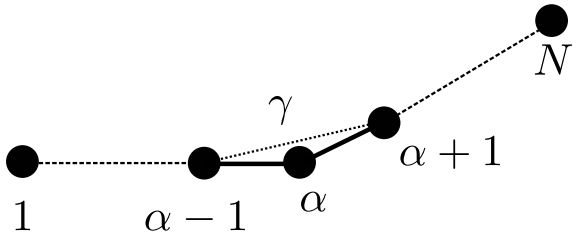

Figure 6.1: Qubit network with an additional interaction at the bend

evaluated by Wigner [Wig59] with the help of the Wigner D-matrix. Specifically, we can calculate

$$\langle N|_e e^{-i\lambda t S_x}|1\rangle_e = \left[-i\sin\left(\frac{\lambda t}{2}\right)\right]^{N-1}. \tag{6.8}$$

This matrix element gives us the overlap of the initial state $|1\rangle_e$ with the target state $|N\rangle_e$ after a time t. We thus find that a perfect state transfer from qubit 1 to qubit N occurs after time $T = \pi/\lambda$, and the phase change is $(-1)^{N-1}$.

Now, assuming the qubit eigenenergies are identical to one another, $\omega_i = \omega$, we find that they commute with the couplings in H_{int},

$$\left[\frac{\omega}{2}Z, H_{int}\right] = 0. \tag{6.9}$$

Thus we can calculate

$$e^{-iH_{PST}T}|1\rangle_e = (-i)^{N-1}e^{-i\frac{\omega}{2}TZ}|N\rangle_e = (-i)^{N-1}e^{i\frac{\omega}{2}T}|N\rangle_e. \tag{6.10}$$

Since we have $e^{-i\frac{\omega}{2}TZ}|0\rangle_e = e^{-i\frac{\omega}{2}T}|0\rangle_e$, the relative phase change of the transferred state is in fact $(-i)^{N-1}e^{i\omega T}$.

6.2 CORRECTING ERRORS IN BENT QUBIT CHAINS

Let us now consider an additional interaction between qubits $\alpha-1$ and $\alpha+1$ on the chain as described by the Hamiltonian

$$H_0 = H_{PST} + \gamma\left(\sigma_1^{(\alpha-1)}\sigma_1^{(\alpha+1)} + \sigma_2^{(\alpha-1)}\sigma_2^{(\alpha+1)}\right), \tag{6.11}$$

with $\gamma \in \mathbb{R}$ and $\alpha \in [2, N-1]$. This situation arises naturally if we consider a physical implementation of a qubit chain in which the coupling strengths between qubits are based on their physical distance. If there is a bend in the chain at qubit α, it is conceivable that the coupling strength between the two neighbouring qubits at the bend becomes large enough so that it is no longer negligible (compare with Fig. 6.1).

This type of perturbation and its effects have been studied in detail in [NHJ12]. It has been shown that such an interaction has severe

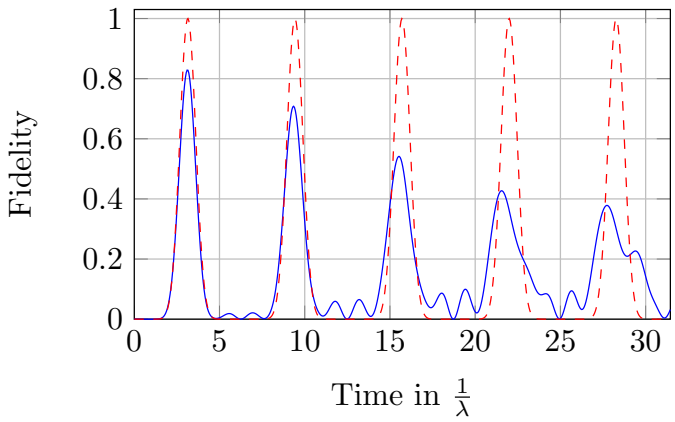

Figure 6.2: Fidelity as a function of time (in units of $1/\lambda$) for a 10-qubit chain with Hamiltonian (6.11):
Ideal unperturbed qubit chain with $\gamma = 0$ (red dashed line);
Perturbed bent qubit chain with γ of (6.14) and $\alpha = 5$ (blue line).

detrimental effects on quantum state transfer in this network. We are going to try to combat these effects with several decoupling schemes. In order to quantify the positive influence of our schemes, we will run numerical simulations. Since the Hamiltonian and the decoupling procedure preserve the total number of excitations, it is sufficient to consider a single excitation transfer [BNJ09]. In this scenario the first qubit of the network is prepared in its excited state and the rest is in the ground state, i.e.

$$|\psi_i\rangle = |1\rangle|0\rangle\cdots|0\rangle = |1\rangle_e. \tag{6.12}$$

We measure the transfer quality by means of the state fidelity F, which in our case is given by

$$\begin{aligned} F(t) &= |\langle\psi_f|\psi(t)\rangle|, \\ |\psi_f\rangle &= |0\rangle\cdots|0\rangle|1\rangle = |N\rangle_e. \end{aligned} \tag{6.13}$$

Perfect state transfer has occurred after time T if $F(T) = 1$.

Numerical results demonstrating the resulting loss of fidelity of quantum state transfer due to a bend in the chain are presented in Fig. 6.2 for a chain of 10 qubits. In this simulation and throughout the remainder of this section, we chose for the unwanted coupling strength

$$\gamma = 0.8 \max\{J_{\alpha-1}, J_\alpha\}, \tag{6.14}$$

and α to be at or close to the middle of the chain. This way, γ is comparable to, but slightly less than the coupling strengths J_i at the bend. As expected, the fidelity never reaches the optimal value of unity. After the time $T = \pi/\lambda$ the fidelity of the bent 10-qubit chain

assumes its maximum at ≈ 0.83. This is the time where we expect perfect quantum state transfer to happen under ideal conditions.

In our subsequent discussion it will be demonstrated how these detrimental effects can be suppressed efficiently by dynamical decoupling. For this discussion, it is helpful to introduce operators

$$h_{i,j} = \sigma_1^{(i)}\sigma_1^{(j)} + \sigma_2^{(i)}\sigma_2^{(j)}, \tag{6.15}$$

which allow us to rewrite the Hamiltonians as

$$\begin{aligned} H_{PST} &= \sum_i \frac{\omega_i}{2}\sigma_3^{(i)} + \sum_i J_i h_{i,i+1}, \\ H_0 &= H_{PST} + \gamma h_{\alpha-1,\alpha+1}. \end{aligned} \tag{6.16}$$

Choosing an operator $g = \sigma_3^{(i)}$ or $g = \sigma_3^{(j)}$, a straight-forward calculation yields

$$g^\dagger h_{i,j} g = -h_{i,j}, \tag{6.17}$$

so that g acts as a time-reversal operator for the Hamiltonian component $h_{i,j}$. If we consider two decoupling scheme operators $g_0 = \mathbb{1}$ and $g_1 = g = \sigma_{\alpha-1}^z$ and insert them into (2.24), we find

$$\begin{aligned} \overline{H}^{[0]} &= \frac{1}{2}(H_{PST} + g^\dagger H_{PST} g + \gamma h_{\alpha-1,\alpha+1} - \gamma h_{\alpha-1,\alpha+1}) && (6.18)\\ &= \frac{1}{2}(H_{PST} + g^\dagger H_{PST} g). && (6.19) \end{aligned}$$

Thus, to lowest order the unwanted coupling appearing in the Hamiltonian (6.11) is eliminated, independent of the actual strength γ of the error. Unfortunately, the remaining term in $\overline{H}^{[0]}$ is not equal to H_{PST} because $g^\dagger H_{PST} g \neq H_{PST}$. Nevertheless, this result allows us to understand how the schemes work, which we will construct in the following.

6.2.1 *Complete selective decoupling scheme*

As a first step, we will employ our method from Ch. 3 to construct a decoupling scheme for the bent chain. Setting up the linear system is straight-forward, however, we are again faced with the problem that due to the exponential growth of the system with the number of qubits N, we can only construct solutions for small chains. We therefore begin with constructing a scheme for $N = 3$, the smallest possible problem size, and then extending the scheme manually to higher N. The scheme we get from our method for $N = 3$ (with $\alpha = 2$) consists of the following four decoupling operators:

$$\begin{aligned} g_0 &= \mathbb{1} \\ g_1 &= \sigma_1^{(1)} \\ g_2 &= \sigma_2^{(3)} \\ g_3 &= \sigma_3^{(1)}\sigma_1^{(2)}. \end{aligned} \tag{6.20}$$

The scaling constant of this scheme is $D = 2$, which is optimal since the scheme was found by employing linear programming. We can easily verify that these operators have the desired effect of eliminating $h_{1,3}$ in the lowest order of the average Hamiltonian, while keeping all the other components, each weakened by the factor $\frac{1}{2}$.

In order to extend this scheme for longer chains, it is clear that the structure of the operators (6.20) must be kept intact for the three qubits at the bend, $\alpha-1$, α and $\alpha+1$. This will ensure that $h_{\alpha-1,\alpha+1}$ is eliminated, and all other components involving those 3 qubits are scaled down appropriately. However, in our extension we must also ensure that the additional interactions along the chain and the eigenenergies of the additional qubits are also scaled down by the factor $\frac{1}{2}$ to ensure a consistent overall scaling factor $D = 2$. It turns out that this is possible by choosing the following decoupling operators:

$$\begin{aligned} g_0 &= \mathbb{1} \\ g_1 &= \sigma_1^{(1)}\sigma_1^{(2)}\dots\sigma_1^{(\alpha-2)}\sigma_1^{(\alpha-1)} \\ g_2 &= \sigma_2^{(\alpha+1)}\sigma_2^{(\alpha+2)}\dots\sigma_2^{(N-1)}\sigma_2^{(N)} \\ g_3 &= \sigma_3^{(2)}\sigma_3^{(4)}\dots\sigma_3^{(\alpha-3)}\sigma_3^{(\alpha-1)}\sigma_1^{(\alpha)}\sigma_3^{(\alpha+2)}\sigma_3^{(\alpha+4)}\dots\sigma_3^{(N-2)}\sigma_3^{(N)}. \end{aligned} \tag{6.21}$$

In the unitary operation g_1, a σ_1 operator acts on all qubits up to $\alpha-1$, and in g_2 a σ_2 operator is applied to all qubits starting from $\alpha+1$. Since $\sigma_1\sigma_3\sigma_1 = \sigma_2\sigma_3\sigma_2 = -\sigma_3$, both the σ_1 and the σ_2 operators act as time reversal operators for the eigenenergy terms of the qubits. Analogously, in the sum of (2.24) the operators g_1 and g_2 introduce minus signs in the eigenenergy terms of all affected qubits. The operator g_3 involves a single σ_1 operator acting on qubit α at the bend. Therefore, for each qubit i there is a decoupling operator yielding a minus sign in the term $\omega_i\sigma_3^{(i)}$ of the sum of (2.24), and in addition there are three operators for each qubit yielding a positive sign. Thus, all of the terms $\omega_i\sigma_3^{(i)}$ are weakened by a scaling factor $D = 2$ as needed.

We still need to confirm that the unwanted coupling between qubits $\alpha-1$ and $\alpha+1$ is removed and the remaining two-qubit couplings are scaled by a factor of $D = 2$. Let us first ignore the qubit α at the bend and let us focus on the rest of the qubit chain. In view of the relation

$$\sigma_1^{(i)}\sigma_1^{(i+1)}h_{i,i+1}\sigma_1^{(i)}\sigma_1^{(i+1)} = \sigma_2^{(i)}\sigma_2^{(i+1)}h_{i,i+1}\sigma_2^{(i)}\sigma_2^{(i+1)} = h_{i,i+1}, \tag{6.22}$$

the operators g_1 and g_2 yield positive signs in the couplings $h_{i,i+1}$ for $i \in [1,\dots,\alpha-2,\alpha+1,\dots,N-1]$. The operator g_3, however, yields a negative sign for these couplings. Therefore, we obtain a scaling of these couplings with $D = 2$ as expected. The relevant couplings at the

bend are $h_{\alpha-1,\alpha}$, $h_{\alpha,\alpha+1}$ and $h_{\alpha-1,\alpha+1}$ the latter of which we want to remove to lowest order of the Magnus expansion. The operators g_j transform these couplings in the following way

$$\begin{aligned}
g_1 h_{\alpha-1,\alpha} g_1 &= \sigma_1^{(\alpha-1)}\sigma_1^{(\alpha)} - \sigma_2^{(\alpha-1)}\sigma_2^{(\alpha)},\\
g_2 h_{\alpha-1,\alpha} g_1 &= \sigma_1^{(\alpha-1)}\sigma_1^{(\alpha)} + \sigma_2^{(\alpha-1)}\sigma_2^{(\alpha)},\\
g_3 h_{\alpha-1,\alpha} g_3 &= -\sigma_1^{(\alpha-1)}\sigma_1^{(\alpha)} + \sigma_2^{(\alpha-1)}\sigma_2^{(\alpha)},\\
g_1 h_{\alpha,\alpha+1} g_1 &= \sigma_1^{(\alpha)}\sigma_1^{(\alpha+1)} + \sigma_2^{(\alpha)}\sigma_2^{(\alpha+1)},\\
g_2 h_{\alpha,\alpha+1} g_2 &= -\sigma_1^{(\alpha)}\sigma_1^{(\alpha+1)} + \sigma_2^{(\alpha)}\sigma_2^{(\alpha+1)},\\
g_3 h_{\alpha,\alpha+1} g_3 &= \sigma_1^{(\alpha)}\sigma_1^{(\alpha+1)} - \sigma_2^{(\alpha)}\sigma_2^{(\alpha+1)},\\
g_1 h_{\alpha-1,\alpha+1} g_1 &= \sigma_1^{(\alpha-1)}\sigma_1^{(\alpha+1)} - \sigma_2^{(\alpha-1)}\sigma_2^{(\alpha+1)},\\
g_2 h_{\alpha-1,\alpha+1} g_2 &= -\sigma_1^{(\alpha-1)}\sigma_1^{(\alpha+1)} + \sigma_2^{(\alpha-1)}\sigma_2^{(\alpha+1)},\\
g_3 h_{\alpha-1,\alpha+1} g_3 &= -\sigma_1^{(\alpha-1)}\sigma_1^{(\alpha+1)} - \sigma_2^{(\alpha-1)}\sigma_2^{(\alpha+1)}.
\end{aligned} \tag{6.23}$$

Using these results and looking at the sum of (2.24) we notice that the coupling $h_{\alpha-1,\alpha+1}$ is indeed eliminated as the applications of operators g_0 and g_3 cancel each other. Similarly, this is valid for the operators g_1 and g_2. In the case of the other two couplings, i.e. $h_{\alpha-1,\alpha}$ and $h_{\alpha,\alpha+1}$, the couplings remain in the result of the sum with a factor of $1/2$ each as required. Therefore, the extended scheme fulfils the necessary decoupling condition with a scaling factor of $D = 2$.

Let us now investigate how well this solution performs in our numerical simulations. For this purpose, we will simulate the time evolution resulting from applying the scheme for a specific number of repetitions during the transfer time T.

Figure 6.3 presents numerical results obtained for a bent 10-qubit chain under the protecting influence of our decoupling scheme. Two cases are depicted with different frequencies of the applied control operations. In the first case (magenta lower line) the decoupling scheme is repeated 12 times with a total number of 48 pulses per π/λ period required for perfect state transfer in the ideal unperturbed case. In the second case the selective dynamical decoupling scheme is repeated 60 times with a total number of 240 pulses per π/λ period. We notice that now the fidelity peak occurs after a time $2\pi/\lambda$ which originates from the decoupling scheme's time scaling factor of $D = 2$. It is also apparent that in both cases the fidelity maximum is higher than in the unprotected case; for 12 repetitions it reaches a value of $F \approx 0.947$ and for 60 repetitions it reaches $F \approx 0.998$. The beneficial influence of higher repetitions is particularly apparent at the subsequent fidelity peaks. In the case of 60 repetitions the achievable fidelities at these maxima are still close to unity. However, for practical purposes the first fidelity maximum at time $t = 2\pi/\lambda$ is the most relevant one. In actual experiments the achievable number of control pulses is likely

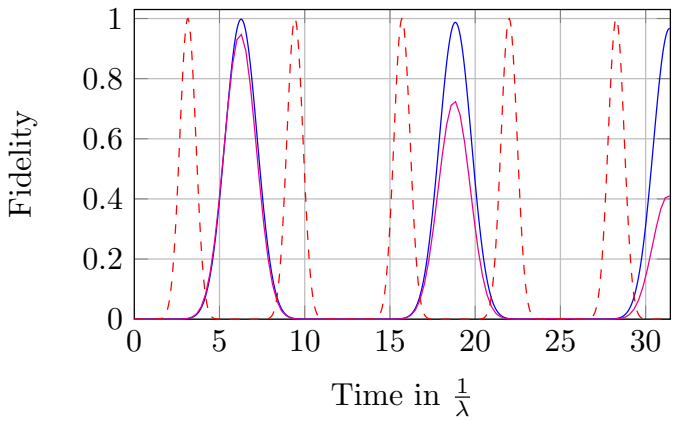

Figure 6.3: Fidelity as a function of time (in units of $1/\lambda$) for a 10-qubit bent chain with Hamiltonian (6.11) protected by the complete selective dynamical decoupling scheme: 12 repetitions of the complete scheme with a total number of 48 pulses per π/λ (magenta lower line); 60 repetitions of the complete scheme with a total number of 240 pulses per π/λ (blue line). The red dashed line shows the time evolution of an ideal unperturbed 10-qubit chain.

to be limited, so it is important to find a reasonable balance between the required number of control pulses and the achieved transfer fidelity.

To improve the performance of the scheme, we can employ the construction (2.25) to generate an SDD version of our scheme. Even though the symmetrized scheme consists of twice as many operations, it should require fewer repetitions than the original sequence to achieve a given degree of error suppression. Numerical results are presented in Fig. 6.4 for the symmetrized scheme. Here, 6 repetitions have been performed involving a total number of 48 control pulses per π/λ period. This is the same number of control pulses as used for obtaining the black curve of Fig. 6.3. The fidelity maximum is now closer to unity at a value of $F \approx 0.997$ which is comparable to simulations involving the original scheme with the significantly larger number of 240 control pulses. This demonstrates that the symmetrized version of the scheme performs significantly better.

6.2.2 *Partial selective decoupling scheme*

The decoupling scheme from Sec. 6.2.1, constructed with our systematic method, has a drawback. It is relatively complicated and requires all three Pauli operators σ_i to be applied to individual qubits, which may be very challenging to do in an experiment. In the following, we will try to find alternative schemes by manual construction. For this,

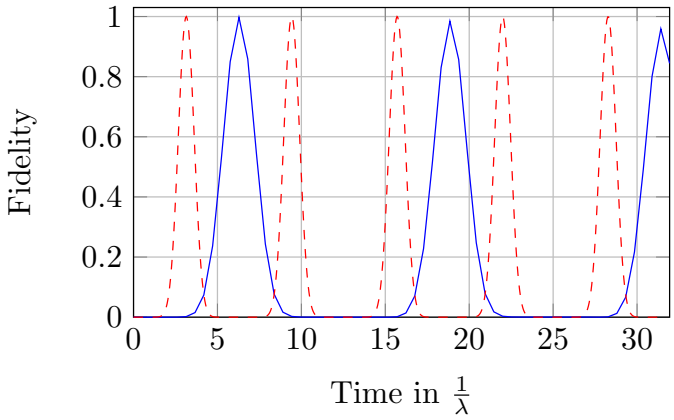

Figure 6.4: Fidelity as a function of time (in units of $1/\lambda$) for a 10-qubit bent chain with Hamiltonian (6.11) protected by the symmetrized scheme with 6 repetitions of the symmetrized complete scheme involving a total number of 48 pulses per π/λ (blue line); the red dashed line shows the time evolution of an ideal unperturbed 10-qubit chain.

we will leverage the knowledge we gained from the insight into the workings of the full scheme.

In order to simplify our task, let us for a moment ignore the eigenenergy terms $\frac{\omega_i}{2}\sigma_3^{(i)}$ in the Hamiltonian (6.11), so that we only have to deal with the coupling terms $h_{i,j}$. We will build on our initial test in Eq. (6.18) and split the decoupling operator g into two operators. One of them acts on the qubit $\alpha-1$ and the other one on qubit $\alpha+1$. Thus, they reverse the sign of $h_{\alpha-1,\alpha+1}$ in a way that the result of (2.24) is proportional to H_{PST}. These operators must be extended to the remaining qubits of the chain such that the scaling of the remaining interaction terms is proportionate. Specifically we choose decoupling operators of the form

$$\begin{aligned} g_0 &= \mathbb{1}, \\ g_1 &= \mathbb{1}, \\ g_2 &= \sigma_3^{(1)}\sigma_3^{(3)}\ldots\sigma_3^{(\alpha-3)}\sigma_3^{(\alpha-1)}, \\ g_3 &= \sigma_3^{(\alpha+1)}\sigma_3^{(\alpha+3)}\ldots\sigma_3^{(N-2)}\sigma_3^{(N)}, \end{aligned} \tag{6.24}$$

where g_2 acts on qubit $\alpha-1$ and every second qubit before it. Similarly, g_3 acts on qubit $\alpha+1$ and every second qubit after it. The unitary transformation g_2 induces a time reversal affecting all operators $h_{i,i+1}$ for $i<\alpha$ and $h_{\alpha-1,\alpha+1}$. Analogously, g_3 acts as a time reversal operation on all operators $h_{i,i+1}$ with $i\geqslant\alpha$ and on $h_{\alpha-1,\alpha+1}$. Since two operators reverse the sign of $h_{\alpha-1,\alpha+1}$, we also need to in-

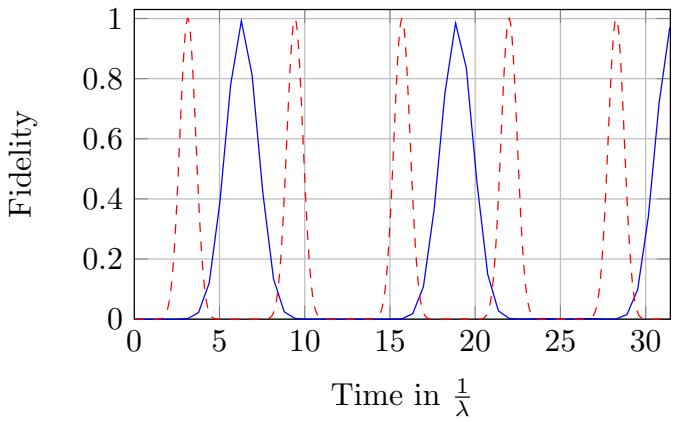

Figure 6.5: Fidelity as a function of time (in units of $1/\lambda$) for a 10-qubit bent chain with Hamiltonian (6.11) protected by the partial scheme with 5 repetitions of the partial scheme involving a total number of 20 pulses per π/λ (blue line); the red dashed line shows the time evolution of an ideal unperturbed 10-qubit chain.

clude $\mathbb{1}$ twice in our decoupling scheme to bring its total sum to zero. Calculating $\overline{H}^{[0]}$ for this decoupling scheme yields

$$\overline{H}^{[0]} = \sum_i \frac{\omega_i}{2}\sigma_3^{(i)} + \frac{1}{2}\sum_i J_i\left(\sigma_1^{(i)}\sigma_1^{(i+1)} + \sigma_2^{(i)}\sigma_2^{(i+1)}\right). \tag{6.25}$$

Compared to H_{PST}, we have all the two-qubit interactions scaled by a factor $\frac{1}{2}$, meaning $D = 2$. However, the eigenenergies of the qubits $\frac{\omega_i}{2}\sigma_3^{(i)}$ are not scaled, so our decoupling scheme is not able to achieve H_{PST} to lowest order perfectly. If all the ω_i are the same, as required for successful state transfer, then the effect of this discrepancy in the scaling is just a relative phase $e^{i\omega T}$ which is picked up by the transferred state and can be corrected after the transfer occurred. As such, the discrepancy may be perfectly acceptable in practice, depending on the specifics of the studied system. On the upside, this scheme is simpler in nature and only requires σ_3 pulses to implement.

Let us now investigate the performance of this simpler scheme. We will see that in some respects it performs even better than the symmetrized version of the original scheme. This feature is attractive for practical application provided the resulting phase change due to the incorrect scaling of the eigenenergy terms can be corrected at the end of a quantum state transfer by other means. Note that the phase change is only relevant if transferring a superposition state $\alpha|0\rangle + \beta|1\rangle$. The transfer fidelity for the state $|1\rangle$, which we use in our simulations, is unaffected.

Figure 6.5 shows the influence of this partial decoupling scheme on the dynamics of a bent 10-qubit chain. In this example 5 repetitions of this scheme are used which involve a total number of 20 control

pulses per π/λ period. This is less than half the number of control pulses used in the symmetric full scheme depicted in Fig. 6.4. Yet the performance is quite comparable. The fidelity maximum reaches a value of $F \approx 0.992$.

6.2.3 *Disorder-resistant decoupling scheme*

The scheme from Sec. 6.2.2 ignores the eigenenergy terms in the Hamiltonian and leaves them untouched. In contrast, the final scheme in this section will eliminate them to lowest order. It consists of the following four operators:

$$\begin{aligned} g_0 &= \mathbb{1}, \\ g_1 &= \sigma_1^{(1)}\sigma_1^{(2)}\dots\sigma_1^{(\alpha)}\sigma_2^{(\alpha+1)}\sigma_1^{(\alpha+2)}\sigma_2^{(\alpha+3)}\dots\sigma_1^{(N)}, \\ g_2 &= \mathbb{1}, \\ g_3 &= \sigma_2^{(1)}\sigma_1^{(2)}\sigma_2^{(3)}\dots\sigma_1^{(\alpha-2)}\sigma_2^{(\alpha-1)}\sigma_1^{(\alpha)}\sigma_1^{(\alpha+1)}\dots\sigma_1^{(N)}. \end{aligned} \tag{6.26}$$

The operator g_1 applies σ_1 to all qubits up to the bend position α, then alternates between σ_2 and σ_1 for the remaining qubits. The operator g_3 is basically a mirror of g_1 and applies σ_1 to all qubits starting from the bend position α to the end of the chain, but alternates between σ_2 and σ_1 before the bend.

With the result from (6.22) and the additional relations

$$\begin{aligned} \sigma_1^{(i)}\sigma_2^{(i+1)}h_{i,i+1}\sigma_2^{(i)}\sigma_1^{(i+1)} &= \sigma_2^{(i)}\sigma_1^{(i+1)}h_{i,i+1}\sigma_1^{(i)}\sigma_2^{(i+1)} \\ &= -h_{i,i+1}, \\ \sigma_1^{(i)}\sigma_3^{(i)}\sigma_1^{(i)} = \sigma_2^{(i)}\sigma_3^{(i)}\sigma_2^{(i)} &= -\sigma_3^{(i)} \end{aligned} \tag{6.27}$$

we can easily verify that the lowest order of the average Hamiltonian takes the form

$$\overline{H}^{[0]} = \frac{1}{2}\sum_i J_i h_{i,i+1}. \tag{6.28}$$

Just like with the previous two schemes, the interactions between the qubits are preserved with a scaling of $D = 2$, while the additional coupling at the bend is eliminated in the lowest order. However, this scheme also eliminates the eigenenergy terms $\frac{\omega_i}{2}\sigma_3^{(i)}$ to lowest order. This means that the relative phase shift from the transfer depends entirely on the length of the chain N and is given by $e^{i\varphi} = (-i)^{N-1}$.

Since $\overline{H}^{[0]}$ does not depend on specific values of the ω_i, the eigenenergies are eliminated even if they are not uniform. This offers a practical advantage over the other two schemes: since non-uniform eigenenergies disturb the transfer, this scheme is robust against this kind of disorder and allows the state transfer to complete successfully even in the presence of diagonal disorder, as long as the eigenenergies

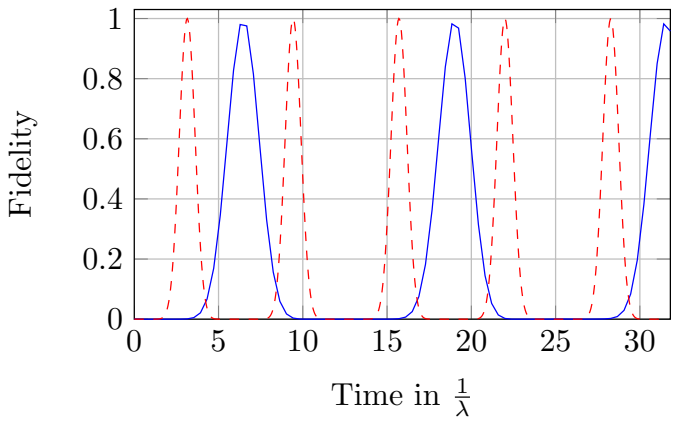

Figure 6.6: Fidelity as a function of time (in units of $1/\lambda$) for a 10-qubit bent chain with Hamiltonian (6.11) protected by the practical decoupling scheme with 8 repetitions of the practical scheme involving a total number of 32 pulses per π/λ (blue line); the red dashed line shows the time evolution of an ideal unperturbed 10-qubit chain.

are not too high so that the higher orders in the Magnus expansion can be neglected. The occuring phase shift is predictable and therefore easily corrected after the transfer. Additionally, this scheme requires only σ_1 and σ_2 pulses, which may be an advantage if the Pauli σ_3 operator is harder to implement in a specific experiment. Since pulses are always applied to all qubits at the same time, in practical realizations only the pulse phase would need to be altered for the individual qubits to differentiate between σ_1 and σ_2 pulses, whereas the source of the pulses may be shared by all qubits, allowing for potentially easier implementation.

We will now investigate the performance of this final decoupling scheme. A representative case of the time evolution numerically simulated is plotted in Fig. 6.6. From our simulations it seems that the number of pulses needed for quantitatively similar effects as the previous two schemes lies somewhere in between the two other schemes, somewhat closer to the number of pulses needed with the complete scheme.

6.2.4 *Scalability considerations for longer qubit chains*

In practical realizations of our decoupling schemes the number of control pulses that can be implemented may be limited. In the following we investigate how the minimal number of control pulses necessary for achieving a satisfactory transfer fidelity scales with the number of qubits in bent qubit chains. For this purpose we concentrate on an achievable transfer fidelity of $F = 0.95$ at the first maximum of

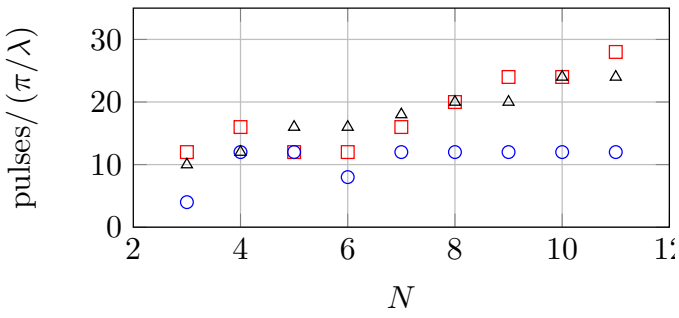

Figure 6.7: Minimum number of control pulses per π/λ period to achieve a transfer fidelity $F \geqslant 0.95$ and its dependence on the number N of qubits in a bent chain with γ given by (6.14) and with α positioned in the middle of the chain: Symmetrized complete selective dynamical decoupling scheme (red squares); partial selective dynamical decoupling scheme (blue circles); practical decoupling scheme (black triangles)

the quantum state transfer protocol in qubit chains involving up to eleven qubits and determine the minimal number of pulses required to reach this transfer fidelity.

Numerical results are depicted in Fig. 6.7 for all of our schemes. Apart from small qubit chains the number of control pulses required in the symmetrized complete scheme and the disorder-resistant scheme grow approximately linearly with the number N of qubits in the chain. For $N < 6$ somewhat more control pulses are required which may originate from the disturbance being too close to the ends of the chain and thus having a particularly strong impact. The partial selective dynamical decoupling scheme also exhibits this phenomenon. But for longer qubit chains it requires an approximately constant number of 12 control pulses per π/λ period. We expect, however, that for even larger qubit chains the number of required control pulses will also eventually grow linearly with N, albeit possibly with a smaller slope than the symmetrized complete selective decoupling scheme.

In [NHJ12] it has been demonstrated that the effect of the perturbing additional coupling at the bend of a linear qubit chain diminishes with increasing numbers N of qubits of the chain. In view of the linearly increasing number of pulses necessary to counteract the influence of the disturbance we expect that for very long qubit chains the effort required to successfully implement decoupling may no longer be worth the expected benefits. Therefore, the presented selective dynamical decoupling schemes are expected to be particularly valu-

able for protecting quantum state transfer in quantum networks of intermediate sizes which are of interest for current realizations of quantum registers.

6.2.5 *Influence of imperfect pulses*

Since we consider the additional coupling in the network to be a result of some imperfection or defect, it is important to investigate how the suggested schemes work under imperfect conditions themselves. So far, we have assumed that both the pulses and the timing between pulses are perfect. In this section, we will study the effects of two different sources of errors. The first are imperfections in the timing of the pulses, which we model by replacing the constant τ with random values from a Gaussian distribution with mean value $\mu = \tau$ and standard deviation $\sigma = q\tau$. The second are systematic errors in the applied Pauli pulses where we replace the perfect pulses σ_i with an imperfect pulse $\sigma_i e^{-i\theta\sigma_i}$ like in Sec. 5.1.4.

The results for imperfect timings can be seen for the disorder-resistant scheme in Fig. 6.8. We have also run simulations for the other schemes, and the results are similar in the sense that the fidelity peaks begin to drop significantly once $q \geqslant 0.2$ and do not change very much for $q \in [0, 0.2)$. In other words: if 95.4% of pulses have a distance between $\tau \pm 0.4\tau$ with Gaussian distribution around τ, the decoupling schemes generally perform close to the case of perfect timing.

For the systematic errors, the results are shown in Fig. 6.9. Judging from our simulations, all three schemes were more sensitive to this kind of systematic error than to the randomized timings. In order to keep the first fidelity peak above 0.9, θ should be kept below 0.1τ.

Our simulation results show that there is a reasonable margin for error in the implementation of the decoupling schemes. The systematic error proved to be slightly more problematic, which is to be expected, since a statistical error can average itself out to a certain extent over time. Unfortunately, there is no obvious way to construct a self-decoupling sequence from the presented decoupling schemes, since they do not remove arbitrary single-qubit terms in the lowest order and thus would not decouple arbitrary pulse errors.

6.3 DESIGNING INTERACTION STRENGTHS FOR STATE TRANSFER

The perfect state transfer Hamiltonian (6.1) requires specifically designed interaction strengths given in Eq. (6.2) between the individual qubit pairs. The couplings are strongest in the middle of the chain and then get gradually weaker to the chain ends, whereby the strengths are symmetric around the middle of the chain. In many practical implementations of qubit chains, the coupling strengths between neighbouring qubits depends on their physical distance to each

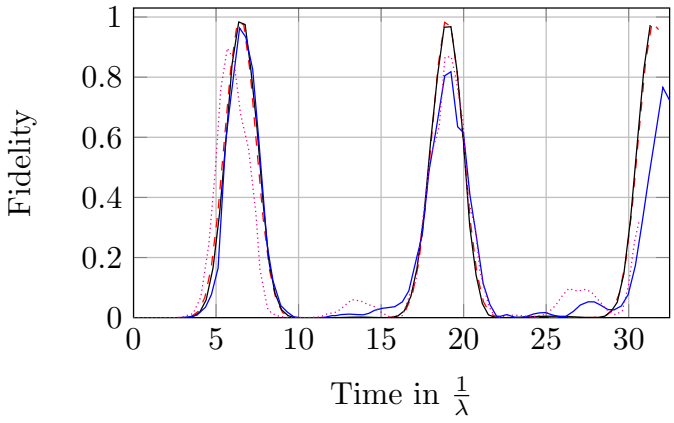

(a) First three peaks in Fidelity

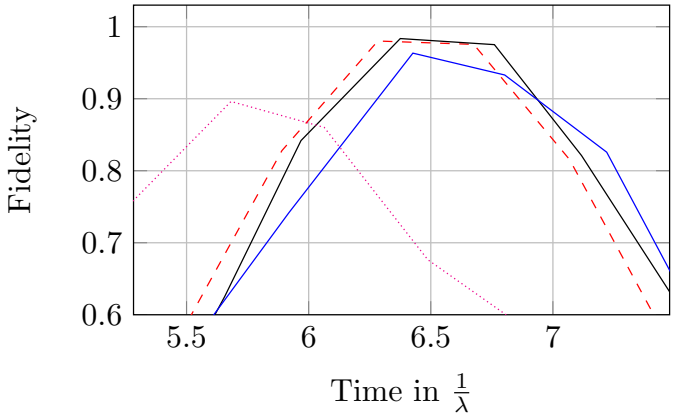

(b) Cut out of the first fidelity peak

Figure 6.8: Fidelity as a function of time (in units of $1/\lambda$) for a 10-qubit bent chain with Hamiltonian (6.11) protected by the disorder-resistant scheme with 8 repetitions of the scheme involving a total number of ≈ 32 pulses per π/λ seconds with pulses placed imperfectly, randomly in time. Notice the imperfect timings and drops in the first fidelity peak depending on the standard deviation σ:
red dashed line: $\sigma = 0$, exactly placed, perfect pulses
black solid line: $\sigma = 0.1\tau$ very similar result to perfectly placed pulses
blue solid line: $\sigma = 0.3\tau$, significant drop in all fidelity peaks behind the first peak
magenta dotted line: $\sigma = 0.5\tau$, biggest drop in the first fidelity peak

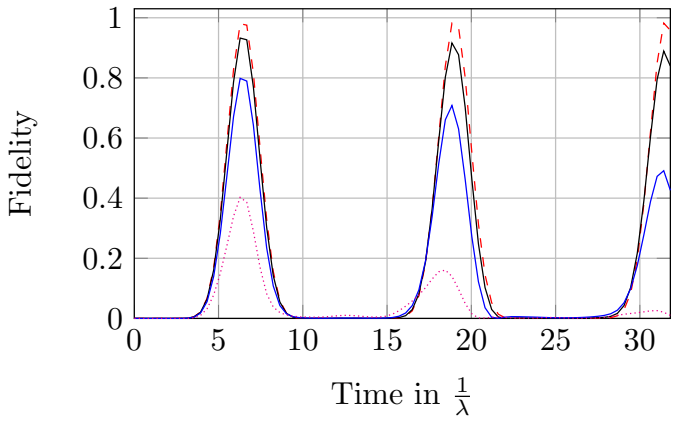

(a) First three peaks in Fidelity

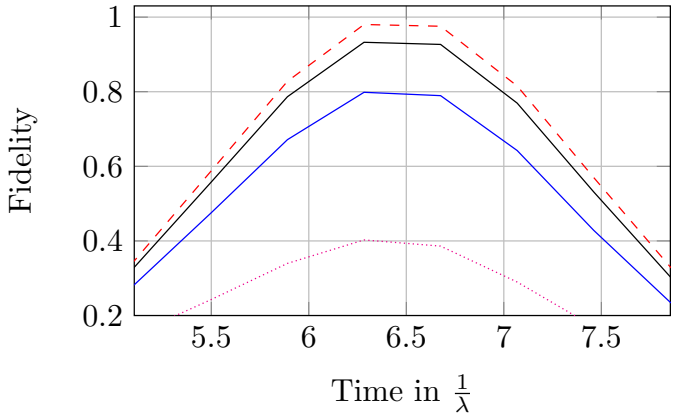

(b) Cut out of the first fidelity peak

Figure 6.9: Fidelity as a function of time (in units of $1/\lambda$) for a 10-qubit bent chain with Hamiltonian (6.11) protected by the disorder-resistant scheme with 8 repetitions of the scheme involving a total number of 32 pulses per π/λ seconds with imperfect pulses - a systematic error is present with all the pulses. Different θ's were selected for the four simulations. Notice the drop in the first fidelity peak and the consequent peaks as well:
red dashed line: $\theta = 0$, perfect pulses
black solid line: $\theta = 0.05\tau$, very similar result to perfect pulses
blue solid line: $\theta = 0.1\tau$, significant drop in all fidelity peaks
magenta dotted line: $\theta = 0.2\tau$, fidelity roughly 0.4 even at the first peak

other, and as such, the required couplings (6.2) could in principle be engineered by placing the qubits at appropriate distances to each other.

However, such a specially designed chain is less useful for other applications. In particular, consider a qubit chain or 2D grid for the purpose of doing quantum computation. In such a system, we need to be able to perform two-qubit gates on neighbouring qubits, a task for which we can exploit the natural coupling between those qubits (see also Ch. 8). If the coupling strengths are engineered according to (6.2), then the speed, and possibly fidelity, of these gate operations is not equivalent between different pairs of qubits, a trait which is not desirable for a general-purpose quantum processor.

Let us instead consider an N-qubit chain governed by a Hamiltonian with equal coupling strengths J throughout,

$$H_0 = \sum_{i=1}^{N} \frac{\omega}{2} \sigma_3^{(i)} + \sum_{i=1}^{N-1} J \left(\sigma_1^{(i)} \sigma_1^{(i+1)} + \sigma_2^{(i)} \sigma_2^{(i+1)} \right). \tag{6.29}$$

We can now try and use dynamical decoupling to modify the average Hamiltonian $\overline{H}$ to have the desired interaction strengths (6.2) required for perfect state transfer. This is an extension of the example given in Sec. 3.3.5.

6.3.1 *Narrowing the search space*

As before, due to the exponential growth of the linear system (3.9), we cannot directly use our method to find a suitable decoupling scheme for arbitrary N. In this case, the smallest relevant problem is $N = 4$, and unfortunately it turns out that the decoupling schemes found by using the particular solution or a linear programming solver are already quite complicated, with no clear structure we could exploit to extend them to higher N. Therefore, for this problem we are going to use a slightly different approach.

Due to the structure of the desired coupling strengths (6.2), we need to gradually weaken the outer couplings. In the decoupling condition (2.24), this means that we need to have a mixture of decoupling operators g_j giving positive and negative sign for a coupling depending on the amount we need to weaken it. Since the couplings in the middle of the chain are supposed to be strongest, our decoupling operators should all give a positive sign for these couplings. The weakest couplings are those at the end of the chain, so these need to have the most operators giving a negative sign for them. Then some of these operators should also reverse the sign for the second-to-outer couplings, and so on.

We know from Eq. (6.17) that a σ_3 operator applied to either qubit of a coupled pair can reverse the sign on the XX-type interaction we

are using. Then we can easily come up with the following set of decoupling operators:

$$\begin{aligned} g_0 &= \mathbb{1} \\ g_1 &= \sigma_3^{(1)}\sigma_3^{(N)} \\ g_2 &= \sigma_3^{(2)}\sigma_3^{(N-1)} \\ g_3 &= \sigma_3^{(1)}\sigma_3^{(3)}\sigma_3^{(N-2)}\sigma_3^{(N)} \\ &\vdots \end{aligned} \tag{6.30}$$

In each operator, a σ_3 operator is added to the second-next qubit from either end of the chain, where the odd-numbered operators start with the qubits directly at the end, and the even-numbered start with the second qubit from the end. This construction gives us $\lfloor N/2 \rfloor$ operators, which gradually reverse the sign on additional couplings, until we reach the middle of the chain. $\lfloor x \rfloor$ means rounding to the nearest integer $\leqslant x$. These operators have no effect on the eigenenergy terms $\frac{\omega}{2}\sigma_3^{(i)}$ of the qubits.

It is clear that these operators are sufficient to achieve our goal of designing the state transfer coupling strengths (6.2). The only remaining question is how often each operator needs to appear in our final decoupling scheme.

6.3.2 *Constructing solutions*

In the previous subsection, we have significantly reduced the search space for our method, since we already know the $\lfloor N/2 \rfloor$ operators which will appear in our decoupling scheme. This means a significant reduction in the size of our linear system (3.8), and so it is now a straight-forward task to compute the number of appearances c_j for each of the decoupling operators g_j in (6.30). We know the ratios of the operators $h_{i,i+1}$,

$$\frac{\nu_i}{\mu_i} = \frac{J_i}{J} = \frac{\lambda}{2J}\sqrt{i(N-i)} = \frac{\sqrt{i(N-i)}}{\sqrt{\lfloor N/2 \rfloor \lceil N/2 \rceil}}, \tag{6.31}$$

where $\lceil x \rceil$ means rounding to the nearest integer $\geqslant x$. We used the fact that we do not intend to scale down the strength of the coupling in the middle of the chain and thus use $J = J_{\lfloor N/2 \rfloor}$ as a reference point. Inserting into (3.9), we get our final linear set of equations,

$$\sum_{j=0}^{i-1} e_j - \sum_{j=i}^{\lfloor N/2 \rfloor - 1} e_j = \frac{\sqrt{i(N-i)}}{\sqrt{\lfloor N/2 \rfloor \lceil N/2 \rceil}} \quad \forall i \in [1, \ldots, \lfloor N/2 \rfloor - 1], \tag{6.32}$$

and the additional restraint $\sum e_j = 1$, since we need our scaling to be $D = 1$.

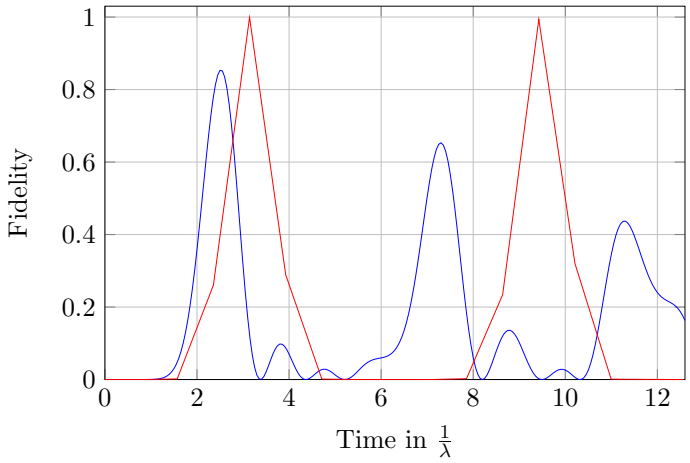

Figure 6.10: State transfer in an 8-qubit chain. The blue line represents the uncorrected evolution of the system according to the Hamiltonian (6.29). The red line employs the proposed dynamical decoupling scheme from Sec. 6.3.2.

This linear system produces real-valued solutions for the e_j due to the square roots on the right-hand side, and so we have to round the solutions to some rational numbers to produce the final integer-valued c_j, as discussed in Sec. 3.2.2. In our numerical solutions we found that this rounding can be quite rough to still produce adequate results. In the following we present a few examples for smaller N which work well in practice:

$$\begin{aligned}
N = 5: &\quad c_0 = 9 \quad c_1 = 1 \\
N = 6: &\quad c_0 = 61 \quad c_1 = 7 \quad c_2 = 2 \\
N = 7: &\quad c_0 = 41 \quad c_1 = 5 \quad c_2 = 2 \\
N = 8: &\quad c_0 = 48 \quad c_1 = 6 \quad c_2 = 3 \quad c_3 = 1
\end{aligned} \tag{6.33}$$

6.3.3 *Numerical results*

We ran numerical simulations for an 8-qubit chain evolving under the influence of the Hamiltonian (6.29). In Fig. 6.10 we see a comparison between the uncorrected evolution (blue line) and the correction with the help of the decoupling scheme from Sec. 6.3.2 (red line). In both cases, the state $|1\rangle$ was prepared on the first qubit of the chain, and the plot shows the fidelity overlap with the target state, where the final qubit of the chain is in the state $|1\rangle$. During the transfer time π/λ, the decoupling scheme was repeated 4 times, which amounts to 232 total pulses, since the scheme consists of 58 operators as per Eq. (6.33). We see that, without the scheme, the maximum fidelity is only at about 0.8, whereas with our scheme, we reach a fidelity of 1 almost perfectly at both the first and second transfer times T and $3T$.

6.4 EXTENDING THE STATE TRANSFER PROTOCOL TO QUDIT CHAINS

Before concluding this chapter, let us have a look at state transfer in qudit chains with dimension $d > 2$. As we will see shortly, the PST Hamiltonian (6.1) can be extended to qudit chains in a natural manner. Although we do not yet know if this approach will be experimentally feasible, it allows us another opportunity to look at how our methods can be applied to qudit systems in principle.

6.4.1 *Perfect state transfer Hamiltonian for qudits*

It turns out that the PST Hamiltonian from Eq. (6.1) has a natural extension to qudit systems by expressing it in the basis of the generalized Gell-Mann operators from Sec. 4.1.1. If we ignore the eigenenergies of the qudits and focus entirely on the interactions, then the PST Hamiltonian for qudit chains is given as

$$H_{PST} = \sum_{i=1}^{N-1} \sum_{j=1}^{d-1} J_i \left(u_{0j}^{(i)} u_{0j}^{(i+1)} + v_{0j}^{(i)} v_{0j}^{(i+1)} \right). \tag{6.34}$$

To prove that the Hamiltonian (6.34) is indeed capable of state transfer on a qudit chain, let us define the operators

$$Z_k = \sum_{i=1}^{N} w_k^{(i)}, \quad 1 \leqslant k < d \tag{6.35}$$

as a generalization of the total z component operator Z in the qubit case. Then we find that each of these operators commutes with H_{PST},

$$[H_{PST}, Z_k] = 0, \tag{6.36}$$

which tells us that the number of excitations of each state $|k\rangle$ is preserved by H_{PST}. This means that, if we prepare the chain initially in the state $|k0\ldots0\rangle$, then the chain's evolution is restricted to the subspace spanned by the N vectors $\{|j\rangle_k\}_{j=1}^{N}$, with $|j\rangle_k$ meaning that the qudit j is in the excited state $|k\rangle$, while all other qudits are in the ground state $|0\rangle$. In this subspace, the Hamiltonian (6.34) takes the familiar form of Eq. (6.7), and so the arguments made in Sec. 6.1 for the qubit case carry over. We thus know that after time $T = \pi/(2\lambda)$, the initial state $|k0\ldots0\rangle$ will have evolved to the state $(-i)^{N-1}|0\ldots0k\rangle$. As this holds for any of the excited states k, if we prepare the first qubit in an arbitary superposition, then the chain will evolve as

$$e^{-iH_{PST}T} \sum_{k=0}^{d-1} a_k |k0\ldots0\rangle = a_0 |00\ldots0\rangle + (-i)^{N-1} \sum_{k=1}^{d-1} a_k |0\ldots0k\rangle. \tag{6.37}$$

The ground state $|00\ldots0\rangle$ is an eigenstate of H_{PST} and does not change, the other states pick up the phase $(-i)^{N-1}$ relative to the ground state. As in the qubit case, this phase change needs to be corrected at some point to complete the perfect state transfer.

6.4.2 *Designing interaction strengths on the qudit chain*

Now that we have established the perfect state transfer Hamiltonian for qudit chains, let us quickly look at how we could generalize the results from Sec. 6.3 to qudits. That is, we want to simulate H_{PST} from Eq. (6.34) by using dynamical decoupling on a given Hamiltonian with equal coupling strengths,

$$H_0 = J \sum_{i=1}^{N-1} \sum_{j=1}^{d-1} \left(u_{0j}^{(i)} u_{0j}^{(i+1)} + v_{0j}^{(i)} v_{0j}^{(i+1)} \right). \tag{6.38}$$

This task was studied by Frederic Hummel in his bachelor thesis [Hum14].

A simple, but not necessarily easy approach to the problem is by using our systematic method for finding decoupling schemes, which we generalized to qudits in Ch. 4. For this task, we need to find the representation of H_{PST} and H_0 in the basis of the generalized spin operators. This is a straight-forward, but time-consuming calculation, and the result is

$$\begin{aligned} H_{PST} &= \sum_{i=1}^{N-1} \sum_{j=1}^{d-1} J_i \sum_{k,l=0}^{d-1} \xi_{jk,jl} \sigma_{j,k}^{(i)} \sigma_{d-j,l}^{(i+1)}, \\ \xi_{k,l} &= \frac{1}{d^2} \left(e^{-2\pi i k/d} + e^{2\pi i l/d} \right). \end{aligned} \tag{6.39}$$

However, a more direct approach is to try and take over the results from the qubit case directly. To do this, we need to find an appropriate replacement for the Pauli operator σ_3 in the decoupling operators of Eq. (6.30). This replacement operator has to act as a reversal operator on u_{0j} and v_{0j} for $1 \leqslant j < d$ and must be unitary.

Formally, one such operator can be written as

$$\zeta = |0\rangle\langle 0| - \sum_{i=1}^{d-1} |i\rangle\langle i|. \tag{6.40}$$

For qubits ($d = 2$), this coincides with σ_3. It is easy to verify that indeed we have

$$\begin{aligned} \zeta^\dagger u_{0j} \zeta &= -u_{0j}, \\ \zeta^\dagger v_{0j} \zeta &= -v_{0j}. \end{aligned} \tag{6.41}$$

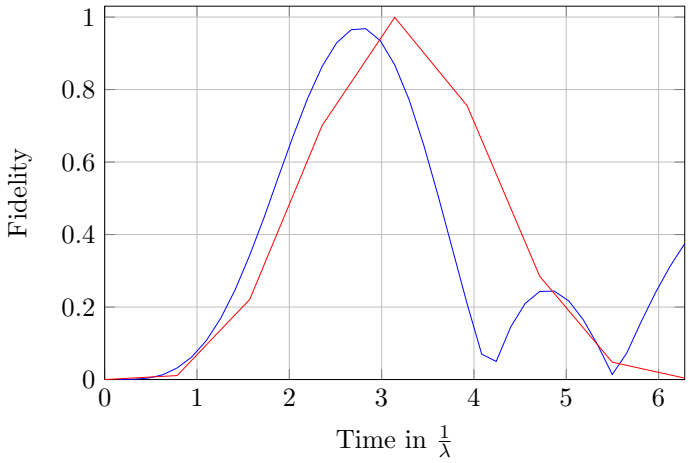

Figure 6.11: State transfer in a 5-qudit chain of dimension $d = 4$. The blue line represents the uncorrected evolution of the system according to the Hamiltonian (6.38). The red line employs the proposed dynamical decoupling scheme.

Therefore, we can now formulate our decoupling scheme operators:

$$\begin{aligned} g_0 &= \mathbb{1} \\ g_1 &= \zeta^{(1)}\zeta^{(N)} \\ g_2 &= \zeta^{(2)}\zeta^{(N-1)} \\ g_3 &= \zeta^{(1)}\zeta^{(3)}\zeta^{(N-2)}\zeta^{(N)} \\ &\vdots \end{aligned} \tag{6.42}$$

The number of occurences c_j of each operator g_j in the scheme do not change and can be taken directly from our results in the qubit case, as determined by the system of equations (6.32). This concludes the formal answer to the problem we were trying to solve, as this decoupling scheme is capable of turning the Hamiltonian H_0 into H_{PST} to lowest order.

On a practical level, however, it is not immediately apparent how to implement the operator ζ as a unitary pulse on the qudits. As such, this result should be understood purely as a theoretical gedankenspiel to understand how our concepts could, in principle, be generalized to qudit systems.

6.4.3 *Numerical simulation*

Due to the higher-dimensional nature of qudits, numerical calculations on qudit systems become increasingly complex and time-consuming. As such, we will restrict ourselves to a 5-qudit chain with $d = 4$. On this chain, we have simulated the time evolution under the Hamilto-

nian (6.38), once without any corrections and once with the proposed decoupling scheme (6.42). The number of occurences of each operator were taken from Eq. (6.33). The qudit chain is initially prepared in the state

$$|\Psi_0\rangle = \frac{1}{\sqrt{3}} \left(|10\ldots0\rangle + |20\ldots0\rangle + |30\ldots0\rangle \right), \tag{6.43}$$

and at each time step we calculate the fidelity overlap with the target state

$$|\Psi_f\rangle = \frac{1}{\sqrt{3}} \left(|0\ldots01\rangle + |0\ldots02\rangle + |0\ldots03\rangle \right). \tag{6.44}$$

The distance between pulses was set to $\tau = \pi/(40\lambda)$, which equals four repetitions of the decoupling scheme during the transport time $T = \pi/\lambda$. The results are presented in Fig. 6.11. The blue line presents the results of the uncorrected time evolution. The maximum is shifted slightly to the left of the expected time T and reaches a fidelity of 0.968. This may actually be an acceptable level, however, both the maximum fidelity and the position of the maximum in the uncorrected case depend on the initial state. Additionally, the fidelity will decrease with increasing number N of qudits. The red line shows the effects of our decoupling scheme. Here, the maximum coincides with the expected time $T = \pi/\lambda$, and the fidelity reaches the value of 1 almost perfectly.

7

DECOUPLING THE CENTRE-OF-MASS MOTION IN MATTER-FIELD INTERACTIONS IN A CAVITY

The qubit chains presented in Ch. 6 are a good way to transfer quantum states over shorter distances. However, for long-range quantum communication it is simply impractical to build a qubit chain over the whole distance, particularly as imperfections are going to make it nearly impossible to successfully transfer states over such a long distance. The medium of choice in these scenarios are photons, transmitted either through air/vacuum [MHS+12, KFF+14, TAAL15] or through optical fibres [MdT+03, UJA+04]. However, the photons will be exposed to decoherence effects, which make a successful transfer of states challenging.

Instead of directly transferring a particular qubit state, an alternative is to prepare an entangled pair of qubits and then distribute one qubit of the pair to each end of the communication line. An arbitrary qubit state could then be transferred between the two end points with the help of quantum teleportation protocols [TBA14]. It is also possible to do quantum cryptography with entangled qubit pairs. Of course, distributing the entangled pair to both end points suffers from the same decoherence problems as the original transport.

A possible way to overcome these problems is provided by quantum repeaters [BDCZ98, DBCZ99]. The repeaters form a network of quantum nodes, and entangled states are prepared and shared between neighbouring pairs of nodes. Entanglement between distant nodes can then be generated by entanglement swapping [ŻZHE93]. To ensure we end up with high-fidelity entangled pairs, entanglement purification procedures [BBP+96, DEJ+96] typically need to be used to distil high-fidelity entangled pairs from a sufficiently large number of low-fidelity entangled pairs. Recently various physical set-ups and entanglement distribution protocols have been proposed for the realization of quantum repeaters [SSdG11].

The proposal of van Loock et al. [vLS+06, LvLN+06, vLMN08] for a hybrid quantum repeater is of particular interest as it is potentially compatible with existing classical optical communication networks. It takes advantage of the transmission of coherent photon states through an optical fibre and subsequent photonic post-selection for the generation of entanglement between distant pairs of material qubits which are, following a recent generalization [BA13] of the original proposal, entangled with the photons by strong resonant interactions. Although a realization of the assumed cavity-fibre couplings is

still challenging, highly promising experimental developments have been taking place in this direction [SCH+06, CSD+07].

An important issue in any implementation of such a photon-mediated entanglement distribution scenario is the physical realisation of the material qubits [SDS09]. Trapped ions or atoms are well suited for this purpose as the quantum technology for controlling their degrees of freedom is already well advanced [LMK+96, LBMW03, BR12]. However, it is important to control the centre-of-mass motion of the qubits properly as it introduces unwanted decoherence and dissipation.

This centre-of-mass motion has so far been neglected in most studies of quantum repeaters, so in this chapter we will take a closer look at its decohering influence on the entanglement generation. We will study its influence on the matter-field interaction in the cavities and then explore the possibility of employing dynamical decoupling to suppress the effects of the motion, a task which involves the decoupling of a quantum harmonic oscillator.

The outline of the chapter is as follows. In section 7.1 we introduce our theoretical model for the matter-field interaction between a trapped atom or ion in a cavity and a single-mode photon field. Formulas are derived for the resulting matter-field state after the interaction. In section 7.2 we address the suppression of these decohering and dissipating effects and propose a dynamical decoupling scheme which acts only on the degrees of freedom of the centre-of-mass motion. The derivation of a proper Baker-Hausdorff formula needed in Sec. 7.1 is given in App. B.

7.1 MATTER-FIELD ENTANGLEMENT IN THE PRESENCE OF CENTRE-OF-MASS MOTION

In a hybrid quantum repeater, entanglement is created between two distant material qubits with the help of photon exchange and subsequent photonic post-selection. We will assume that the material qubits are represented by internal states of trapped atoms or ions. In a Ramsey-type interaction scenario, the first qubit interacts shortly with the radiation field inside a cavity resulting in an entangled state between this qubit and the photon field. After transmitting the resulting photon wave packet to the second distant cavity by an optical fibre it interacts shortly with the second qubit. The process is depicted in Fig. 7.1. If the photon state transfer between both cavities is perfect, the resulting entanglement between the two distant material qubits and the photons can be used to prepare an almost perfectly entangled state between the two qubits by an appropriate photonic measurement with post-selection. It was found [BA13] that in this scenario the maximal success probability is 25%. This occurs during the collapse phenomenon of the Jaynes-Cummings-Paul model.

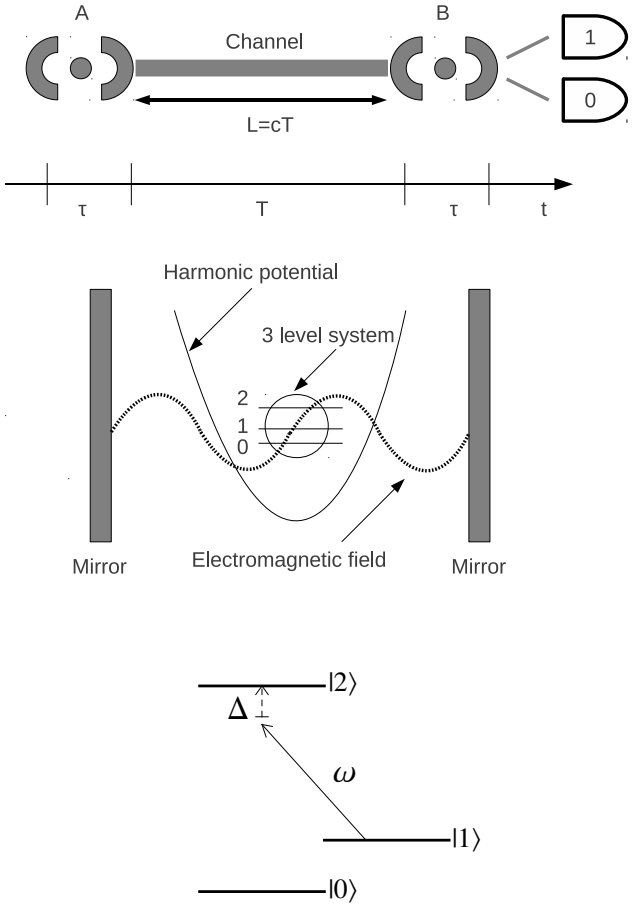

Figure 7.1: Generation of photon-assisted entanglement: The first interaction of duration τ results in an entangled state between the material quantum system and the radiation field in cavity A; after transferring the photons by an optical fibre with length L into the second cavity B, the propagated photons interact in a similar way with the second material quantum system B. The resulting state of the radiation field is projected by a minimum-error two-valued POVM measurement with measurement results 1 or 0. The measurement result 1 prepares both material quantum systems approximately in a Bell state $|\Psi^+\rangle$ of states $|0\rangle$ and $|1\rangle$ with success probability P_{Bell} and with fidelity F_{opt}. Schematic diagrams of the structure of internal states and their coupling to the centre-of-mass motion are depicted.

However, the centre-of-mass motion of the trapped atoms or ions has to be taken into account as these degrees of freedom also participate in the formation of the entanglement between the material quantum systems and the photons involved, thus causing decoherence and dissipation. Taking the centre-of-mass motion into account, we found [BFA13] that the success probability and fidelity are very sensitive to the trap frequency. If we consider a trap frequency for which the results resemble the ideal case, then for a four times smaller trap frequency the best fidelity achieved is 0.5 with a probability of 11%. These results are consistent with the expectation that the centre-of-mass motion introduces a significant amount of decoherence in the system. This decoherence prohibits the creation of high-fidelity pairs. In order to increase the characteristic quantities we must increase the frequency of the trap. The increase of the trap frequency corresponds to a steeper harmonic potential, which is reducing the centre-of-mass motion. However, in the case of an already built experimental apparatus the eigenfrequency of the trap might not be a freely controllable parameter. Therefore, the preparation of high-fidelity Bell states is limited by the centre-of-mass motion even if the post-selection is performed by minimum-error POVM measurements.

In this section we will study the model for the interactions of the radiation field with the material qubits in the cavities A and B, as this is where the centre-of-mass motion influences the results. We will later try to remove this influence by decoupling. A full treatment of the complete hybrid quantum repeater model with a study of the resulting loss of success probability and fidelity in the created entanglement pairs was done in [BFA13].

7.1.1 *Model Hamiltonian for the qubit-field interaction*

We consider a three-level trapped system (ion or atom) in a harmonic trap potential with frequency ω_t, placed inside an optical cavity with frequency ω_c. The internal energy eigenstates are $|0\rangle$, $|1\rangle$ and $|2\rangle$ with associated energies E_0, E_1 and E_2. The internal states are treated as a ladder system with two hyperfine-split components $|0\rangle$ and $|1\rangle$ acting as the qubit states, of which only the state $|1\rangle$ participates in the interaction with the cavity mode and the centre-of-mass motion. These two states have long radiative lifetimes.

Assuming that the electric field does not change considerably over the size of the atom or ion, the total Hamiltonian in the dipole approximation reads [Scho1]

$$\begin{aligned} H_0 =& \frac{p^2}{2m\hbar} + \frac{m\omega_t^2 x^2}{2\hbar} + \omega_0 |0\rangle\langle 0| + \frac{1}{2}\omega_{21}\sigma_3 + \omega_c a^\dagger a \\ &+ \left(\sigma_+ + \sigma_-\right)\left(g^*(kx)a^\dagger + g(kx)a\right), \end{aligned} \tag{7.1}$$

where in this instance $\sigma_3 = |2\rangle\langle 2| - |1\rangle\langle 1|$, $\sigma_+ = |2\rangle\langle 1|$ and $\sigma_- = |1\rangle\langle 2|$ with $\omega_{21} = (E_2 - E_1)/2\hbar$ and $\omega_0 = E_0 + (E_1 + E_2)/2\hbar$. The Hamiltonian includes the kinetic energy operator $\frac{p^2}{2m}$ of the centre-of-mass motion with mass m in the harmonic potential $\frac{m\omega_t^2 x^2}{2}$. a ($a^\dagger$) is the annihilation (creation) operator of the electromagnetic field mode. The coupling operator $g(kx)$ characterizes the strength of the interaction of the material system with the single mode of the radiation field and is given by

$$g(kx) = -\sqrt{\frac{\hbar\omega_c}{2\epsilon_0}}\langle 1|\vec{d}|2\rangle \cdot \vec{u}(x, 0, 0), \tag{7.2}$$

where $\vec{d}$ is the dipole operator and k is the wave number of the field. (ϵ_0 is the permittivity of vacuum.) The normalized mode function $\vec{u}(\vec{r})$ is a solution to the Helmholtz equation

$$\left(\nabla^2 + \frac{\omega_c^2}{c^2}\right)\vec{u}(\vec{r}) = 0 \tag{7.3}$$

and fulfils the boundary conditions of the cavity and the Coulomb gauge condition.

We now define the position and momentum operator in terms of the annihilation and creation operators b and $b^\dagger$ of the harmonic trap, that is

$$x = \sqrt{\frac{\hbar}{2m\omega_t}}\left(b + b^\dagger\right), \quad p = \sqrt{\frac{m\hbar\omega_t}{2}}\frac{1}{i}\left(b - b^\dagger\right). \tag{7.4}$$

The minimum of the harmonic potential is in the position $\vec{x} = 0$ and we are going to Taylor expand the coupling operator around this point. There are two necessary conditions to justify this expansion, namely the function $g(\vec{x})$ is smooth in the neighbourhood of the origin and the Lamb-Dicke parameter

$$\eta = k\sqrt{\frac{\hbar}{2m\omega_t}} \ll 1 \tag{7.5}$$

is small. The smoothness of $g(x)$ is guaranteed by $\vec{u}$, which is a solution to the Helmholtz equation. The Lamb-Dicke parameter η measures the deviation

$$\Delta x = \sqrt{\frac{\hbar}{2m\omega_t}} \tag{7.6}$$

of the centre-of-mass motion with respect to the wave length λ of the field

$$\eta = k\sqrt{\frac{\hbar}{2m\omega_t}} = 2\pi\frac{\Delta x}{\lambda}. \tag{7.7}$$

The wavelength of a single-mode cavity is around $\lambda = 600$ nm, and with a typical experimentally used trapped ion, Yb^{2+}, in a 100 MHz oscillatory potential, the Lamb-Dicke parameter yields $\eta \sim 4 \times 10^{-2}$.

Since both conditions for the Taylor expansion are fulfilled, the coupling operator can be written as

$$g(kx) \cong g + \eta g'(x)\,|_{x=0}\,\left(b + b^\dagger\right). \tag{7.8}$$

With the help of the rotating wave approximation for the interaction between the radiation field and the internal states we arrive at

$$\begin{aligned} H_0 =& \omega_t b^\dagger b + \omega_0 |0\rangle\langle 0| + \frac{1}{2}\omega_{21}\sigma_3 + g\sigma_+ a + g^*\sigma_- a^\dagger \\ &+ \omega_c a^\dagger a + \gamma\sigma_+ a\left(b + b^\dagger\right) + \gamma^*\sigma_- a^\dagger\left(b + b^\dagger\right), \end{aligned} \tag{7.9}$$

where $\gamma = \eta g'(0)$.

We now switch to an interaction picture by applying the unitary transformation

$$\begin{aligned} U(t) &= e^{-iH_S t}, \\ H_S &= \omega_0 |0\rangle\langle 0| + \frac{1}{2}\omega_c\sigma_3 + \omega_c a^\dagger a. \end{aligned} \tag{7.10}$$

The Hamiltonian in this interaction picture reads

$$\begin{aligned} H_I =& \omega_t b^\dagger b + \frac{1}{2}\Delta\sigma_3 + g a\sigma_+ + g^* a^\dagger\sigma_- \\ &+ \gamma\sigma_+ a\left(b + b^\dagger\right) + \gamma^*\sigma_- a^\dagger\left(b + b^\dagger\right), \end{aligned} \tag{7.11}$$

where we introduced the detuning $\Delta = \omega_{21} - \omega_c$.

7.1.2 *Dressing the model*

The theoretical treatment of the system is simplified by introducing dressed states, which are eigenstates of the radiation field Hamiltonian. For a pair of bare states with n excitations in the radiation field mode, there are two dressed states $|+, n\rangle$ and $|-, n\rangle$. We express these as superpositions of the bare states $|1\rangle|n\rangle$ and $|2\rangle|n-1\rangle$ so that

$$|+, n\rangle = \alpha_+(n)|1\rangle|n\rangle + \beta_+(n)|2\rangle|n-1\rangle, \tag{7.12}$$

$$|-, n\rangle = \alpha_-(n)|1\rangle|n\rangle + \beta_-(n)|2\rangle|n-1\rangle. \tag{7.13}$$

The eigenvalue equation reads

$$\begin{aligned} \left(\frac{1}{2}\Delta\sigma_3 + g a\sigma_+ + g^* a^\dagger\sigma_-\right)|\pm, n\rangle &= \pm\Omega_R(n)|\pm, n\rangle, \\ \Omega_R(n) &= \sqrt{\Delta^2/4 + |g|^2 n}, \end{aligned} \tag{7.14}$$

where $\Omega_R(n)$ is the Rabi frequency for n photons, and the coefficients $\alpha_\pm(n)$ and $\beta_\pm(n)$ are given by

$$\alpha_-(n) = \beta_+(n) = \left(\frac{\Omega_R(n) + \Delta/2}{2\Omega_R(n)}\right)^{1/2}, \tag{7.15}$$

$$\alpha_+(n) = \left(\frac{\Omega_R(n) - \Delta/2}{2\Omega_R(n)}\right)^{1/2} e^{-i\varphi}, \tag{7.16}$$

$$\beta_-(n) = -\left(\frac{\Omega_R(n) - \Delta/2}{2\Omega_R(n)}\right)^{1/2} e^{i\varphi}. \tag{7.17}$$

We used the orthogonality condition $\langle +, n|-, n\rangle = 0$ and the notation $g = |g|e^{i\varphi}$.

Now, motivated by the results of the resonant interaction [BA13], where a maximally entangled state can be post-selected by a von Neumann measurement, we simplify our model to $\Delta = 0$. This leads to the following identities

$$\begin{aligned}\Big(g a\sigma_+ + g^* a^\dagger \sigma_-\Big)|\pm, n\rangle &= \pm|g|\sqrt{n}|\pm, n\rangle,\\ \Big(\gamma a\sigma_+ + \gamma^* a^\dagger \sigma_-\Big)|\pm, n\rangle &= \pm|\gamma|\sqrt{n}|\pm, n\rangle,\end{aligned} \tag{7.18}$$

where we used the relation $\gamma/g = |\gamma|/|g|$ supported by the definition $\gamma = \eta g'(0)$.

We recall the Hamiltonian in (7.11), which is block-diagonal in regards to the sectors of $|+, n\rangle$ and $|-, n\rangle$

$$\begin{aligned}\langle +, n|H_I|+, n\rangle &= \omega_t b^\dagger b + |g|\sqrt{n} + |\gamma|\sqrt{n}\big(b + b^\dagger\big),\\ \langle -, n|H_I|-, n\rangle &= \omega_t b^\dagger b - |g|\sqrt{n} - |\gamma|\sqrt{n}\big(b + b^\dagger\big),\\ \langle +, n|H_I|-, n\rangle &= \langle -, n|H_I|+, n\rangle = 0.\end{aligned} \tag{7.19}$$

Let us consider that the centre-of-mass motion state is initially in the ground state. We get the following equations by using a general Baker-Hausdorff identity, derived in App. B:

$$\begin{aligned}&e^{-iH_I t}|+, n, 0\rangle = e^{-i\omega_t b^\dagger b t - i|\gamma|\sqrt{n}\left(b+b^\dagger\right)t - i|g|\sqrt{n}t}|+, n, 0\rangle\\ &= e^{-i\omega_t b^\dagger b t - i|\gamma|\sqrt{n}\left(b+b^\dagger\right)t - i|g|\sqrt{n}t} e^{i\omega_t b^\dagger b t} e^{-i\omega_t b^\dagger b t}|+, n, 0\rangle\\ &= e^{i\Phi_n(t) - i|g|\sqrt{n}t} e^{\alpha_n(t) b^\dagger - \alpha_n^*(t) b} e^{-i\omega_t b^\dagger b t}|+, n, 0\rangle\\ &= e^{i\Phi_n(t) - i|g|\sqrt{n}t}|+, n, -\alpha_n(t)\rangle,\end{aligned} \tag{7.20}$$

and for the state $|-, n, 0\rangle$

$$e^{-iH_I t}|-, n, 0\rangle = e^{i\Phi_n(t) + i|g|\sqrt{n}t}|-, n, \alpha_n(t)\rangle, \tag{7.21}$$

where we introduced

$$\alpha_n(t) = \frac{|\gamma|\sqrt{n}}{\omega_t}\left(1 - e^{-i\omega_t t}\right), \tag{7.22}$$

$$\Phi_n(t) = \frac{|\gamma|^2 n}{\omega_t^2}\left(\omega_t t - \sin(\omega_t t)\right). \tag{7.23}$$

We can see that the oscillator states of the centre-of-mass motion and the joint states of the radiation field and of the three-level system get entangled if we start from a superposition of dressed states. This entanglement is detrimental to the quantum repeater and needs to be eliminated, if possible. We observe that the coherent state displacement $\alpha_n(t)$ in the oscillator space oscillates with the trap frequency ω_t and vanishes for times $T = k\frac{2\pi}{\omega_t}, k \in [0, 1, 2, \dots]$ for all n. Since this oscillation is faster than the interaction time τ, one should try and

choose $\tau = k\frac{2\pi}{\omega_t}$ while ensuring that τ remains in the immediate vicinity of the occurence of the collapse phenomenon. Doing so ensures that the oscillator state is separable at the end of the interaction. However, the motion-field interaction still introduces relative phase shifts $e^{i\Phi_n(t)}$ which do not cancel so easily. To have all the phases vanish simultaneously, one would require that $T = m\frac{2\pi\omega_t}{|\gamma|^2}, m \in [0, 1, 2, \dots]$, in addition to $T = k\frac{2\pi}{\omega_t}$. This is fulfilled if $\frac{k}{m} = \frac{\omega_t^2}{|\gamma|^2}$ which will generally lead to very large $T \gg \tau$ and is hardly achievable in the constraints of this setup.

7.2 DECOUPLING THE CENTRE-OF-MASS MOTION

In this section we look at a dynamical decoupling approach to suppress the unwanted interaction between the centre-of-mass motion on the one hand and the radiation field and the internal states on the other hand.

There are two notable differences in this scenario compared to our previous dealings with dynamical decoupling. First, our goal is to protect the subspace consisting of the finite internal three-level state and the radiation field. But in contrast to usual applications of dynamical decoupling we cannot act on the internal states of the qubits because that would decouple not only the unwanted interaction with the centre-of-mass motion, but also the required interaction with the radiation field. Instead, we have to act on our environment, which is the harmonic oscillator space of the centre-of-mass motion. This immediately results in the second difference, since the system we want to act on with decoupling is now an infinite-dimensional system.

7.2.1 *Finding a decoupling scheme*

We want to suppress the coupling between the atomic motion and the rest of the system in the Hamiltonian (7.11) with $\Delta = 0$. Since the harmonic oscillator is an infinite-dimensional system, we cannot use our previously developed methods for finding decoupling schemes and will therefore have to take a different approach. To that end we assume that we are able to apply instantaneously a single unitary operator p to the motion subspace repeatedly. We will see shortly that a single pulse operator is sufficient in this case. The resulting time evolution after application of N equidistant pulses at time t is

$$U_N(t) = \left(pe^{-iH_I\frac{t}{N}}\right)^N. \tag{7.24}$$

By calculating the time derivative of $U_N(t)$ we can define an effective Hamiltonian $H_N(t)$ which generates the same time evolution:

$$\begin{aligned}\frac{d}{dt}U_N(t) &= -\frac{i}{N}\sum_{k=0}^{N-1}\left(pe^{-iH_I\frac{t}{N}}\right)^k pH_Ip^\dagger\left(e^{iH_I\frac{t}{N}}p^\dagger\right)^k U_N(t)\\ &\equiv -iH_N(t)U_N(t). \end{aligned} \tag{7.25}$$

This is similar to what we did in Sec. 5.2.2, minus the stochastic noise component. In order for our decoupling scheme to have the desired effect, we want the average Hamiltonian H_N to be as close to the ideal Hamiltonian as possible,

$$H_{id} = \omega_t b^\dagger b + g a\sigma_+ + g^* a^\dagger \sigma_-. \tag{7.26}$$

To find suitable candidates for the operator p we regard the limit of continuous control, i.e. $N \to \infty$. We are going to derive the generator of the time evolution in this limit by following the method given in the work of Facchi et. al. [FLP04]. The limiting unitary evolution

$$\mathcal{U}(t) = \lim_{N\to\infty} U_N(t) \tag{7.27}$$

satisfies the equation

$$\begin{aligned}\frac{d}{dt}\mathcal{U}(t) &= -i\mathcal{H}\mathcal{U}(t),\\ \mathcal{H} &= \lim_{N\to\infty}\frac{1}{N}\sum_{k=0}^{N-1} p^{k+1}H_I\left(p^\dagger\right)^{k+1}. \end{aligned} \tag{7.28}$$

If we can choose p such that $\mathcal{H} = H_{id}$, then we know that with increasing number N of pulses, H_N approaches the ideal Hamiltonian in the limit $N \to \infty$. Since p acts on the subspace of the centre-of-mass motion and $H_I - H_{id} \sim b + b^\dagger$, it turns out that the solution is to choose p as a diagonal operator in the oscillator eigenstates,

$$p = \sum_{n=0}^{\infty} e^{-i\lambda_n}|n\rangle_t\langle n|_t \otimes \mathbb{1}_c \otimes \mathbb{1}_3, \tag{7.29}$$

where $|n\rangle_t$ ($n \in \mathbb{N}$) is the number state representation of the centre-of-mass motion, $\mathbb{1}_c$ is the identity operator on the Fock space of the radiation field and $\mathbb{1}_3$ stands for the three-dimensional identity matrix. $b^\dagger b$ is a diagonal operator, which means that it commutes with p. Facchi et. al. [FLP04] studied the effects of decoupling operators in the form of (7.29) with non-degenerate spectra, i.e. $\lambda_n \neq \lambda_m$

$(\mathrm{mod}\ 2\pi)$ for $n \neq m$, but we choose not to make this restriction. Inserting (7.29) into (7.28) we find:

$$\begin{aligned}
\mathcal{H} &= H_{id} + \lim_{N\to\infty} \frac{1}{N} \sum_{k=1}^{N} p^k (H_I - H_{id})(p^\dagger)^k \\
&= H_{id} + \left(\gamma \sigma_+ a + \gamma^* \sigma_- a^\dagger\right) \lim_{N\to\infty} \sum_{n,m=0}^{\infty} \\
&\quad \left(\frac{1}{N} \sum_{k=1}^{N} e^{-i(\lambda_n - \lambda_m)k}\right) |n\rangle_t \langle n|_t (b + b^\dagger) |m\rangle_t \langle m|_t \qquad (7.30) \\
&= H_{id} + \left(\gamma \sigma_+ a + \gamma^* \sigma_- a^\dagger\right) \sum_{\substack{\lambda_n = \lambda_{n+1} \\ (\mathrm{mod}\ 2\pi)}} \sqrt{n+1} \times \\
&\quad (|n\rangle_t \langle n+1|_t + |n+1\rangle_t \langle n|_t) \qquad (7.31)
\end{aligned}$$

The limit of $N \to \infty$ eliminates all pairs of the sum in (7.30) where $\lambda_n \neq \lambda_m \pmod{2\pi}$. Of the remaining pairs only direct neighbours contribute due to the ladder operators b and $b^\dagger$. Therefore, in order for $\mathcal{H}$ to be equal to H_{id}, we require that $\lambda_n \neq \lambda_{n+1} \pmod{2\pi}$ for any n.

With this result, we found a suitable class of unitary operations for p of the form given in Eq. (7.29), with the condition that any two neighbors λ_n and λ_{n+1} are not allowed to be in the same 2π modulo class. While this concludes the search from a mathematical viewpoint, in the next section we will look at actual unitary operators that fulfill these conditions and look at how they might be implemented experimentally.

7.2.2 *Suitable decoupling operators and physical implementation*

There is one particular choice for the decoupling operator p which fulfils the conditions $\lambda_n \neq \lambda_{n+j} \pmod{2\pi}$ for all odd j. That is the parity operator

$$\mathcal{P} = \sum_{n=0}^{\infty} (-1)^n |n\rangle\langle n|, \qquad (7.32)$$

whose λ_n are $0, \pi, 2\pi, 3\pi, \ldots$ This choice of decoupling operator has already been proposed by Vitali and Tombesi [VT99] for the case of two harmonic oscillators interacting in the rotating wave approximation.

The parity operator can be written in terms of the number operator $b^\dagger b$ as $\mathcal{P} = e^{-i\pi b^\dagger b}$. If we replace π by an arbitrary phase $\varphi \in (0, \pi)$, then we get a more general class of decoupling operators

$$p = e^{-i\varphi b^\dagger b} \qquad (7.33)$$

with λ_n values of $0, \varphi, 2\varphi, 3\varphi, \ldots$ Therefore they still fulfil the necessary condition $\lambda_n \neq \lambda_{n+1} \pmod{2\pi}$.

So far, this class of operators is a purely theoretical result, as there is no obvious way to implement the parity operator, or the more general p, experimentally. For this, we would require an additional external control Hamiltonian of the form

$$H_p = \chi b^\dagger b \tag{7.34}$$

with some parameter χ that is activated for a time t_p such that $\chi t_p = \varphi$. Then the induced unitary evolution operator is

$$U(t_p) = e^{-i\chi b^\dagger b t_p} = p \tag{7.35}$$

as required. In our search for an experimental realization of such a Hamiltonian, we note that the Hamiltonian of the harmonic oscillator contains a term of exactly this nature: $\omega_t b^\dagger b$. Unfortunately this term does not commute with the rest of the interaction Hamiltonian and therefore does not act undisturbed, otherwise it would implement a perfect decoupling pulse on its own. Even so, the presence of this term does imply a sort of self-decoupling that depends on the trap frequency ω_t - for very high frequencies the term $\omega_t b^\dagger b$ dominates the Hamiltonian and can thus implement the decoupling pulse almost perfectly, but with decreasing frequency the other parts of the Hamiltonian disturb the purity of the pulse. This offers another view on why a higher trap frequency improves the overall fidelity of the entanglement process.

Still, for lower trap frequencies ω_t this gives us an idea of how to implement the Hamiltonian H_p: In our scenario a possibility is to switch off interactions during short time intervals of motion t_p during the interaction time τ, such that within the time interval t_p only the term $\omega_t b^\dagger b$ remains in the interaction picture. In the Lamb-Dicke regime this could be achieved by a Stark-switching procedure, since the coupling of the internal states with the centre-of-mass motion without a radiation field is small during the interaction time τ. This has the additional effect that the time used to implement the pulses does not contribute to the interaction time τ, since no interaction is taking place. Therefore, the whole process now takes a time $T = \tau + Nt_p$ depending on the number of pulses N. Keep in mind, though, that the time T cannot grow arbitrarily large due to experimental constraints. When T grows larger, spontaneous emission will eventually become a problem. Therefore, there is a practical limit on the time Nt_p available to implement all of the pulses. If Γ is the rate of spontaneous decay of the internal state $|2\rangle$ of either material qubit, then we require that

$$T = \tau + Nt_p \ll \frac{1}{\Gamma}. \tag{7.36}$$

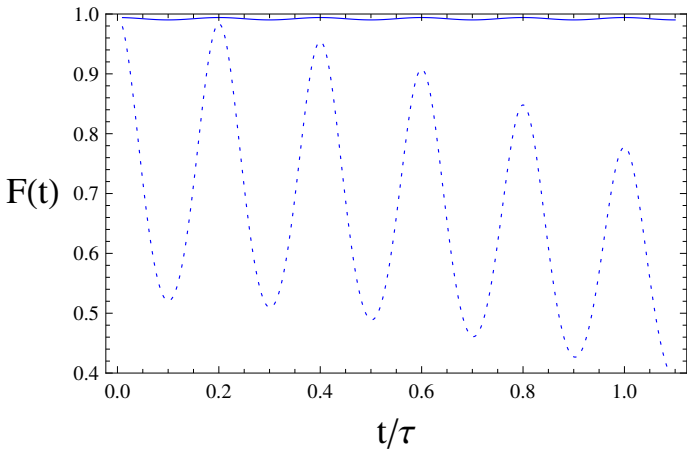

Figure 7.2: The fidelity $F(t)$ of the system compared to its ideal evolution during the interaction time τ. Without decoupling (dotted line) there is a steady drop in the fidelity and also oscillations with frequency $2\omega_t$ as explained by the induced oscillations in the coherent motion states. With active parity kick decoupling, using 200 $\mathcal{P}$ pulses in total during the interaction time, the system effectively remains at unit fidelity throughout the process.

Since the interaction time τ is determined by the occurence of the collapse phenomenon and is of the order $\tau \sim \frac{1}{2|g|}$, we can roughly estimate that the available time to implement our decoupling pulses is limited by

$$N t_p \ll \frac{|g|}{\Gamma}\tau, \tag{7.37}$$

where $\frac{|g|}{\Gamma}$ depends on the specific experimental setup. Recent experimental developments look very promising: whereas in 2003 an experiment by McKeever *et al.* [MBB+03] achieved the ratio $\frac{|g|}{\Gamma} = 6.15$, in 2007 an experiment by Colombe *et al.* [CSD+07] was performed with a significantly improved ratio of $\frac{|g|}{\Gamma} = 71.66$.

This leads to the question of how large N and t_p need to be to see a positive effect of the decoupling procedure. Remember that the class of operators p was derived in the continuous control limit $N \to \infty$. As a consequence, very high repetitions of applications of p may be necessary to observe a positive effect of the decoupling procedure. In order to examine just how large N should be and what phase φ is preferable for the decoupling operator p, we will look at some numerical simulations next.

7.2.3 *Numerical simulation*

We have run a numerical simulation for the trapped system under the influence of the interaction Hamiltonian H_I. For our simulation we

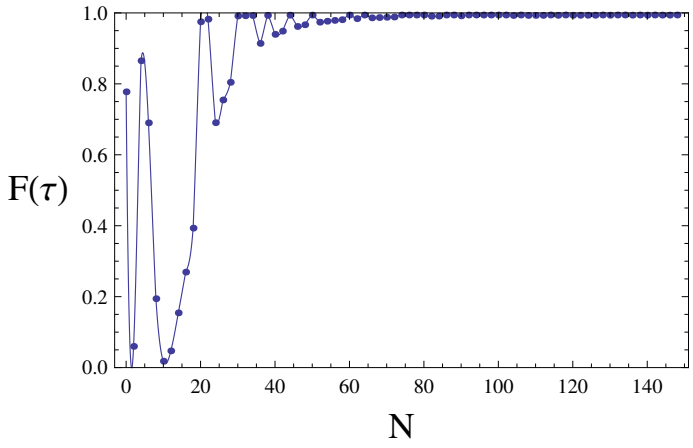

Figure 7.3: The final fidelity $F(\tau)$ of the system at the end of the interaction depending on the number N of parity kicks $\mathcal{P}$ used. The fidelity stabilizes at $N \sim 50$ kicks at high fidelity values.

assume that the material qubit and the radiation field are initially in the state

$$|\Psi_0\rangle = \frac{1}{\sqrt{2}}(|0\rangle|\alpha\rangle_c|0\rangle_t + |1\rangle|\alpha\rangle_c|0\rangle_t), \tag{7.38}$$

meaning that the centre-of-mass motion is in the oscillator ground state while the internal states are in the superposition $\frac{1}{\sqrt{2}}(|0\rangle + |1\rangle)$ and the driving field is in the coherent state $|\alpha\rangle_c$ with $|\alpha|^2 = 100$ the mean photon number. The coupling strengths are chosen such that $\frac{|\gamma|}{|g|} = 0.4$ and $\frac{\omega_t}{|g|} = 10$. Figure 7.2 shows plots of the fidelity

$$F(t) = \left|\langle\Psi_0|U_{id}^{\dagger}(t)U(t)|\Psi_0\rangle\right| \tag{7.39}$$

over the course of the interaction time τ, comparing the time evolution under the actual Hamiltonian H_I and the ideal Hamiltonian H_{id}. First is plotted the fidelity as it evolves without decoupling. There is some oscillation with a frequency of $2\omega_t$, and one can clearly see that the fidelity is steadily decreasing. The oscillation is expected due to the oscillatory behaviour in the coherent state displacement, see (7.23). The second plot demonstrates the effect of our decoupling scheme, where we chose the parity operator $\mathcal{P}$ as the decoupling operator and applied it evenly 200 times over the whole interaction time. There is no visible drop of the fidelity, and even the minimal points of the still present oscillation are well above $F > 0.99$.

Encouraged by this result we studied how many parity kicks one actually needs to achieve a high fidelity at the end of the interaction. We therefore ran additional simulations calculating the final fidelity $F(\tau)$ depending on the number N of parity kicks employed during that time. The results are plotted in figure 7.3; as one can see the

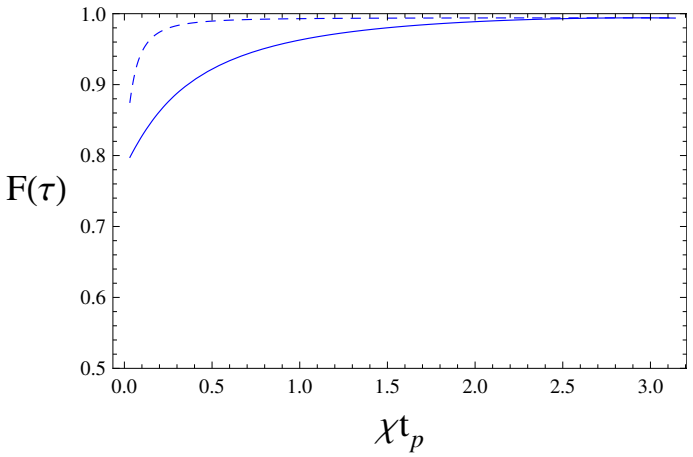

Figure 7.4: The final fidelity $F(\tau)$ of the system at the end of the interaction depending on the parameter χ when using a Hamiltonian $H_p = \hbar\chi b^\dagger b$ to implement a non-parity decoupling pulse p. The fidelity $F(\tau)$ is plotted for different numbers of pulses $N = 50$ (solid) and $N = 400$ (dotted line). It improves with χt_p approaching the parity operator value π. The fidelity is also generally higher for higher number of pulses used.

fidelity stabilizes on a high level at around $N \sim 50$ parity kicks. Below that threshold the fidelity is unpredictable which suggests that the time between pulses is too high and, as a consequence, the system evolution is governed by higher terms of the average Hamiltonian.

The parity operator is only a special case of the class of decoupling operators we found. Indeed, in the experimental realization we proposed the parity operator might need an unacceptably long time t_p to be implemented. Therefore, we ran additional simulations with a decoupling pulse implemented by the Hamiltonian $H_p = \chi b^\dagger b$ over a time t_p, as explained previously. We plotted the dependency of the fidelity $F(\tau)$ after the interaction time τ on the phase χt_p for different numbers N of total pulses. The results are shown in figure 7.4. As we can see, the fidelity improves the closer χt_p comes to the parity value π, which makes the parity operator $\mathcal{P}$ the preferred choice for the decoupling procedure. The fidelity also improves with the number of pulses N, so the smaller the parameter χt_p is in the experimental setup, the more pulses must be employed to get a good fidelity at the end of the interaction.

But as explained before, in actual experimental realizations the number of pulses one can implement is not independent of the pulse width χt_p due to constraints on the overall process time T, expected to be primarily given by the rate of spontaneous decay Γ. Given this constraint, we need to figure out what the best choice of number of pulses N is, considering that the choice of N also fixes the maximal pulse time t_p by the inequality in (7.37). We ran simulations under

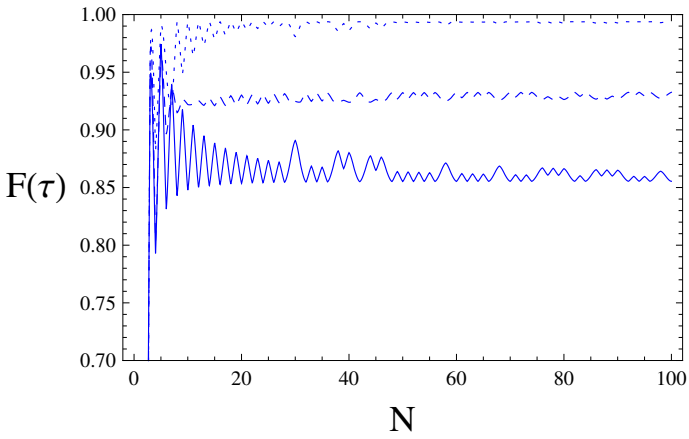

Figure 7.5: The final fidelity $F(\tau)$ of the system at the end of the interaction with time-constrained decoupling. The fidelity is plotted over the number of pulses used, while the number of pulses N also determines the pulse width $\omega_t t_p$ - the higher N, the shorter t_p. The solid curve shows the final fidelity assuming that the additional time Nt_p to implement pulses is τ, whereas the dashed curve assumes it to be 2τ and the dotted curve is for 4τ. All curves converge to an almost constant fidelity value at higher pulse numbers, but show unpredictable behaviour below $N = 20$ pulses. The more time is available for pulse implementation, the higher the achieved fidelity.

the assumptions that the overall process time $T = \tau + Nt_p$ should not exceed 2τ, 3τ and 5τ, respectively. The results are shown in figure 7.5. Unsurprisingly the results are better if more time is available for pulse implementation. Somewhat surprsingly, however, is that the achievable fidelity stabilizes at higher pulse numbers N, so the choice of whether to do larger numbers of short pulses or smaller numbers of longer pulses has little influence as long as the number of pulses does not fall below a certain threshold. For small numbers of pulses the results are unpredictable, suggesting that the delay between pulses is large enough that higher orders of the average Hamiltonian govern the time evolution. For optimal results, judging from our combined numerical simulations, we recommend to aim for $N = 50$ pulses and then make the pulses as close to the parity operator as possible.

8

IMPLEMENTING QUANTUM GATE SEQUENCES ON A COUPLED QUBIT CHAIN

In the final chapter of this thesis, we will take a look at how dynamical decoupling can be integrated with and used for quantum computation. To achieve the goal of building a working quantum computer, we require an architecture that is capable of strongly coupling qubits to implement fast multi-qubit gates, but that can also isolate qubits from each other and the environment when no gate operation is performed. However, current implementations of qubits are typically either well isolated from noise, but difficult to couple, or strongly coupled, but difficult to isolate.

In quantum optics, extensive work has been done using trapped ions or atoms as qubits, and scalable architectures that can trap and address a large number of qubits simultaneously exist [STKB11]. These qubits feature excellent coherence times, yet the implementation of two-qubit gates in these architectures is still a topic of ongoing research, although recently promising proposals were made in this regard [ALB$^+$07, WGE$^+$10, IUZ$^+$10].

Likewise, we have seen significant progress in solid state qubit architectures [MDL$^+$14, ZHS$^+$12, BAN11], and there exist promising candidates for scalable qubit architectures. Gate-defined spin qubits [DS13, ABD$^+$13] feature excellent coherence properties [BFN$^+$11], but coupling two qubits remains a challenge despite proposals for efficient coupling [JMSS12, SDH$^+$12]. For superconducting qubits, both indirect coupling via a resonator [DRS$^+$10] and direct capacitive coupling of detuned qubits [SAB$^+$06] have been demonstrated and are comparatively easy to realize. Recently, good coherence properties were achieved for flux qubits [SCK$^+$14], a particular type of superconducting qubit with a very large anharmonicity. This anharmonicity allows them to be strongly coupled [MPt$^+$05], which makes them particularly interesting for the implementation of fast two-qubit gates. However, their tunability is limited by the need for an optimal operating point, which makes it difficult to isolate the qubits when no gate operation should be performed.

We already established that dynamical decoupling can be used both to suppress environmental influences as well as decouple individual interactions in a qubit network. Indeed, in Sec. 3.3.2 we presented a decoupling scheme to isolate two interacting qubits, which could offer an alternative to switching off the couplings of, e.g., flux qubits. However, if these interactions are strong, as we would like them to be to implement fast multi-qubit gates, then the instanta-

neous bang-bang decoupling may no longer be a suitable approximation. In this chapter, we therefore study a strongly coupled qubit chain and simulate a pulse generator to implement finite-width decoupling pulses. We will develop suitable self-decoupling sequences which can implement both single- and two-qubit gates with high fidelity despite the imperfect controls. As a demonstration, we will simulate a gate sequence on the qubit chain which entangles all the qubits in the chain in a GHZ state [GHZ07] with high fidelity.

The chapter is organized as follows. In Sec. 8.1 we present the physical model of our qubit chain and the type of control we have over the system. Section 8.2 shows how to use dynamical decoupling to implement the two-qubit iSWAP gates between any two neighbouring qubits on the chain. We also discuss how to make this procedure robust against the imperfections of realistic pulses and discuss what kind of constraints these pulses may face in realistic experiments. In Sec. 8.3 we explain how to achieve single-qubit gates with high fidelity by modifying the Eulerian path decoupling approach from Sec. 5.1.3 to implement a dynamically corrected gate. Finally, in Sec. 8.4 we combine all of the components to develop a sequence of gate operations which entangles all the qubits on the chain in a GHZ state.

8.1 THE COUPLED QUBIT SYSTEM MODEL

We consider a system of N qubits in a chain with nearest-neighbor couplings described by the Hamiltonian

$$H_0 = \frac{1}{2}\sum_{i=1}^{N} \epsilon_i \sigma_3^{(i)} - g\sum_{i=1}^{N-1} \sigma_1^{(i)}\sigma_1^{(i+1)}, \tag{8.1}$$

where ϵ_i are the qubits' eigenenergies, and the coupling between the qubits is assumed to be uniform and characterized by the coupling strength g. This model is strongly inspired by a system of coupled flux qubits [MPt+05], however, alternative qubit designs may exist which are also described by this Hamiltonian. Additionally, in our model there is a pulse generator with frequency ω which can exert external control on the qubits. It is described by the control Hamiltonian

$$H_c(t) = \sum_{i=1}^{N} f_i(t)\sigma_1^{(i)} \cos(\omega t + \varphi_i(t)) \tag{8.2}$$

and is governed by the pulse amplitudes $f_i(t)$ and phases $\varphi_i(t)$, which can be controlled for each qubit individually.

For the remainder of the chapter, it is convenient to switch to a rotating frame by transforming to the interaction picture given by the

unitary operator $U_\omega = \exp(-i\frac{\omega}{2}t\sum_i \sigma_3^{(i)})$. In the rotating frame, the system and control Hamiltonians equal

$$\begin{aligned} H_I =& \frac{1}{2}\sum_{i=1}^{N}\Delta_i\sigma_3^{(i)} - \frac{g}{2}\sum_{i=1}^{N-1}\left(\sigma_1^{(i)}\sigma_1^{(i+1)} + \sigma_2^{(i)}\sigma_2^{(i+1)}\right), \\ H_{c,I}(t) =& \frac{1}{2}\sum_{i=1}^{N} f_i(t)\left(\cos(\varphi_i(t))\sigma_1^{(i)} + \sin(\varphi_i(t))\sigma_2^{(i)}\right), \end{aligned} \tag{8.3}$$

where we also applied the rotating wave approximation and dropped the quickly oscillating terms $e^{2i\omega t}$. The $\Delta_i = \epsilon_i - \omega$ indicate the detuning between the individual qubits' eigenenergies and the frequency of the driving field and should ideally be zero for our purposes. If the eigenenergies are different, then we have disorder, which can disrupt the gate operations we intend to implement in the following. However, as we will see, our approach is robust to disorder due to our use of decoupling, as long as the Δ_i do not become too large.

8.2 IMPLEMENTING TWO-QUBIT ISWAP GATES ON THE CHAIN

The coupling between the qubits according to Eq. (8.3) is of XX type. Schuch and Siewert [SS03] studied natural gate operations resulting from such an interaction. They showed that, after an interaction time $T = \pi/(2g)$, this type of coupling between two qubits produces a unitary iSWAP gate:

$$\begin{aligned} U_{\text{iSWAP}} :=& \exp\left[iT\frac{g}{2}\left(\sigma_1^{(i)}\sigma_1^{(i+1)} + \sigma_2^{(i)}\sigma_2^{(i+1)}\right)\right] \\ =& \begin{pmatrix} 1 & & & \\ & 0 & i & \\ & i & 0 & \\ & & & 1 \end{pmatrix}. \end{aligned} \tag{8.4}$$

This gate, like the better known SWAP gate, exchanges the state of two qubits, but introduces an additional phase on the swapped qubit states. However, in our model we have additional couplings to the qubits $(i-1)$ and $(i+2)$ as well as the disorder terms $\frac{\Delta_i}{2}\sigma_3^{(i)}$ and $\frac{\Delta_{i+1}}{2}\sigma_3(i+1)$. In order to successfully use the natural couplings to implement the iSWAP gate, we need to decouple the two qubits involved in the gate operation.

8.2.1 *Selective decoupling on the qubit chain*

In Sec. 3.3.2 we constructed a decoupling scheme which decouples two qubits from environmental influences while keeping a Heisenberg type interaction between the two qubits alive. This is exactly

what we need. In order to implement it, we would thus need to execute a series of alternating XY pulses on the two gate qubits (i) and $(i+1)$ during the gate time T. More precisely, we require four pulses,

$$\begin{aligned} p_1 &= \sigma_1^{(i)}\sigma_1^{(i+1)}, \\ p_2 &= \sigma_2^{(i)}\sigma_2^{(i+1)}, \\ p_3 &= p_1, \\ p_4 &= p_2. \end{aligned} \tag{8.5}$$

This sequence will keep the couplings between qubits (i) and $(i+1)$ alive, but remove those to the qubits $(i-1)$ and $(i+2)$ as well as decouple the disorder terms for the gate qubits. However, this is not enough. If we intend to do sequences of quantum gates on the whole chain, then we must also keep the other qubits isolated during the gate operation, because otherwise the state of the whole chain will be disturbed by the remaining qubit interactions and the disorder.

Fortunately, it is straight-forward to extend this sequence to the whole chain. First we note that if we reverse the pulse order on one of the qubits, so that our pulse sequence is, e.g.,

$$\begin{aligned} p_1' &= \sigma_1^{(i)}\sigma_2^{(i+1)}, \\ p_2' &= \sigma_2^{(i)}\sigma_1^{(i+1)}, \\ p_3' &= p_1', \\ p_4' &= p_2', \end{aligned} \tag{8.6}$$

then the XX type couplings between qubits (i) and $(i+1)$ are eliminated to first order by this decoupling sequence, as is easy to verify. From here, it is easy to see how our decoupling sequence on the whole chain should look like. On each qubit, we do alternating XY pulse sequences, but the order of the X and Y pulses is chosen such that we keep alive those qubit couplings that we want. Two neighbouring qubits whose interaction should be kept intact will have the same ordering of pulse. For those qubits for which the coupling is to be eliminated, the pulse order will be reversed. For example, if we wanted to protect the interaction between the first and last qubit pairs on a 5-qubit chain, but eliminate the couplings with the middle qubit, we would use the following pulse sequence:

$$\begin{aligned} p_1 &= \sigma_1^{(1)}\sigma_1^{(2)}\sigma_2^{(3)}\sigma_1^{(4)}\sigma_1^{(5)}, \\ p_2 &= \sigma_2^{(1)}\sigma_2^{(2)}\sigma_1^{(3)}\sigma_2^{(4)}\sigma_2^{(5)}, \\ p_3 &= p_1, \\ p_4 &= p_2. \end{aligned} \tag{8.7}$$

This allows us to selectively decouple only specific interactions on the chain, which in turn allows us to even do several iSWAP gates in parallel, as long as they are not on neighbouring qubit pairs. All disorder terms $\frac{\Delta_i}{2}\sigma_3^{(i)}$ are also eliminated in the lowest order.

8.2.2 *Decoupling pulses with the pulse generator*

In order to implement the required decoupling pulses σ_1 and σ_2 on the individual qubits, we will make use of the pulse generator. For each qubit, we can select the required pulse by setting the phase function $\varphi_i(t)$ to the appropriate value. In the rotating frame, the unitary operator implemented by the control Hamiltonian alone is

$$U_{c,I}(t) = \exp\left[-\frac{i}{2}\sum_{i=1}^{N}\int_0^t dt' f_i(t')\left(\cos(\varphi_i(t'))\sigma_1^{(i)} - \sin(\varphi_i(t'))\sigma_2^{(i)}\right)\right] \tag{8.8}$$

For the pulse amplitudes we can choose any smooth function such that

$$\int_0^{t_p} dt\, f_i(t) = \pi, \tag{8.9}$$

where t_p is the finite time it will take to implement a pulse. If we then choose a phase $\varphi_i = 0$, then $U_{c,I}(t_p) = \sigma_1^{(i)}$ for this particular qubit. Similarly, a phase $\varphi_i = \pi/2$ will give us a σ_2 pulse after time t_p. Implementing the decoupling sequence is a matter of selecting the appropriate phases for each qubit and then switching on the pulse generator with the amplitude functions $f_i(t)$ for a time t_p.

Since we expect the qubit couplings to be strong in order to implement the iSWAP gate quickly, we cannot assume that $t_p \ll T$, i.e. that the pulse implementation time t_p is negligible compared to the gate time T. However, this means that the decoupling pulses cannot be treated as instantaneous, and as such we have to expect that the finite width of the pulses will cause a noticeable error. As a consequence, we should adopt the results about self-decoupling sequences in Sec. 5.1. Thankfully, this is rather straight-forward. Since our decoupling sequences contain the annihilator scheme for each individual qubit, we can simply replace it with a first-order self-decoupling sequence. For instance, the 5-qubit sequence in Eq. (8.7) is replaced by

$$\begin{aligned} p_1 = p_3 = p_6 = p_8 &= \sigma_1^{(1)}\sigma_1^{(2)}\sigma_2^{(3)}\sigma_1^{(4)}\sigma_1^{(5)}, \\ p_2 = p_4 = p_5 = p_7 &= \sigma_2^{(1)}\sigma_2^{(2)}\sigma_1^{(3)}\sigma_2^{(4)}\sigma_2^{(5)}. \end{aligned} \tag{8.10}$$

We should note that, due to the multi-qubit pulses and interactions between the pulses, the terms occurring in the lowest order of the pulse errors $\Phi_j^{[0]}$ cannot all be suppressed by our scheme. The reason is that it was designed specifically to allow certain interaction terms to be kept alive, some of which appear in $\Phi_j^{[0]}$. However, it still suppresses a significant amount of the errors, and as we will see shortly, the achievable fidelities are generally high.

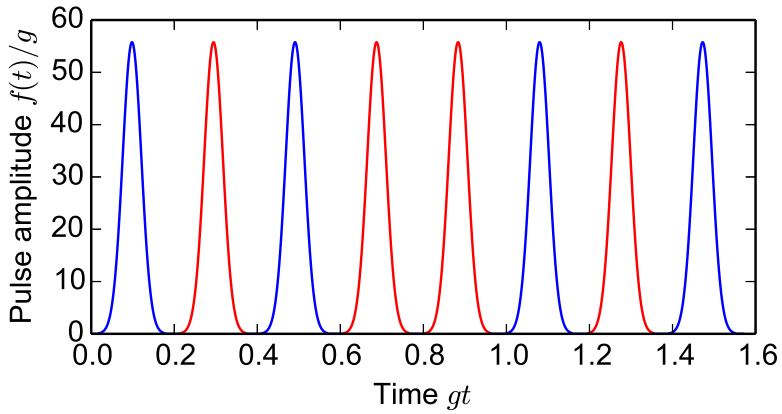

Figure 8.1: The pulse sequence used to implement the iSWAP gate. This figure shows the pulse sequence used for both of the gate qubits, where blue signifies a pulse in X direction and red signifies a pulse in Y direction. Neighbouring qubits use the same pulse sequence, but with X and Y swapped.

8.2.3 *Physical limits and numerical simulations*

The pulse implementation time t_p should be made as small as possible. However, there are some fundamental obstacles which prevent us from making t_p infinitely short. For one, a physical pulse generator will have limitations on how quickly it can steer the pulse amplitude and on the maximal achievable pulse amplitude, which in turn limits the minimal pulse duration. Additionally, the rotating frame Hamiltonian in Eq. (8.3) was derived in the rotating wave approximation. In order to ensure validity of this approximation, we require $1 \ll 2\omega t_p$. Another fundamental problem is the fact that many physical implementations of qubits are only approximately two-level systems. If we probe the physical system hard enough, which in our case means if we choose $t_p \to 0$, eventually we will excite higher states or invoke additional interactions and thus invalidate our two-level approximation.

With that in mind, let us look at what kind of pulse duration we would have to achieve to actually implement the iSWAP gate with high fidelity. Given the implementation time $T = \pi/(2g)$ of the iSWAP gate and the necessity to implement a series of 8 pulses during that time, the upper limit for the pulse time is given as $t_p \leqslant \pi/(16g)$. In our simulation, we have used pulse times

$$t_p \in [\pi/(16g), \pi/(32g), \pi/(48g), \pi(64g), \pi/(96g)].$$

We simulated a qubit chain of varying length and implemented the iSWAP gate in the middle of the chain. We used Gaussian pulse shapes for the decoupling pulses, and Fig. 8.1 depicts the pulse sequence used. We simulated the time-dependent Schrödinger equa-

$t_p = \pi/(16g)$	$\pi/(32g)$	$\pi/(48g)$	$\pi/(64g)$	$\pi/(96g)$
0.9922	0.9979	0.9990	0.9994	0.9997

Table 8.1: Numerical simulation results for the achievable fidelity of the iSWAP gate, depending on the pulse duration t_p.

tion for the full pulse sequence and calculated the emerging state of the qubit chain, where we then traced out all of the qubits except for the two gate qubits. The resulting state ρ was then compared to the expected state $|\Psi\rangle = U_{iSWAP}|\Psi_{in}\rangle$ by means of the state fidelity

$$F(T) = |\langle\Psi|\rho|\Psi\rangle| . \tag{8.11}$$

As initial states $|\Psi_{in}\rangle$ we used all four basis states $|00\rangle$, $|01\rangle$, $|10\rangle$ and $|11\rangle$ and took the average over the achieved fidelities. The remaining qubits were always prepared in the state $|0\rangle$. The average fidelities depending on the pulse duration t_p are given in table 8.1. The results were virtually independent of the number of total qubits N in the chain. We can see that even for the longest possible pulse duration $t_p = \pi/(16g)$, the gate fidelity is quite good.

Are these pulse durations realistic? Let us consider as a concrete example two superconducting flux qubits. Flux qubits with always-on couplings of the order of $g \sim 500\,\mathrm{MHz}$ were realized in [MPt+05], which would allow for a fast implementation of the iSWAP gate. Additionally, flux qubits feature a rather large anharmonicity, meaning that the higher energy levels are separated from the two qubit states by a significant gap. As such, we could in theory have a pulse amplitude of several GHz before we risk exciting the higher states. Let us assume that we could safely employ a maximum pulse amplitude $f_{max} = 10\mathrm{GHz}$. Then the achievable minimal pulse duration for that amplitude depends on the specific pulse shape. For a Gauss pulse like we used in our simulations we find that for $t_p = \pi/(16g)$, the required maximal pulse amplitude is $\sim 45g$. However, with the assumed value of g and f_{max} for the flux qubits, we only achieve a ratio of $f_{max}/g \sim 20$. As a consequence, we would have to reduce the coupling constant by a factor of about 2. Alternatively, one could also look at different pulse shapes. For example, a sine-shaped pulse would only require $f_{max}/g \sim 25$, which is much closer. However, we found in our simulations that the sine pulse performs slightly worse in terms of achievable gate fidelity. As such, there is a compromise to be made between minimizing the gate duration T and maximizing the gate fidelity.

Let us assume that we choose to engineer a coupling strength of $g = 100\,\mathrm{MHz}$, which gives us some additional reserves and allows us to aim for a pulse duration of $t_p = \pi/(32g) \approx 1\,\mathrm{ns}$ without exciting higher states. With the driving field frequency ω tuned to the

approximate qubit level splitting of 5 GHz, this pulse time is then one order of magnitude larger than $1/(2\omega)$, so that the rotating wave approximation is still valid. The implementation time of the iSWAP gate is $T \approx 16\,\mathrm{ns}$, during which 8 pulses need to be applied, resulting in a pulse frequency of 500 MHz. The requirements for our pulse generator are ambitious, but not impossible. Even more encouragingly, in recent experiments flux qubits have been demonstrated with decoherence times of the order of $10\,\mu\mathrm{s}$ [BGY+11, SCK+14]. This means that the gate operation time is almost three orders of magnitude faster than the decoherence time, making this procedure viable for flux qubits. Other implementations of the basic model from Sec. 8.1 may impose very different limitations.

In the interest of maximizing the fidelity, we should also point out that there exist more sophisticated pulse shapes than Gaussian or sine-shaped pulses. Some of these pulse shapes were specifically engineered to reduce their own error (see, e.g., [VC05] for a review of NMR pulse shapes or [PS08] for a more recent design), or are less likely to excite higher states in the system [SMC03, MGRW09, MW13]. Both of these properties might help to improve the gate fidelity further. However, specifically with the self-correcting pulse shapes, the price to pay is typically a significantly higher ratio $f_{\max}/g$ to implement a particular pulse in the same time span. Thus the qubit interaction strength g would have to be reduced even further, meaning that decoherence becomes a potentially larger concern. Which pulse shape is the most adequate depends on the specific needs of a particular experiment. In our numerical simulations, Gaussian shaped pulses proved to provide a suitable compromise between achievable fidelity and required maximal pulse amplitude.

8.3 DYNAMICALLY CORRECTED SINGLE-QUBIT GATES

In addition to the two-qubit iSWAP gate, we will also need to be able to perform single-qubit gates on the individual qubits. For the implementation of the single-qubit gates, we will again make use of the pulse generator. This means that the available gate operations are given by the unitary propagator of Eq. (8.8). In particular, we can implement rotation operations around the X and Y axes,

$$\begin{aligned} R_x(\phi) &= e^{-i\sigma_1\phi/2}, \\ R_y(\phi) &= e^{-i\sigma_2\phi/2} \end{aligned} \tag{8.12}$$

which can be realised by choosing the phase φ_i appropriately and engineering the pulse amplitude function such that $\int_0^{t_p} dt\, f_i(t) = \phi/2$. However, as with the decoupling pulses in Sec. 8.2.2, the gate operation is disturbed by the system Hamiltonian H_0, which limits the achievable gate fidelity. For a single-qubit gate, we typically want

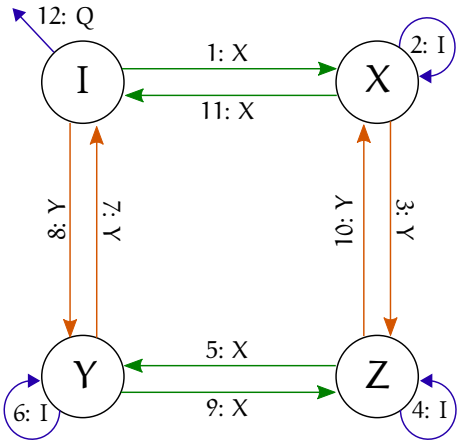

Figure 8.2: A Eulerian path for a dynamically corrected gate operation Q.

to achieve fidelities well above 0.99, which is a requirement to add quantum error correction later.

8.3.1 *Dynamically corrected gates with Eulerian path decoupling*

Fortunately, there is a way to embed a gate operation Q into a Eulerian path decoupling sequence such that it decouples the error of the gate. This technique is called *dynamically corrected gates* and was introduced in [KV09a, KV09b]. The idea is deceptively simple. Remember in the original Eulerian path construction in Fig. 5.1, each generator (decoupling pulse) formed an outgoing edge from every node (toggling operator), ensuring that its error would be decoupled to lowest order. We can add the identity operation $\mathbb{1}$ as another "generator" to this picture, represented as loops which go out from each node and point back to that same node. Let us now consider that our identity operations are not perfect, but in fact given by $I = \mathbb{1}e^{-i\Phi_I}$, carrying an error Φ_I like the other decoupling pulses. Then this error is decoupled to first order by design of the Eulerian path construction. Finally, let us replace the final identity operation with the actual gate Q that we want to implement, and let us assume that Q has the same error as the faulty identity operation, $\Phi_Q = \Phi_I$. The updated graph for the resulting decoupling sequence is depicted in Fig. 8.2. The net operation of this sequence without any errors would be the gate Q, as intended. Furthermore, the errors of all occurring operations are corrected to first order by the Eulerian path design.

This design hinges on the question whether we can find a faulty identity operation which has the same error as the gate Q. It turns out this is possible at least to first order of the error. Consider an arbitrary gate Q with its time propagator given by $U_Q(t)$ during the

implementation time t_Q. The first order of its associated error is given as

$$\Phi_Q^{[0]} = \int_0^{t_Q} U_Q^\dagger(t) H_0 U_Q(t) dt. \tag{8.13}$$

We will now construct the faulty identity operation as $I = Q^\dagger Q$ with time propagator

$$U_I(t) = \begin{cases} U_Q(t), & 0 \leqslant t < t_Q, \\ U_Q(2t_q - t), & t_Q \leqslant t \leqslant 2t_Q. \end{cases} \tag{8.14}$$

Its error to first order can be calculated to be

$$\begin{aligned} \Phi_I^{[0]} &= \int_0^{2t_Q} U_I^\dagger(t) H_0 U_I(t) dt \\ &= 2\int_0^{t_Q} U_Q^\dagger(t) H_0 U_Q(t) dt = 2\Phi_Q^{[0]}. \end{aligned} \tag{8.15}$$

This is almost what we need, except for the factor 2. However, we can accomodate the original gate Q such that it matches this error. This is done by scaling it such that it takes twice as long to execute. Let us call this scaled gate $Q_{1/2}$ with time propagator $U_{Q_{1/2}}(t) = U_Q(t/2)$, which obviously needs an implementation time of $2t_Q$. Its error to first order is given by

$$\begin{aligned} \Phi_{Q_{1/2}}^{[0]} &= \int_0^{2t_Q} U_Q^\dagger(t/2) H_0 U_Q(t/2) dt \\ &= 2\int_0^{t_Q} U_Q^\dagger(t) H_0 U_Q(t) dt = 2\Phi_Q^{[0]}, \end{aligned} \tag{8.16}$$

just as we wanted. In our control scheme, for any of the possible rotation gates $R_a(\phi)$, the gates I and $Q_{1/2}$ can be implemented in a straight-forward manner by modifying the phase amplitude functions $f_i(t)$. For the faulty identity gate we need

$$f_i'(t) = \begin{cases} f_i(t), & 0 \leqslant t < t_Q, \\ -f_i(2t_Q - t), & t_Q \leqslant t \leqslant 2t_Q, \end{cases} \tag{8.17}$$

meaning that we append the negative reverse of the original pulse shape of gate Q. For the gate $Q_{1/2}$ we need to scale both the time and the amplitude by 1/2, meaning

$$f_i'(t) = \frac{1}{2} f_i(t/2). \tag{8.18}$$

If our minimal gate time is given by t_p, then each of the faulty identity operations and the final gate Q will take $2t_p$ to implement. As a consequence, the total duration to implement a single-qubit gate is $16t_p$. For the case of flux qubits as discussed in Sec. 8.2.3, the operation times for a single qubit gate and the iSWAP gate are thus comparable.

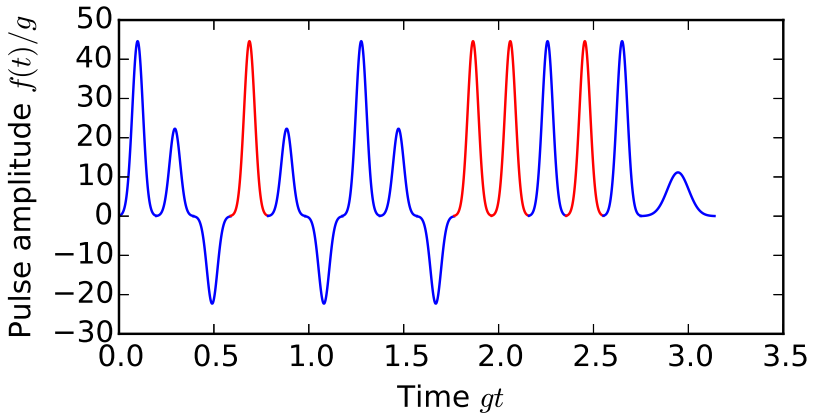

Figure 8.3: The pulse sequence applied to a single qubit to implement a dynamically corrected $R_x(\pi/2)$ gate with Gaussian pulse shapes. Blue indicates that the pulse generator is acting along the X axis, red indicates a pulse along the Y axis.

8.3.2 *Implementation and numerical simulations*

Figure 8.3 shows the concrete pulse sequence we are employing in our numerical simulations to implement a dynamically corrected $R_x(\pi/2)$ gate with the decoupling sequence from Fig. 8.2. The blue parts indicate pulses along the X axis, red parts indicate pulses along the Y axis. All qubits in the chain are subjected to the same sequence, except that neighbouring qubits will have the X and Y pulses interchanged such that the couplings between the qubits are decoupled. Qubits on which no gate is implemented will leave the pulse amplitude set to 0 during the I and Q phases in the sequence. Note that several single-qubit gates can, in principle, be applied in parallel to different qubits, however not on neighbouring qubits. The reason is that on neighbouring qubits, the error associated with the gate $Q = Q_1 \otimes Q_2$ contains terms which cannot be decoupled by our decoupling scheme, and as a consequence the fidelity reduces significantly. Therefore, single-qubit gates on neighbouring qubits should be performed sequentially.

As with the iSWAP gate, we simulated the pulse sequence from Fig. 8.3 on the middle qubit of a chain with N qubits by simulating the time-dependent Schrödinger equation, then tracing out all qubits but the gate qubit. The remaining traced state ρ was compared to the expected state. As input states, we simulated both $|0\rangle$ and $|1\rangle$ and took the average of the resulting fidelities. The results for the implementation of the $R_x(\pi/2)$ gate can be found in table 8.2. Results for different single-qubit gates are very similar. We can see that even for $t_p = \pi/(16g)$ the fidelity is excellent.

$t_p = \pi/(16g)$	$\pi/(24g)$	$\pi/(32g)$	$\pi/(40g)$	$\pi/(48g)$
0.99929	0.99986	0.99996	0.99998	0.99999

Table 8.2: Numerical simulation results for the achievable fidelity of the $R_x(\pi/2)$ gate, depending on the pulse duration t_p.

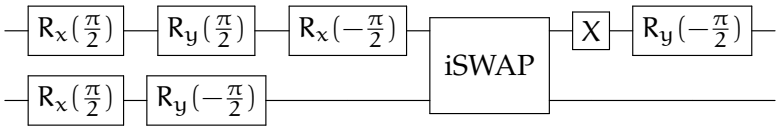

Figure 8.4: The quantum circuit to implement a CNS gate with the help of the iSWAP gate and a number of single-qubit rotations.

8.4 ENTANGLING THE CHAIN QUBITS WITH THE HELP OF A CNS GATE SEQUENCE

In the following, we investigate how to implement an entangling two-qubit gate in our model. An entangling gate is a necessity for universal quantum computing, and the previously implemented iSWAP gate on its own is not sufficient. Although the underlying model from Sec. 8.1 can, in principle, generate entanglement for different interaction times $T \neq \pi/(2g)$, a more reliable way to generate controlled entanglement is to combine the iSWAP gate with a sequence of single-qubit gates to perform the so-called CNS gate [SS03]. The CNS gate is a combination of a standard CNOT followed by a SWAP operation. The action of the gate on the basis states of a two-qubit Hilbert space is defined as follows:

$$\begin{aligned} |00\rangle &\xrightarrow{\text{CNS}} |00\rangle & |01\rangle &\xrightarrow{\text{CNS}} |10\rangle \\ |10\rangle &\xrightarrow{\text{CNS}} |11\rangle & |11\rangle &\xrightarrow{\text{CNS}} |01\rangle \end{aligned} \tag{8.19}$$

Here, the first qubit acts as the control. If it is in the state 1, then the state of the second qubit is flipped. Afterwards, the states of both qubits are swapped. This gate is able to generate entanglement between two qubits.

The gate sequence depicted in Fig. 8.4 implements a CNS gate with the upper qubit being the control qubit.

In [SS03], Hadamard gates and rotations around the Z axis were used. We rearranged the gate sequence to use rotations around the X and Y axes instead, as these are the operations accessible in our model with the help of the pulse generator.

We already have all the pieces of the puzzle to implement the CNS gate. Given that the single-qubit gates must be performed sequentially due to being on neighbouring qubits, the CNS gate will take

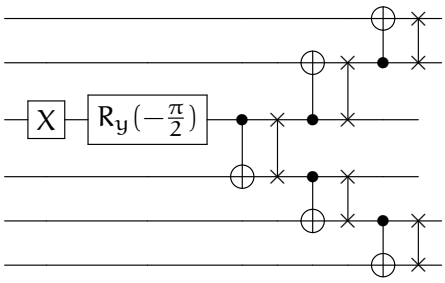

Figure 8.5: A quantum circuit to entangle all qubits in a quantum register in a GHZ state. In this figure, the CNS gates are represented by a directed CNOT gate followed by a SWAP gate.

time $\pi/(2g) + 112t_p$ to implement. For our flux qubit example with a coupling strength of $g = 100\,\mathrm{MHz}$ and $t_p = \pi/(32g)$, this yields a time of approximately 126 ns, which is still a factor of 80 below the decoherence time.

As a final experiment in this chapter, we will perform a sequence of CNS gates to entangle all the qubits in the chain.

8.4.1 *An entangling sequence of CNS gates*

If we perform a CNS gate on two qubits, of which the first (control) is prepared in the superposition $(|0\rangle + |1\rangle)/\sqrt{2}$ and the second in the state $|0\rangle$, then by Eq. (8.19) the resulting state is $(|00\rangle + |11\rangle)/\sqrt{2}$, which is an entangled Bell state. If we now take a third qubit, initially also in the state $|0\rangle$, and perform a CNS gate an qubits 2 and 3, then we get a three-qubit entangled state $(|000\rangle + |111\rangle)/\sqrt{2}$. With each additional execution of a CNS gate, we can bring an additional qubit into the entangled state. This type of multi-qubit entangled states is called a GHZ state [GHZ07]:

$$|\mathrm{GHZ}\rangle = \frac{|0\rangle^{\otimes N} + |1\rangle^{\otimes N}}{\sqrt{2}}. \tag{8.20}$$

Let us assume that all qubits on the chain are initially prepared in the state $|0\rangle$. Then we bring a qubit in the middle of the chain into the superposition $(|0\rangle + |1\rangle)/\sqrt{2}$. This is done by applying a Hadamard gate to it, which in our model we can express as an X gate followed by a rotation $R_y(-\pi/2)$. From there on we apply CNS gates to entangle this qubit with all the other qubits in the chain, where we can in fact apply CNS gates in parallel, except not on directly neighbouring qubit pairs, as that would apply single-qubit gates on neighbouring qubits. A gate sequence for a 6-qubit chain is depicted in Fig. 8.5.

We conducted numerical simulations for this gate sequence by calculating the resulting state $|\Psi\rangle$ by simulating the time-dependent Schrödinger equation, where we assume that all qubits are initially in the

N	$t_p = \pi/(16g)$	$\pi/(32g)$	$\pi/(48g)$	$\pi/(64g)$	$\pi/(96g)$
3	0.964	0.989	0.995	0.997	0.999
4	0.933	0.982	0.992	0.995	0.998
5	0.882	0.974	0.988	0.993	0.997
6	0.835	0.967	0.986	0.992	0.996
7	0.821	0.962	0.983	0.990	0.996
8	0.784	0.956	0.981	0.989	0.995
9	0.710	0.947	0.977	0.987	0.994

Table 8.3: Numerical simulation results for the achievable fidelity of the GHZ state, depending on the number N of qubits and the pulse duration t_p.

state $|0\rangle$. We calculated the fidelity F_{GHZ} of the GHZ state depending on the pulse duration t_p for Gaussian pulse shapes,

$$F_{GHZ} = |\langle GHZ|\Psi\rangle| . \tag{8.21}$$

We simulated qubit chains of up to 9 qubits. The results are shown in table 8.3. Given pulses which are sufficiently quick compared to the coupling strength g, a high fidelity of 0.99 for the entangled state can theoretically be achieved even for $N = 9$ qubits. However, at least in the flux qubit case, this would require us to reduce the coupling strength g to the point that the full gate sequence will approach the flux qubit decoherence time. For the more realistic pulse duration $t_p = \pi/(32g)$ the achieved fidelities are not as spectacular, but still promising.

It is clear that with increasing N, the fidelities will steadily drop. This is a consequence of the increased number of imperfect gate operations. Additionally, the longer the gate sequence, the closer we get to the decoherence time, at which point everything breaks down. In order to achieve scalability, the addition of quantum error correction is therefore necessary. We believe that the demonstrated gate fidelities for single-qubit gates and the iSWAP gate are sufficiently high that error correction is feasible. For a possible implementation, we would propose to extend the qubit chain model to a two-dimensional grid, on which we could then employ a surface code. The extension to the grid requires modifications to the decoupling scheme, which are not trivial, but should be possible. Such a scenario has been accomplished recently for Ising-type qubit couplings by De and Pryadko in [DP13, DP14].

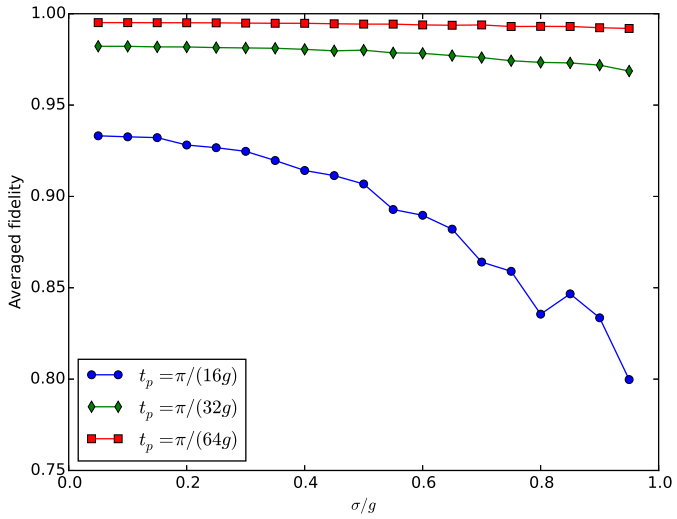

Figure 8.6: Averaged fidelity for a GHZ state achievable on a 4-qubit chain for different values of the pulse duration t_p (Gaussian pulse shapes were used), when the qubit eigenenergies differ from each other. The Δ_i are randomly sampled from a Gaussian distribution with standard deviation σ. The plotted results were averaged over 100 runs.

8.4.2 *Influence of disorder*

The results in table 8.3 were achieved under the assumption that the qubits' eigenergies are all the same, meaning that the Δ_i in Eq. (8.3) are all zero in the rotating frame. Non-zero Δ_i have a detrimental effect on the achievable fidelity. However, our decoupling scheme offers limited robustness against these effects. We ran additional simulations where we sampled the Δ_i randomly from a Gaussian distribution with mean value $\mu = 0$ and standard deviation σ. Results of the achievable fidelity depending on σ, averaged over 100 runs, are plotted in Fig. 8.6 for a chain of four qubits. We can see that the drop in the averaged fidelity is noticeable for $t_p = \pi/(16g)$, but with faster pulses becomes negligible, at least up to the simulated maximal value of $\sigma/g = 1$. In a recent experiment with 20 flux qubits [MOR+14], deviations of up to 1 GHz were observed in the eigenenergies, which may be two to ten times larger than the coupling g, depending on how strongly the qubits are engineered to interact. As such, current experimental deviations may be larger than our decoupling scheme can handle. We can expect that with improved manufacturing processes the qubit eigenenergy discrepancies will become sufficiently small in the future so that the detrimental influence of the disorder is negligible with sufficiently fast pulses.

9

CONCLUSIONS AND OUTLOOK

Dynamical decoupling is a powerful method by which a quantum system is rotated in its state space by means of repeated applications of strong external control pulses. A careful design of the pulse sequence allows us to average out certain parts of a Hamiltonian acting on the system, at least to a certain order of the average Hamiltonian. A natural application of the technique is to suppress couplings to an environment, which will significantly reduce the effects of decoherence and dissipation and thus significantly improve the lifetime and fidelity of a quantum system. However, removing or weakening certain parts of a system Hamiltonian can also be a viable method for simulating other Hamiltonian interactions.

In the first part of this thesis, we introduced the theoretical foundations of dynamical decoupling and then developed a new approach to design pulse sequences on networks of qubits formed entirely from Pauli pulses. This method employs a linear set of equations which depends on the actual system Hamiltonian H_0 and a target Hamiltonian H_{id} and allows us to determine a possible set of decoupling pulses and their relative frequency to turn H_0 into H_{id} to lowest order. The construction is more general than previous techniques, and while it does not scale to systems with a large number of qubits, it performs well on small systems and often provides the basis to construct a scalable scheme with some minor manual adjustments. This method was then extended to networks of qudits, where the generalized spin operators take the place of the Pauli pulses. Finally, we studied the effects of imperfections in the control pulses and how to deal with them. Here, we were able to extend previous results on self-stabilizing pulse sequences to higher orders and also introduced a stochastic noise model, which we analysed in detail.

In the second part, we looked at practical applications of dynamical decoupling to concrete problems in quantum information theory. We developed several pulse sequences to protect or engineer quantum state transfer on a qubit chain, which we also extended to the qudit case. Then we studied the effects of atomic motion in a cavity during interaction with a radiation field. For instance, this is a relevant source of fidelity loss in the distribution of entanglement over long distances in a quantum repeater. We developed a dynamical decoupling technique to counter the atomic motion in this scenario. Finally, we considered how decoupling techniques can be used to implement a universal set of quantum gate operations on a coupled qubit chain. Our approach exploits the natural interaction of the

qubits to implement a two-qubit gate operation, while decoupling is used to isolate the qubits where necessary and to implement high-fidelity single-qubit gates. Our approach is capable of dealing with realistic finite-width pulses and also discusses the physical viability specifically for superconducting flux qubits.

As a next step, we would like to extend the coupled qubit chain to a two-dimensional grid and adapt our quantum gate implementations to this new structure. In particular, this would allow us to implement a certain set of quantum error correction codes on the grid to achieve true scalability. We would also like to explore possibilities to generalise our scheme construction method to sets of elementary pulses different from the Pauli or generalised spin operators. Given that the current method relies on a specific property of these operators, it may require some modification to work with a different set of operators.

To conclude, we believe that dynamical decoupling is a vital technique in the realisation of quantum computation architectures, both for suppressing environmental influences and for modifying existing Hamiltonians. The scheme construction method we presented is versatile and can accommodate both cases, which we demonstrated in several applications throughout this thesis. We believe that it will therefore be a valuable tool in practical decoupling scheme design.

Part III

APPENDIX

A

HIGHER-ORDER SELF-STABILIZING SEQUENCES

In this appendix, we list self-stabilizing sequences of higher orders that we found by a search algorithm. Due to the length of the sequences, we give them as a list of numbers, where 1 represents a σ_1 pulse and 2 a σ_2 pulse. All sequences decouple any time-independent Hamiltonian on a single qubit at least to first order, and the systematic control errors as described in Sec. 5.1 to the order specified.

ORDER 1 (Length 8)

22121121 (A.1)

ORDER 2 (Length 16)

2212112121221211 (A.2)

ORDER 3 (Length 32)

22121211212211212212112121221211 (A.3)

ORDER 4 (Length 64)

2212121122121121212212112122112122121211212211212
2212112121221211 (A.4)

ORDER 5 (Length 128)

2212121122121121212212112122112122121211212211212
2212112121222121122121211212221122121121212211
2212112122121211212211211 (A.5)

ORDER 6 (Length 256)

2212121122121121212212112122112122121211212211212
2212112121222121122121211212221122121121212211
2212112122121211212211212122112122121211222121121
2122121112221121222121211212211212212112121221211
2212121122121121212211212212121122121122121121
2122121122121121 (A.6)

ORDER 7 (Length 512)

221212112212112121221211212211212212121121221121
221211212122121122121211212212112212112121221211
221211212212121121221121212211212212121122121121
212212112121221121221212112122112122121121212211
221212112122112121221121221212112122121122121121
212212112212112122121211221211212122121121221121
221212112122112122121121212211212212121121221211
221211212122121122121121221212112122112121221211
212211212212121121221121221211212122121122121211
221211212122112122121211212212112212112121221211
22121121221212112122112121221211 (A.7)

ORDER 8 (Length 1024)

221212112212112121221211212211212212121121221121
221211212122121122121211221211212122112122121211
212212112212112121221211221211212212121121221121
212212112212121122121121212212112122112122121211
212211212212112121221121221212112122121122121121
212212112212112122121211212211212122121121221121
221212112122112122121121212212112212121121221211
221211212122121122121121221212112122112121221121
221212112212112121221211212211212212121121221121
221211212122121122121211212211212122112122121211
212212112212112121221211221211212212121122121121
212212112122112122121211212211212212112121221211
221212112122121122121121212212112212112122121211
212211212122112122121211221211212122121121221121
221212112122112122121121212212112212121121221121
212211212212121121221211221211212122121122121121
221212112212112121221211212211212212121121221121
221211212122112122121211212212112212112121221211
221211212212121121221121212212112122112122121211
212211212212112121221211221212112212112121221121
221212112122121122121121212212112212112122121211
2122112121221211 (A.8)

ORDER 9 (Length 2048)

22121211221211212122121121221121221212112122112122121121
21221211221212112212112121221121221212112122121122121121
21221211221211212212121121221121212212112212121122121121
21221211212211212212121121221121221211212122112122121211
21221211221211212122121122121121221212112122112121221211
21221121221212112122112122121121212212112212121121221211
22121121212212112212112122121211212211212122112122121211
22121121212212112122112122121211212211212212112121221211
22121211212211212122112122121211212212112212112121221211
22121121221212112212112121221211212211212212121121221121
22121121212212112212121121221211221211212122121122121121
22121211212211212122112122121211221211212122121121221121
22121211212211212212112121221211221212112122112121221121
22121211212212112212112121221211221211212212121122121121
21221211212211212212121121221121221211212122112122121211
21221211221211212122121122121121221212112122112121221211
21221121221212112122112122121121212212112212121122121121
21221121221212112122121122121121212212112212112122121211
21221121212212112212121122121121212212112122112122121211
21221121221211212122121122121211212212112212112121221211
22121121221212112122112121221211212211212212121121221121
22121121212212112212121122121121212211212212121121221211
22121121212212112212112122121211212211212122121122121211
22121121212212112122112122121211212211212212112121221121
22121211212212112212112121221211221211212212121121221121
21221211212211212212121121221121221211212122121122121211
22121121212211212212121121221211221211212122121122121121
22121211212211212122121122121211221211212122121121221121
22121211212211212212112121221121221212112122121122121121
21221211221211212212121122121121212212112122112122121211
21221121221211212122121122121211212212112212112121221211
22121121221212112122112121221121221212112212112121221211
21221121221212112122112122121121212212112212121121221121
21221121221212112122121122121121212212112212112122121211
21221121212211212212121122121121212212112122112122121211
21221121221211212122121122121211212211212122112122121211
21221211221211212122121122121121 (A.9)

B

BAKER-HAUSDORFF FORMULA FOR CENTRE-OF-MASS MOTION

In this appendix we derive a general Baker-Hausdorff identity which is used in Eq. (7.20). Let us define the unitary operator

$$U(t) = e^{i\omega_t b^\dagger b t} e^{-i\omega_t b^\dagger b t - i|\gamma|\sqrt{n}\left(b+b^\dagger\right)t}, \tag{B.1}$$

which fulfils the following equation of motion

$$\begin{aligned}\frac{dU(t)}{dt} &= -i|\gamma|\sqrt{n}e^{i\omega_t b^\dagger b t}\left(b+b^\dagger\right)e^{-i\omega_t b^\dagger b t}U(t)\\ &= \Big(A(t)+B(t)\Big)U(t),\end{aligned} \tag{B.2}$$

where

$$\begin{aligned}A(t) &= -i|\gamma|\sqrt{n}e^{-i\omega_t t}b,\\ B(t) &= -i|\gamma|\sqrt{n}e^{i\omega_t t}b^\dagger.\end{aligned} \tag{B.3}$$

This follows from the fact that

$$\begin{aligned}e^{i\omega_t b^\dagger b t}be^{-i\omega_t b^\dagger b t} &= e^{-i\omega_t t}b,\\ e^{i\omega_t b^\dagger b t}b^\dagger e^{-i\omega_t b^\dagger b t} &= e^{i\omega_t t}b^\dagger.\end{aligned} \tag{B.4}$$

The operators $A(t)$ and $B(t)$ obey the commutation relations

$$\begin{aligned}\left[A(t),A(t')\right] &= \left[B(t),B(t')\right] = 0,\\ \left[A(t),B(t')\right] &= -|\gamma|^2 n e^{-i\omega_t(t-t')}.\end{aligned} \tag{B.5}$$

Consider now the operator V defined as

$$V(t) = e^{\int_0^t dt' B(t')}e^{\int_0^t dt' A(t')}, \tag{B.6}$$

whose equation of motion is

$$\begin{aligned}\frac{dV(t)}{dt} &= e^{\int_0^t dt' B(t')}\Big(B(t)+A(t)\Big)e^{\int_0^t dt' A(t')},\\ &= \Big(B(t)+e^{\int_0^t dt' B(t')}A(t)e^{-\int_0^t dt' B(t')}\Big)V(t).\end{aligned} \tag{B.7}$$

Now using the identity

$$e^B A e^{-B} = A + [B,A] + \frac{1}{2!}[B,[B,A]] + \dots \tag{B.8}$$

and the fact that the commutator of $A(t)$ and $B(t)$ is a number, the equation of motion for V takes the form

$$\frac{dV(t)}{dt} = \Big(B(t)+A(t)+\int_0^t dt'\left[B(t'),A(t)\right]\Big)V(t). \tag{B.9}$$

Now comparing (B.2) with (B.9) and knowing that $[B(t'), A(t)]$ is a number, we get

$$U(t) = e^{\int_0^t dt' B(t')} e^{\int_0^t dt' A(t')} e^{-\int_o^t dt' \int_0^{t'} dt'' [B(t''), A(t')]}. \tag{B.10}$$

In Eq. (7.20), an operator of the form $e^{-i\omega_t b^\dagger b t} U(t) e^{i\omega_t b^\dagger b t}$ appears. With Eq. (B.10) we can then express this operator as

$$\begin{aligned}
&e^{-i\omega_t b^\dagger b t} U(t) e^{i\omega_t b^\dagger b t} \\
&= e^{-i\omega_t b^\dagger b t} e^{\int_0^t dt' B(t')} e^{i\omega_t b^\dagger b t} e^{-i\omega_t b^\dagger b t} e^{\int_0^t dt' A(t')} e^{i\omega_t b^\dagger b t} \\
&\quad \times e^{-\int_o^t dt' \int_0^{t'} dt'' [B(t''), A(t')]}, \\
&= e^{-i|\gamma|\sqrt{n}\int_0^t dt' e^{i\omega_t t'} e^{-i\omega_t t} b^\dagger} e^{-i|\gamma|\sqrt{n}\int_0^t dt' e^{-i\omega_t t'} e^{i\omega_t t} b} \\
&\quad \times e^{-|\gamma|^2 n \int_o^t dt' \int_0^{t'} dt'' e^{i\omega(t''-t')}}, \\
&= e^{-\frac{|\gamma|\sqrt{n}}{\omega_t}\left(1-e^{-i\omega_t t}\right) b^\dagger} e^{\frac{|\gamma|\sqrt{n}}{\omega_t}\left(1-e^{i\omega_t t}\right) b} e^{-\frac{|\gamma|^2 n}{\omega_t^2}\left(1-i\omega_t t - e^{-i\omega_t t}\right)} \\
&= e^{i\Phi_n(t)} e^{-\alpha_n(t) b^\dagger + \alpha_n^*(t) b},
\end{aligned} \tag{B.11}$$

where we introduced the parameters

$$\alpha_n(t) = \frac{|\gamma|\sqrt{n}}{\omega_t}\left(1 - e^{-i\omega_t t}\right), \tag{B.12}$$

$$\Phi_n(t) = \frac{|\gamma|^2 n}{\omega_t^2}\left(\omega_t t - \sin(\omega_t t)\right). \tag{B.13}$$

In the derivation we used the identity

$$e^{e^{-iB} A e^{iB}} = \sum_{n=0}^{\infty} \frac{\left(e^{-iB} A e^{iB}\right)^n}{n!} = \sum_{n=0}^{\infty} e^{-iB} \frac{A^n}{n!} e^{iB} = e^{-iB} e^{A} e^{iB} \tag{B.14}$$

together with Eqs. (B.4) to move the operators $e^{\pm i\omega_t b^\dagger b t}$ into the exponents. We also used the fact that since $[b, [b, b^\dagger]] = [b^\dagger, [b^\dagger, b]] = 0$, we can write

$$e^{-\alpha_n(t) b^\dagger} e^{\alpha_n^*(t) b} = e^{-\alpha_n(t) b^\dagger + \alpha_n^*(t) b} e^{\frac{1}{2}|\alpha_n(t)|^2 [b, b^\dagger]}. \tag{B.15}$$

BIBLIOGRAPHY

[ABD+13] David D. Awschalom, Lee C. Bassett, Andrew S. Dzurak, Evelyn L. Hu, and Jason R. Petta. Quantum spintronics: Engineering and manipulating atom-like spins in semiconductors. *Science*, 339(6124):1174–1179, August 2013. (Cited on page 115.)

[ALB+07] Marco Anderlini, Patricia J. Lee, Benjamin L. Brown, Jennifer Sebby-Strabley, William D. Phillips, and J. V. Porto. Controlled exchange interaction between pairs of neutral atoms in an optical lattice. *Nature*, 448(7152):452–456, July 2007. (Cited on page 115.)

[BA13] J. Z. Bernád and G. Alber. Photon-assisted entanglement creation by minimum-error generalized quantum measurements in the strong-coupling regime. *Physical Review A*, 87(1):012311, January 2013. (Cited on pages 99, 100, and 105.)

[Bal14] Leslie E. Ballentine. *Quantum Mechanics*. World Scientific Publishing Co Pte Ltd, Hackensack, New Jersey, 2 ed. edition, October 2014. (Cited on page 6.)

[BAN11] Iulia Buluta, Sahel Ashhab, and Franco Nori. Natural and artificial atoms for quantum computation. *Reports on Progress in Physics*, 74(10):104401, October 2011. (Cited on page 115.)

[BBC+93] Charles H. Bennett, Gilles Brassard, Claude Crépeau, Richard Jozsa, Asher Peres, and William K. Wootters. Teleporting an unknown quantum state via dual classical and einstein-podolsky-rosen channels. *Physical Review Letters*, 70(13):1895–1899, March 1993. (Cited on pages 5 and 45.)

[BBP+96] Charles H. Bennett, Gilles Brassard, Sandu Popescu, Benjamin Schumacher, John A. Smolin, and William K. Wootters. Purification of noisy entanglement and faithful teleportation via noisy channels. *Physical Review Letters*, 76(5):722–725, January 1996. (Cited on page 99.)

[BDCZ98] H.-J. Briegel, W. Dür, J. I. Cirac, and P. Zoller. Quantum repeaters: The role of imperfect local operations in quantum communication. *Physical Review Letters*, 81(26):5932–5935, December 1998. (Cited on page 99.)

[BF14] J. Z. Bernád and H. Frydrych. Effects of stochastic noise on dynamical decoupling procedures. *Physical Review A*, 89(6):062327, June 2014. (Cited on page 5.)

[BFA13] J Z Bernád, H Frydrych, and G Alber. Centre-of-mass motion-induced decoherence and entanglement generation in a hybrid quantum repeater. *Journal of Physics B: Atomic, Molecular and Optical Physics*, 46(23):235501, November 2013. (Cited on pages 5 and 102.)

[BFAJ15] P. Bažant, H. Frydrych, G. Alber, and I. Jex. Suppressing systematic control errors to high orders. *Physical Review A*, 92(2):022325, August 2015. (Cited on pages 5, 56, and 57.)

[BFN+11] Hendrik Bluhm, Sandra Foletti, Izhar Neder, Mark Rudner, Diana Mahalu, Vladimir Umansky, and Amir Yacoby. Dephasing time of GaAs electron-spin qubits coupled to a nuclear bath exceeding 200 μs. *Nature Physics*, 7(2):109–113, February 2011. (Cited on pages 17 and 115.)

[BGY+11] Jonas Bylander, Simon Gustavsson, Fei Yan, Fumiki Yoshihara, Khalil Harrabi, George Fitch, David G. Cory, Yasunobu Nakamura, Jaw-Shen Tsai, and William D. Oliver. Noise spectroscopy through dynamical decoupling with a superconducting flux qubit. *Nature Physics*, 7(7):565–570, July 2011. (Cited on pages 17 and 122.)

[BK08] Reinhold A. Bertlmann and Philipp Krammer. Bloch vectors for qudits. *Journal of Physics A: Mathematical and Theoretical*, 41(23):235303, June 2008. (Cited on pages 44 and 45.)

[BMM+10] C. Barthel, J. Medford, C. M. Marcus, M. P. Hanson, and A. C. Gossard. Interlaced dynamical decoupling and coherent operation of a singlet-triplet qubit. *Physical Review Letters*, 105(26):266808, December 2010. (Cited on page 17.)

[BNJ09] T. Brougham, G. M. Nikolopoulos, and I. Jex. Communication in quantum networks of logical bus topology. *Physical Review A*, 80(5):052325, November 2009. (Cited on page 79.)

[Bos03] Sougato Bose. Quantum communication through an unmodulated spin chain. *Physical Review Letters*, 91(20):207901, November 2003. (Cited on pages 5 and 75.)

[BR12] R. Blatt and C. F. Roos. Quantum simulations with trapped ions. *Nature Physics*, 8(4):277–284, April 2012. (Cited on page 100.)

[Bur81] D. P. Burum. Magnus expansion generator. *Physical Review B*, 24(7):3684–3692, October 1981. (Cited on page 21.)

[BUV+09a] Michael J. Biercuk, Hermann Uys, Aaron P. VanDevender, Nobuyasu Shiga, Wayne M. Itano, and John J. Bollinger. Experimental uhrig dynamical decoupling using trapped ions. *Physical Review A*, 79(6):062324, June 2009. (Cited on page 17.)

[BUV+09b] Michael J. Biercuk, Hermann Uys, Aaron P. VanDevender, Nobuyasu Shiga, Wayne M. Itano, and John J. Bollinger. Optimized dynamical decoupling in a model quantum memory. *Nature*, 458(7241):996–1000, April 2009. (Cited on page 17.)

[CDEL04] Matthias Christandl, Nilanjana Datta, Artur Ekert, and Andrew J. Landahl. Perfect state transfer in quantum spin networks. *Physical Review Letters*, 92(18):187902, May 2004. (Cited on pages 5, 75, 76, and 77.)

[CL83] A. O Caldeira and A. J Leggett. Quantum tunnelling in a dissipative system. *Annals of Physics*, 149(2):374–456, September 1983. (Cited on page 71.)

[CL04] W. A. Coish and Daniel Loss. Hyperfine interaction in a quantum dot: Non-markovian electron spin dynamics. *Physical Review B*, 70(19):195340, November 2004. (Cited on pages 67 and 69.)

[CP54] H. Y. Carr and E. M. Purcell. Effects of diffusion on free precession in nuclear magnetic resonance experiments. *Physical Review*, 94(3):630–638, May 1954. (Cited on pages 4 and 17.)

[CSD+07] Yves Colombe, Tilo Steinmetz, Guilhem Dubois, Felix Linke, David Hunger, and Jakob Reichel. Strong atom–field coupling for bose–einstein condensates in an optical cavity on a chip. *Nature*, 450(7167):272–276, November 2007. (Cited on pages 100 and 110.)

[DBCZ99] W. Dür, H.-J. Briegel, J. I. Cirac, and P. Zoller. Quantum repeaters based on entanglement purification. *Physical Review A*, 59(1):169–181, January 1999. (Cited on page 99.)

[DEJ+96] David Deutsch, Artur Ekert, Richard Jozsa, Chiara Macchiavello, Sandu Popescu, and Anna Sanpera. Quantum privacy amplification and the security of quantum cryptography over noisy channels. *Physical Review Letters*, 77(13):2818–2821, September 1996. (Cited on page 99.)

[DLDG+09] S. Damodarakurup, M. Lucamarini, G. Di Giuseppe, D. Vitali, and P. Tombesi. Experimental inhibition of decoherence on flying qubits via "Bang-bang" control. *Physical Review Letters*, 103(4):040502, July 2009. (Cited on page 17.)

[dLWR+10] G. de Lange, Z. H. Wang, D. Ristè, V. V. Dobrovitski, and R. Hanson. Universal dynamical decoupling of a single solid-state spin from a spin bath. *Science*, 330(6000):60–63, January 2010. (Cited on page 17.)

[DNBT02] Jennifer L. Dodd, Michael A. Nielsen, Michael J. Bremner, and Robert T. Thew. Universal quantum computation and simulation using any entangling hamiltonian and local unitaries. *Physical Review A*, 65(4):040301, April 2002. (Cited on page 18.)

[DP13] Amrit De and Leonid P. Pryadko. Universal set of scalable dynamically corrected gates for quantum error correction with always-on qubit couplings. *Physical Review Letters*, 110(7):070503, February 2013. (Cited on page 128.)

[DP14] Amrit De and Leonid P. Pryadko. Dynamically corrected gates for qubits with always-on ising couplings: Error model and fault tolerance with the toric code. *Physical Review A*, 89(3):032332, March 2014. (Cited on page 128.)

[DRS+10] L. DiCarlo, M. D. Reed, L. Sun, B. R. Johnson, J. M. Chow, J. M. Gambetta, L. Frunzio, S. M. Girvin, M. H. Devoret, and R. J. Schoelkopf. Preparation and measurement of three-qubit entanglement in a superconducting circuit. *Nature*, 467(7315):574–578, September 2010. (Cited on page 115.)

[DRZ+09] Jiangfeng Du, Xing Rong, Nan Zhao, Ya Wang, Jiahui Yang, and R. B. Liu. Preserving electron spin coherence in solids by optimal dynamical decoupling. *Nature*, 461(7268):1265–1268, October 2009. (Cited on page 17.)

[DS13] M. H. Devoret and R. J. Schoelkopf. Superconducting circuits for quantum information: An outlook. *Science*, 339(6124):1169–1174, August 2013. (Cited on page 115.)

[FAB14] Holger Frydrych, Gernot Alber, and Pavel Bažant. Constructing pauli pulse schemes for decoupling and quantum simulation. *Physical Review A*, 89(2):022320, February 2014. (Cited on pages 4 and 5.)

[FHJA15] H. Frydrych, A. Hoskovec, I. Jex, and G. Alber. Selective dynamical decoupling for quantum state transfer. *Journal of Physics B: Atomic, Molecular and Optical Physics*, 48(2):025501, January 2015. (Cited on page 6.)

[FLP04] P. Facchi, D. A. Lidar, and S. Pascazio. Unification of dynamical decoupling and the quantum zeno effect. *Physical Review A*, 69(3):032314, March 2004. (Cited on page 107.)

[FMA15] Holger Frydrych, Michael Marthaler, and Gernot Alber. Pulse-controlled quantum gate sequences on a strongly coupled qubit chain. *Physical Review A*, 92:062322, December 2015. (Cited on page 5.)

[GHZ07] Daniel M. Greenberger, Michael A. Horne, and Anton Zeilinger. Going beyond bell's theorem. *arXiv:0712.0921 [quant-ph]*, December 2007. (Cited on pages 6, 116, and 127.)

[GKL08] Goren Gordon, Gershon Kurizki, and Daniel A. Lidar. Optimal dynamical decoherence control of a qubit. *Physical Review Letters*, 101(1):010403, July 2008. (Cited on page 24.)

[GKS76] Vittorio Gorini, Andrzej Kossakowski, and E. C. G. Sudarshan. Completely positive dynamical semigroups of n-level systems. *Journal of Mathematical Physics*, 17(5):821–825, May 1976. (Cited on page 62.)

[Hae76] Ulrich Haeberlen. *High Resolution NMR in Solids Selective Averaging*. Academic Press, 1976. (Cited on pages 4, 17, and 21.)

[Hah50] E. L. Hahn. Spin echoes. *Physical Review*, 80(4):580–594, November 1950. (Cited on pages 4 and 17.)

[HE81] F. T. Hioe and J. H. Eberly. n-level coherence vector and higher conservation laws in quantum optics and quantum mechanics. *Physical Review Letters*, 47(12):838–841, September 1981. (Cited on page 44.)

[HSS99] A. S. Hedayat, N. J. A. Sloane, and John Stufken. *Orthogonal Arrays*. Springer Series in Statistics. Springer New York, New York, NY, 1999. (Cited on page 36.)

[Hum14] Frederic Hummel. *Perfect State Transfer in Qudit Networks via Dynamical Decoupling*. Bachelor thesis, Technische Universität Darmstadt, Darmstadt, 2014. (Cited on page 96.)

[IUZ+10] L. Isenhower, E. Urban, X. L. Zhang, A. T. Gill, T. Henage, T. A. Johnson, T. G. Walker, and M. Saffman. Demonstration of a neutral atom controlled-NOT quantum gate. *Physical Review Letters*, 104(1):010503, January 2010. (Cited on page 115.)

[JMSS12] Pei-Qing Jin, Michael Marthaler, Alexander Shnirman, and Gerd Schön. Strong coupling of spin qubits to a transmission line resonator. *Physical Review Letters*, 108(19):190506, May 2012. (Cited on page 115.)

[KA05] O. Kern and G. Alber. Controlling quantum systems by embedded dynamical decoupling schemes. *Physical Review Letters*, 95(25):250501, December 2005. (Cited on page 24.)

[KAS05] O. Kern, G. Alber, and D. L. Shepelyansky. Quantum error correction of coherent errors by randomization. *The European Physical Journal D - Atomic, Molecular, Optical and Plasma Physics*, 32(1):153–156, January 2005. (Cited on page 24.)

[Kay10] Alastair Kay. Perfect, efficient, state transfer and its application as a constructive tool. *International Journal of Quantum Information*, 08(04):641–676, June 2010. (Cited on page 75.)

[KFF+14] Mario Krenn, Robert Fickler, Matthias Fink, Johannes Handsteiner, Mehul Malik, Thomas Scheidl, Rupert Ursin, and Anton Zeilinger. Communication with spatially modulated light through turbulent air across vienna. *New Journal of Physics*, 16(11):113028, November 2014. (Cited on page 99.)

[KL05] K. Khodjasteh and D. A. Lidar. Fault-tolerant quantum dynamical decoupling. *Physical Review Letters*, 95(18):180501, October 2005. (Cited on pages 23 and 51.)

[KL07] Kaveh Khodjasteh and Daniel A. Lidar. Performance of deterministic dynamical decoupling schemes: Concatenated and periodic pulse sequences. *Physical Review A*, 75(6):062310, June 2007. (Cited on page 23.)

[KV09a] Kaveh Khodjasteh and Lorenza Viola. Dynamical quantum error correction of unitary operations with bounded

controls. *Physical Review A*, 80(3):032314, September 2009. (Cited on page 123.)

[KV09b] Kaveh Khodjasteh and Lorenza Viola. Dynamically error-corrected gates for universal quantum computation. *Physical Review Letters*, 102(8):080501, February 2009. (Cited on page 123.)

[LB13] Daniel A. Lidar and Todd A. Brun. *Quantum Error Correction*. Cambridge University Press, Cambridge, United Kingdom ; New York, auflage: new. edition, September 2013. (Cited on pages 18 and 23.)

[LBMW03] D. Leibfried, R. Blatt, C. Monroe, and D. Wineland. Quantum dynamics of single trapped ions. *Reviews of Modern Physics*, 75(1):281–324, March 2003. (Cited on page 100.)

[LDGD+11] M. Lucamarini, G. Di Giuseppe, S. Damodarakurup, D. Vitali, and P. Tombesi. Suppression of polarization decoherence for traveling light pulses via bang-bang dynamical decoupling. *Physical Review A*, 83(3):032320, March 2011. (Cited on page 17.)

[Leu02] D. W. Leung. Simulation and reversal of n-qubit hamiltonians using hadamard matrices. *Journal of Modern Optics*, 49(8):1197–1197, July 2002. (Cited on page 25.)

[Lin75] Göran Lindblad. Completely positive maps and entropy inequalities. *Communications in Mathematical Physics*, 40(2):147–151, June 1975. (Cited on page 62.)

[LMK+96] D. Leibfried, D. M. Meekhof, B. E. King, C. Monroe, W. M. Itano, and D. J. Wineland. Experimental determination of the motional quantum state of a trapped atom. *Physical Review Letters*, 77(21):4281–4285, November 1996. (Cited on page 100.)

[LvLN+06] T. D. Ladd, P. van Loock, K. Nemoto, W. J. Munro, and Y. Yamamoto. Hybrid quantum repeater based on dispersive CQED interactions between matter qubits and bright coherent light. *New Journal of Physics*, 8(9):184, September 2006. (Cited on pages 5 and 99.)

[LWDS08] B. Lee, W. M. Witzel, and S. Das Sarma. Universal pulse sequence to minimize spin dephasing in the central spin decoherence problem. *Physical Review Letters*, 100(16):160505, April 2008. (Cited on page 24.)

[Mag54] Wilhelm Magnus. On the exponential solution of differential equations for a linear operator. *Communications on*

Pure and Applied Mathematics, 7(4):649–673, 1954. (Cited on pages 4 and 20.)

[MBB+03] J. McKeever, A. Boca, A. D. Boozer, J. R. Buck, and H. J. Kimble. Experimental realization of a one-atom laser in the regime of strong coupling. *Nature*, 425(6955):268–271, September 2003. (Cited on page 110.)

[MDL+14] Juha T. Muhonen, Juan P. Dehollain, Arne Laucht, Fay E. Hudson, Rachpon Kalra, Takeharu Sekiguchi, Kohei M. Itoh, David N. Jamieson, Jeffrey C. McCallum, Andrew S. Dzurak, and Andrea Morello. Storing quantum information for 30 seconds in a nanoelectronic device. *Nature Nanotechnology*, 9(12):986–991, December 2014. (Cited on page 115.)

[MdT+03] I. Marcikic, H. de Riedmatten, W. Tittel, H. Zbinden, and N. Gisin. Long-distance teleportation of qubits at telecommunication wavelengths. *Nature*, 421(6922):509–513, January 2003. (Cited on page 99.)

[MG58] S. Meiboom and D. Gill. Modified spin-echo method for measuring nuclear relaxation times. *Review of Scientific Instruments*, 29(8):688, 1958. (Cited on pages 4 and 17.)

[MGRW09] F. Motzoi, J. M. Gambetta, P. Rebentrost, and F. K. Wilhelm. Simple pulses for elimination of leakage in weakly nonlinear qubits. *Physical Review Letters*, 103(11):110501, September 2009. (Cited on page 122.)

[MHS+12] Xiao-Song Ma, Thomas Herbst, Thomas Scheidl, Daqing Wang, Sebastian Kropatschek, William Naylor, Bernhard Wittmann, Alexandra Mech, Johannes Kofler, Elena Anisimova, Vadim Makarov, Thomas Jennewein, Rupert Ursin, and Anton Zeilinger. Quantum teleportation over 143 kilometres using active feed-forward. *Nature*, 489(7415):269–273, September 2012. (Cited on page 99.)

[MOR+14] Pascal Macha, Gregor Oelsner, Jan-Michael Reiner, Michael Marthaler, Stephan André, Gerd Schön, Uwe Hübner, Hans-Georg Meyer, Evgeni Il'ichev, and Alexey V. Ustinov. Implementation of a quantum metamaterial using superconducting qubits. *Nature Communications*, 5:5146, October 2014. (Cited on page 129.)

[MPt+05] J. B. Majer, F. G. Paauw, A. C. J. ter Haar, C. J. P. M. Harmans, and J. E. Mooij. Spectroscopy on two coupled superconducting flux qubits. *Physical Review Letters*, 94(9):090501, March 2005. (Cited on pages 115, 116, and 121.)

[MW13] F. Motzoi and F. K. Wilhelm. Improving frequency selection of driven pulses using derivative-based transition suppression. *Physical Review A*, 88(6):062318, December 2013. (Cited on page 122.)

[NC00] Michael A. Nielsen and Isaac L. Chuang. *Quantum Computation and Quantum Information*. Cambridge University Press, October 2000. (Cited on page 13.)

[NHJ12] G. M. Nikolopoulos, A. Hoskovec, and I. Jex. Analysis and minimization of bending losses in discrete quantum networks. *Physical Review A*, 85(6):062319, June 2012. (Cited on pages 5, 75, 78, and 88.)

[NJ13] Georgios M. Nikolopoulos and Igor Jex. *Quantum State Transfer and Network Engineering*. Springer Science & Business Media, October 2013. (Cited on page 75.)

[NPL04] G. M. Nikolopoulos, D. Petrosyan, and P. Lambropoulos. Coherent electron wavepacket propagation and entanglement in array of coupled quantum dots. *EPL (Europhysics Letters)*, 65(3):297, February 2004. (Cited on pages 5, 75, and 76.)

[Par92] K. R. Parthasarathy. *An Introduction to Quantum Stochastic Calculus*. Springer Science & Business Media, 1992. (Cited on page 59.)

[PNL10] David Petrosyan, Georgios M. Nikolopoulos, and P. Lambropoulos. State transfer in static and dynamic spin chains with disorder. *Physical Review A*, 81(4):042307, April 2010. (Cited on pages 75 and 77.)

[PR04] Arthur O. Pittenger and Morton H. Rubin. Mutually unbiased bases, generalized spin matrices and separability. *Linear Algebra and its Applications*, 390:255–278, October 2004. (Cited on page 45.)

[PS08] Leonid P. Pryadko and Pinaki Sengupta. Second-order shaped pulses for solid-state quantum computation. *Physical Review A*, 78(3):032336, September 2008. (Cited on page 122.)

[PSB14] Sima Pouyandeh, Farhad Shahbazi, and Abolfazl Bayat. Measurement-induced dynamics for spin-chain quantum communication and its application for optical lattices. *Physical Review A*, 90(1):012337, July 2014. (Cited on page 75.)

[PSK+13] Ch. Piltz, B. Scharfenberger, A. Khromova, A. F. Varón, and Ch. Wunderlich. Protecting conditional quantum

gates by robust dynamical decoupling. *Physical Review Letters*, 110(20):200501, May 2013. (Cited on page 58.)

[Rud91] Walter Rudin. *Functional Analysis*. McGraw-Hill Science/Engineering/Math, New York, 2 edition edition, January 1991. (Cited on page 59.)

[RW06] M. Rotteler and P. Wocjan. Equivalence of decoupling schemes and orthogonal arrays. *IEEE Transactions on Information Theory*, 52(9):4171–4181, September 2006. (Cited on page 25.)

[SAB+06] Matthias Steffen, M. Ansmann, Radoslaw C. Bialczak, N. Katz, Erik Lucero, R. McDermott, Matthew Neeley, E. M. Weig, A. N. Cleland, and John M. Martinis. Measurement of the entanglement of two superconducting qubits via state tomography. *Science*, 313(5792):1423–1425, August 2006. (Cited on page 115.)

[SÁS11] Alexandre M. Souza, Gonzalo A. Álvarez, and Dieter Suter. Robust dynamical decoupling for quantum computing and quantum memory. *Physical Review Letters*, 106(24):240501, June 2011. (Cited on page 24.)

[Sch01] Wolfgang P. Schleich. *Quantum Optics in Phase Space*. Wiley-VCH Verlag GmbH & Co. KGaA, Berlin ; New York, auflage: 1. auflage edition, February 2001. (Cited on page 102.)

[SCH+06] T. Steinmetz, Y. Colombe, D. Hunger, T. W. Hänsch, A. Balocchi, R. J. Warburton, and J. Reichel. Stable fiber-based fabry-pérot cavity. *Applied Physics Letters*, 89(11):111110, September 2006. (Cited on page 100.)

[SCK+14] M. Stern, G. Catelani, Y. Kubo, C. Grezes, A. Bienfait, D. Vion, D. Esteve, and P. Bertet. Flux qubits with long coherence times for hybrid quantum circuits. *Physical Review Letters*, 113(12):123601, September 2014. (Cited on pages 115 and 122.)

[SDH+12] M. D. Shulman, O. E. Dial, S. P. Harvey, H. Bluhm, V. Umansky, and A. Yacoby. Demonstration of entanglement of electrostatically coupled singlet-triplet qubits. *Science*, 336(6078):202–205, April 2012. (Cited on page 115.)

[SDS09] Nicolas Sangouard, Romain Dubessy, and Christoph Simon. Quantum repeaters based on single trapped ions. *Physical Review A*, 79(4):042340, April 2009. (Cited on page 100.)

[SK03] Y. G. Semenov and K. W. Kim. Effect of an external magnetic field on electron-spin dephasing induced by hyperfine interaction in quantum dots. *Physical Review B*, 67(7):073301, February 2003. (Cited on page 67.)

[SM01] Marcus Stollsteimer and Günter Mahler. Suppression of arbitrary internal coupling in a quantum register. *Physical Review A*, 64(5):052301, October 2001. (Cited on page 25.)

[SMC03] Matthias Steffen, John M. Martinis, and Isaac L. Chuang. Accurate control of josephson phase qubits. *Physical Review B*, 68(22):224518, December 2003. (Cited on page 122.)

[SS03] Norbert Schuch and Jens Siewert. Natural two-qubit gate for quantum computation using the XY interaction. *Physical Review A*, 67(3):032301, March 2003. (Cited on pages 34, 117, and 126.)

[SSdG11] Nicolas Sangouard, Christoph Simon, Hugues de Riedmatten, and Nicolas Gisin. Quantum repeaters based on atomic ensembles and linear optics. *Reviews of Modern Physics*, 83(1):33–80, March 2011. (Cited on page 99.)

[STKB11] Malte Schlosser, Sascha Tichelmann, Jens Kruse, and Gerhard Birkl. Scalable architecture for quantum information processing with atoms in optical microstructures. *Quantum Information Processing*, 10(6):907–924, December 2011. (Cited on page 115.)

[SV06] Lea F. Santos and Lorenza Viola. Enhanced convergence and robust performance of randomized dynamical decoupling. *Physical Review Letters*, 97(15):150501, October 2006. (Cited on page 24.)

[Syl67] J.J. Sylvester. LX. thoughts on inverse orthogonal matrices, simultaneous signsuccessions, and tessellated pavements in two or more colours, with applications to newton's rule, ornamental tile-work, and the theory of numbers. *Philosophical Magazine Series 4*, 34(232):461–475, December 1867. (Cited on page 30.)

[TAAL15] N. Trautmann, G. Alber, G.S. Agarwal, and G. Leuchs. Time-reversal-symmetric single-photon wave packets for free-space quantum communication. *Physical Review Letters*, 114(17):173601, April 2015. (Cited on page 99.)

[TBA14] J. M. Torres, J. Z. Bernád, and G. Alber. Quantum teleportation and entanglement swapping of matter qubits

with coherent multiphoton states. *Physical Review A*, 90(1):012304, July 2014. (Cited on page 99.)

[Uhr07] Götz S. Uhrig. Keeping a quantum bit alive by optimized $$\pi${}$-pulse sequences. *Physical Review Letters*, 98(10):100504, March 2007. (Cited on page 23.)

[UJA+04] Rupert Ursin, Thomas Jennewein, Markus Aspelmeyer, Rainer Kaltenbaek, Michael Lindenthal, Philip Walther, and Anton Zeilinger. Communications: Quantum teleportation across the danube. *Nature*, 430(7002):849–849, August 2004. (Cited on page 99.)

[VC05] L. M. K. Vandersypen and I. L. Chuang. NMR techniques for quantum control and computation. *Reviews of Modern Physics*, 76(4):1037–1069, January 2005. (Cited on page 122.)

[VK03] Lorenza Viola and Emanuel Knill. Robust dynamical decoupling of quantum systems with bounded controls. *Physical Review Letters*, 90(3):037901, January 2003. (Cited on pages 5, 51, 52, and 55.)

[VK05] Lorenza Viola and Emanuel Knill. Random decoupling schemes for quantum dynamical control and error suppression. *Physical Review Letters*, 94(6):060502, February 2005. (Cited on page 24.)

[VKL99] Lorenza Viola, Emanuel Knill, and Seth Lloyd. Dynamical decoupling of open quantum systems. *Physical Review Letters*, 82(12):2417–2421, March 1999. (Cited on pages 4 and 17.)

[VL98] Lorenza Viola and Seth Lloyd. Dynamical suppression of decoherence in two-state quantum systems. *Physical Review A*, 58(4):2733–2744, October 1998. (Cited on pages 4, 17, and 22.)

[VLK99] Lorenza Viola, Seth Lloyd, and Emanuel Knill. Universal control of decoupled quantum systems. *Physical Review Letters*, 83(23):4888–4891, December 1999. (Cited on page 17.)

[vLMN08] Peter van Loock, Norbert Lütkenhaus, W. J. Munro, and Kae Nemoto. Quantum repeaters using coherent-state communication. *Physical Review A*, 78(6):062319, December 2008. (Cited on pages 5 and 99.)

[vLS+06] P. van Loock, T. D. Ladd, K. Sanaka, F. Yamaguchi, Kae Nemoto, W. J. Munro, and Y. Yamamoto. Hybrid quan-

tum repeater using bright coherent light. *Physical Review Letters*, 96(24):240501, June 2006. (Cited on pages 5 and 99.)

[VT99] D. Vitali and P. Tombesi. Using parity kicks for decoherence control. *Physical Review A*, 59(6):4178–4186, June 1999. (Cited on pages 70 and 108.)

[WGE+10] T. Wilk, A. Gaëtan, C. Evellin, J. Wolters, Y. Miroshnychenko, P. Grangier, and A. Browaeys. Entanglement of two individual neutral atoms using rydberg blockade. *Physical Review Letters*, 104(1):010502, January 2010. (Cited on page 115.)

[Wig59] Eugene P. Wigner. *Group Theory and its Application to the Quantum Mechanics of Atomic Spectra*. Academic Press, New York, NY, expanded and improved edition edition edition, January 1959. (Cited on page 78.)

[WRJB02a] Pawel Wocjan, Martin Rötteler, Dominik Janzing, and Thomas Beth. Simulating hamiltonians in quantum networks: Efficient schemes and complexity bounds. *Physical Review A*, 65(4):042309, March 2002. (Cited on page 25.)

[WRJB02b] Pawel Wocjan, Martin Rötteler, Dominik Janzing, and Thomas Beth. Universal simulation of hamiltonians using a finite set of control operations. *Quantum Info. Comput.*, 2(2):133–150, February 2002. (Cited on page 17.)

[WS07] W. M. Witzel and S. Das Sarma. Multiple-pulse coherence enhancement of solid state spin qubits. *Physical Review Letters*, 98(7):077601, February 2007. (Cited on page 24.)

[WZ82] W. K. Wootters and W. H. Zurek. A single quantum cannot be cloned. *Nature*, 299(5886):802–803, October 1982. (Cited on page 75.)

[YBB10] Song Yang, Abolfazl Bayat, and Sougato Bose. Spin-state transfer in laterally coupled quantum-dot chains with disorders. *Physical Review A*, 82(2):022336, August 2010. (Cited on pages 75 and 77.)

[Zan99] Paolo Zanardi. Symmetrizing evolutions. *Physics Letters A*, 258(2–3):77–82, July 1999. (Cited on page 17.)

[ZHS+12] Nan Zhao, Jan Honert, Bernhard Schmid, Michael Klas, Junichi Isoya, Matthew Markham, Daniel Twitchen, Fedor Jelezko, Ren-Bao Liu, Helmut Fedder, and Jörg

Wrachtrup. Sensing single remote nuclear spins. *Nature Nanotechnology*, 7(10):657–662, October 2012. (Cited on page 115.)

[ŻZHE93] M. Żukowski, A. Zeilinger, M. A. Horne, and A. K. Ekert. "Event-ready-detectors" bell experiment via entanglement swapping. *Physical Review Letters*, 71(26):4287–4290, December 1993. (Cited on page 99.)

CURRICULUM VITÆ

PERSONAL INFORMATION

Holger Frydrych

Email: holger.frydrych@physik.tu-darmstadt.de

Born: January 3rd, 1986 in Lauterbach (Germany)

PHD STUDIES

2011-2015	Ph. D. Studies at Technische Universität Darmstadt, Institut für Angewandte Physik (supervised by Prof. Dr. Gernot Alber)

HIGHER EDUCATION

2008-2011	Master of Science in physics Technische Universität Darmstadt
2005-2008	Bachelor of Science in physics Technische Universität Darmstadt

CIVILIAN SERVICE

2004-2005	Akademie BURG FÜRSTENECK, Eiterfeld (Germany)

EDUCATION

2001-2004	Higher Education Entrance Qualification Wigbertschule Hünfeld (Germany), Secondary School (Principal subjects: Mathematics and Physics)
1995-2001	Lichtbergschule Eiterfeld (Germany), Secondary School
1992-1995	Grundschule Eiterfeld (Germany), Primary School

PUBLICATIONS

- J. Z. Bernád, H. Frydrych, and G. Alber. Centre-of-mass motion-induced decoherence and entanglement generation in a hybrid quantum repeater. *Journal of Physics B*, 46:235501, November 2013.
- H. Frydrych, G. Alber, and P. Bažant. Constructing Pauli pulse schemes for decoupling and quantum simulation. *Physical Review A*, 89:022320, February 2014.
- J. Z. Bernád and H. Frydrych. Effects of stochastic noise on dynamical decoupling procedures. *Physical Review A*, 89:062327, June 2014.
- H. Frydrych, A. Hoskovec, I. Jex, and G. Alber. Selective dynamical decoupling for quantum state transfer. *Journal of Physics B*, 48:025501, December 2014.
- P. Bažant, H. Frydrych, G. Alber, and I. Jex. Suppressing systematic control errors to high orders. *Physical Review A*, 92:022325, August 2015.
- H. Frydrych, M. Marthaler, and G. Alber. Pulse-controlled quantum gate sequences on a strongly coupled qubit chain. *Physical Review A*, 92:062322, December 2015.